
**UCGE Reports**
**Number 20095**

Department of Geomatics Engineering

# Accuracy and Reliability of Various DGPS Approaches

**(URL: http://www.geomatics.ucalgary.ca/links/GradTheses.html)**

**by**

**Chuanya Tang**

**May 1996**

THE UNIVERSITY OF CALGARY

# Accuracy and Reliability of Various DGPS Approaches

by

Chuanya Tang

A THESIS
SUBMITTED TO THE FACULTY OF GRADUATE STUDIES
IN PARTIAL FULFILLMENT OF THE REQUIREMENTS FOR THE
DEGREE OF MASTER OF SCIENCE

DEPARTMENT OF GEOMATICS ENGINEERING

CALGARY, ALBERTA
MAY, 1996

## ABSTRACT

The accuracy and reliability of various DGPS approaches are investigated. Real-time DGPS accuracy performance using RTCM message Types 1/9 for different receiver technologies is assessed and intercompared. The effects of receiver selection and latency on accuracy performance are quantified. Effects of WGS 84 reference station position errors on DGPS remote station positions are theoretically analyzed and quantified using specific datasets for static and kinematic DGPS positioning. DGPS accuracy performance with height constraints is analyzed using least-squares with inequality constraints (LSI) and weighted least-squares (LS) constraint approaches. Reliability performance results and analysis are also presented to demonstrate the advantage of using height constraint approaches for DGPS horizontal positioning instead of the standard LS method. DGPS accuracy and reliability performance using receivers aided with external precise clocks is explored. Results show that the accuracy and reliability performance improvement can, in some case, be significant when positioning with the differential receiver clock bias fixed.

## ACKNOWLEDGMENTS

I would like to express my sincere gratitude to my supervisor, Professor Gérard Lachapelle, for his continuous support and encouragement throughout the course of my graduate studies. His careful guidance and thoughtful advice were essential for the completion of this thesis.

Special thanks go to Professor M.E. Cannon for her willingness to provide SEMIKIN™ and C3NAV™ software packages. Messrs. Huangqi Sun, Nobuyuki Hayashi, and Dr. Ming Wei are sincerely thanked for sharing their knowledge in GPS and computer systems. Messrs. Chris Varner, Jamie Henriksen, John Brown, Douglas Roberts, Bryan Townsend, Hubiao Lan, Zhaonian Zhang, Nobuyuki Hayashi and Alex Bruton are all thanked for their help in data collection. Mr. Shawn Weisenburger is gratefully acknowledged for proofreading the manuscript.

Parts of my graduate studies were financially supported through grants and contracts from the Natural Science and Engineering Research Council, the Canadian Coast Guard, and the Naval Air Warfare Center, and the U.S. Department of the Navy.

Sincere thanks should also go to my family friends, Freda and Wally, for their continuous encouragement and help. Finally, my deepest thanks are for my wife, Sue X. Sun, for sharing the troubles and pleasures of my life.

## TABLE OF CONTENTS

## LIST OF TABLES

## LIST OF FIGURES

# NOTATION

## i) Symbols

| | |
|---|---|
| $\mathbf{A}$ | design matrix |
| c | speed of light |
| $\mathbf{C}$ | covariance matrix |
| $d_{ion}$ | ionospheric delay |
| $d_{trop}$ | tropospheric delay |
| $\mathbf{G}$ | constraint matrix |
| h | geodetic height |
| dt | satellite clock error |
| dT | receiver clock error |
| $d\rho$ | orbital error |
| N | carrier phase integer ambiguity |
| p | pseudoange observation |
| $P_{ll}$ | weight matrix |
| $P_k$ | measured pseudorange |
| $\hat{P}_k$ | computed smoothed pseudorange |
| $\mathbf{Q}$ | cofactor matrix |
| r | total redundancy number |
| $r_i$ | redundancy contribution of the ith observation to r |

| | |
|---|---|
| $R_f$ | position vector of fixed reference station |
| t | GPS time |
| $W_{p_k}$ | weight on the measured pseudorange |
| $W_{\Phi_k}$ | weight on the carrier phase component |
| $\alpha$ | significance level for Type I error |
| $\beta$ | significance level for Type II error |
| $\rho$ | geometrical distance between the receiver and the satellite |
| $\rho_c$ | calculated range between the reference receiver and the satellite |
| $\rho_{obs}$ | observed range between the reference receiver and the satellite |
| $\varphi$ | geodetic latitude |
| $\Phi$ | carrier phase observation (m) |
| $\lambda$ | carrier phase wavelength, and geodetic longitude |
| $\varepsilon_p$ | pseudorange observation noise and multipath |
| $\varepsilon_\Phi$ | carrier phase observation noise and multipath |
| $\upsilon$ | residual vector |
| ^ | denotes estimated quantity |

**ii) Defined Operators**

| | |
|---|---|
| $A^T$ | matrix transpose |
| $\mathbf{C}^{-1}$ | matrix inverse |
| $\nabla$ | single difference between satellites |
| $\Delta$ | single difference between receivers |

| | |
|---|---|
| $\nabla\Delta$ | double difference |
| $\| \|$ | quadratic norm |
| $\Sigma$ | summation |
| $\delta$ | correction |
| $\dot{\rho}$ | derivative with respect to time |

### iii) Acronyms

| | |
|---|---|
| AS | Anti-Spoofing |
| C/A code | Coarse/Acquisition code |
| DGPS | Differential GPS |
| DND | Department of National Defense |
| DOP | Dilution Of Precision |
| ER | External Reliability |
| GPS | Global Positioning System |
| IR | Internal Reliability |
| ITRF | International Terrestrial Reference Frame |
| LDP | Least Distance Programming |
| LS | Least Squares |
| LSI | Least Squares with Inequality constraints |
| MDB | Minimum Detectable Blunder |
| MF | Medium Frequency |
| PRC | Pseudorange Correction |
| PRN | Pseudo Random Noise |
| RAIM | Receiver Autonomous Integrity Monitoring |
| RMS | Root Mean Square |
| RTCM | Radio Technical Commission for Maritime Services |

| | |
|---|---|
| RRC | Range Rate Correction |
| SA | Selective Availability |
| SV | Space Vehicle |
| SVD | Singular Value Decomposition |
| WGS 84 | World Geodetic System 1984 |

# CHAPTER 1

# INTRODUCTION

## 1.1 Background and Objectives

The instantaneous accuracy of GPS single point positioning is limited by orbital, atmospheric, receiver and multipath errors. The prescribed accuracy of a single frequency user is of the order of 20 m (2drms) horizontally and 30 m ($2\sigma$) vertically when Selective Availability (SA) is off. When SA is turned on, the above errors grow to 100 m horizontally and 156 m vertically at the same probability level [Lachapelle et al., 1995a]. Differential operation of GPS offers the possibility of accuracies of 1-10 m for dynamic navigation applications [Wells et al., 1986; Lachapelle et al., 1988]. Utilizing kinematic carrier phase techniques, differential GPS can achieve an accuracy better than 10 cm for short baselines, e.g., less than about 20 km [Cannon, 1987; Cannon, 1990a; Cannon and Lachapelle, 1992]. Differential operation of GPS is achieved by placing a reference station with a GPS receiver at a known location, determining corrections to the satellite ranging signals, and broadcasting these corrections to users of the service. This removes most of the bias errors common to all receivers and significantly improves the position accuracy [RTCM, 1994].

In real-time DGPS positioning, a remote station has to apply the pseudorange corrections generated by the reference station at a previous time. The time latency will raise the error level of DGPS. In addition, the measurement accuracies of pseudoranges for various receivers are different. Therefore, it is important to investigate the effects of latency on

DGPS accuracy performance using various receiver technologies [Lachapelle et al., 1996a].

In DGPS positioning, we usually assume the position of the reference station is exactly known in WGS 84. In practice, however, the position of the reference station in WGS 84 may not be exactly known due to some practical difficulties. One situation is that there are no known points available in the positioning area and we have to use a point positioning method to determine the position of the reference station. Another case is that we have known points available in the working area, but the coordinates may not be in WGS 84 and we have to transfer the coordinates to WGS 84 [Gryglaszewski, 1995]. Therefore, it is of significance to investigate the effect of the reference station position errors on the remote station position.

For marine and vehicular navigation, the height can be constrained because the height component is normally known to within a few metres [Wells et al., 1986; Lu et al., 1993]. Two methods can be used to constrain height. One is weighted constraints, in which the 'known' height information is treated as a quasi-observation and goes into the standard Least-Squares (LS) solution [Krakiwsky, 1992; Leick, 1995]. Another method is the Least-Squares with Inequality constraints (LSI) [Lawson and Hanson, 1974], in which the *a priori* height information is considered by adding inequality constraints.

Research has shown that the receiver clock bias may be predictable depending on the stability characteristics of the clock [Misra et al., 1995a]. This characteristic of the receiver clock stability has previously been exploited for navigation and integrity monitoring with 'clock coasting' over a relatively short period while the satellite geometry is poor [Sturza, 1983; Lee, 1993]. Since the receiver clock bias is relatively stable over such a period, we can adaptively model the clock bias from the past measurements and expect to be able to predict the clock bias for the future. Then we can take advantage of

the estimated clock stability characteristic regularly and continuously to improve the positioning and reliability performance by constraining the receiver clock bias after we have modeled and predicted it.

The objective of this research is to investigate and analyze accuracy and reliability performance of various DGPS approaches, namely: real-time DGPS accuracy performance using RTCM message Types 1/9 for different receiver technologies, DGPS performance with height constraints, and DGPS performance aided with external precise clocks. In addition, effects of WGS 84 reference station coordinate errors on DGPS remote station coordinates are also analyzed.

## 1.2 Thesis Outline

The thesis consists of six chapters. The contents of the remaining chapters are as follows:

In Chapter 2, real-time DGPS positioning accuracy performance using RTCM message Types 1/9 for different receiver technologies is investigated and intercompared. The RTCM Type 1/9 messages using code or carrier phase smoothed code are used in single differencing mode to obtain DGPS positions. The RTCM message Types 1/9 are described and the algorithm for carrier phase smoothing of code is examined. Receiver selection and field measurements are also described. The results of DGPS without latency and with different simulated latencies are presented and compared using RTCM message Types 1/9 for different receiver technologies.

In Chapter 3, the effects of WGS 84 reference station position errors on DGPS remote station positions are investigated. A theoretical analysis of the effects of WGS 84 reference station position errors on static and kinematic DGPS is presented. The results of static and kinematic DGPS using specific sets of observed data are presented.

In Chapter 4, DGPS performance with height constraints is investigated. Inequality constraint least-squares and the theory of reliability are introduced. Different datasets are processed and analyzed to show the effectiveness of DGPS with height constraints. Accuracy performance is analyzed and intercompared using the LSI and the weighted constraint LS for height constraints. Reliability performance results and analysis are presented.

Chapter 5 investigates DGPS performance aided with external precise clocks. The impact of precise clock augmentation of GPS receivers is described. Receiver clock adaptive modeling at the remote station is presented. A test using two NovAtel GPSCard™ receivers with external precise clocks is conducted, and the results are given to demonstrate the performance improvement.

Finally, the main conclusions of the thesis and recommendations for further investigations are given in Chapter 6.

# CHAPTER 2

## REAL-TIME DGPS ACCURACY PERFORMANCE USING RTCM MESSAGE TYPES 1/9 FOR DIFFERENT RECEIVER TECHNOLOGIES

The Canadian Coast Guard is implementing a marine DGPS service in Canadian waters. This service will be based on MF (radiobeacon) transmitters. It is expected to serve the needs of commercial navigation, Coast Guard Fleet operations and other government operations. Its availability is expected to promote the widespread use of electronic chart navigation and thereby enhance the safety and efficiency of marine commerce [Forbes et al., 1994]. A horizontal accuracy of 5 m (95th percentile) is anticipated.

In order for the Coast Guard to properly implement the above system, it is very important to evaluate various receiver technologies and their performance in real-time differential environments. The purpose of this chapter is to assess and intercompare DGPS accuracy performance using RTCM message Types 1/9 for three receiver technologies, namely C/A code wide correlator spacing, C/A code Narrow Correlator™ spacing and semicodeless P-W technology assuming that the same or different technologies are employed by reference and user stations. The DGPS method used here is the single difference method of one reference station and one user receiver using code only and carrier phase smoothed code. Latencies of up to 25 seconds are used to simulate real-time operations.

## 2.1 RTCM Message Types 1, 2 and 9

The Radio Technical Commission for Maritime Services (RTCM) Special Committee (SC) No. 104 has recommended message types and message structures required for the real-time transmission of GPS data from a reference station to various differential GPS users to correct, to the extent possible, for GPS errors that are common to the reference station and the users. Message Types 1, 2 and 9 are the main message types which will be used in marine DGPS [RTCM, 1994].

The RTCM Type 1 message, differential GPS corrections, contains data for all satellites in view of the reference station. The reference station clock offset will be a common offset in all pseudorange corrections, and this will not affect position calculations at the user station.

The RTCM Type 2 message, delta differential GPS corrections added to the normal correction for a satellite, is provided for situations where the user equipment may not immediately decode new satellite ephemerides in the satellite data, which allows a user to operate with old satellite ephemeris and satellite clock data while the reference station is operating with the most recent data. It contains the difference in the pseudorange and range rate corrections caused by the change in satellite navigation data.

The RTCM Type 9 message, partial satellite set differential corrections, serves the same purpose as the Type 1 message, in that it contains the primary differential corrections. The average correction age is reduced by packing the corrections in groups of 3 satellites, thereby improving performance. A more stable clock may be required at the reference station, because the corrections for different satellites may have different time references.

In order to simulate in a conservative manner real-time operation with the Type 9 message format which uses asynchronous corrections, it was decided to use synchronous corrections for all satellites which implies the use of message Type 1 and represents the worst case obtained by simulating a latency corresponding to the longest delay which may occur using Type 9 message [Lachapelle et al., 1995b]. For this purpose, the two message Types will be referred to as Type 1/9.

In order to avoid the difference caused by using different ephemerides for the reference station and the user, the time of ephemeris is included in the correction message that ensures that the user calculations and the reference station corrections are based on the same ephemeris parameters.

## 2.2 Processing Approaches

The kinematic positioning calculations were performed successively using code and carrier phase smoothed code measurements in DGPS mode with C$^3$NAV™ (Combination of Code and Carrier for NAVigation), a software package that uses a recursive filter suitable for simulation of real-time DGPS [ Cannon and Lachapelle, 1992, 1993]. C$^3$NAV™ post-processes the DGPS data in two steps, namely (i) generation of differential range corrections at the reference station, and (ii) computation of differentially corrected positions at the user station. In step (i), the known coordinates of the reference station are used as input values [Lachapelle et al., 1995b].

### 2.2.1 Generation and Application of Differential GPS Corrections

A range correction is the parameter required to cancel out or reduce the effects of Selective Availability (S. A.), the satellite clock error, the ionosphere and troposphere. It

is computed by comparing the calculated range $\rho_c$ based on the known coordinates $R_f$ of a fixed reference station and computed satellite position **r** to the measured range $\rho_{obs}$, i.e.

$$PRC=\rho_c-\rho_{obs}=\left\|r^s-R_f\right\|-\rho_{obs} \tag{2.1}$$

where PRC is the pseudorange correction in metres.

It has been shown that the behaviour of pseudorange correction mimics SA, which is expected because SA is the largest component of the range error, and is linear over a short time period such as 20 seconds. Figure 2.1 demonstrates the pseudorange correction variation over long and short time periods. The pseudorange correction over a long period (3000 seconds) for PRN 4 does mimic SA, but it is linear over a short period (40 seconds). Based on this linear behaviour of the pseudorange correction over a short time period, the most direct approach to computing the range rate correction is to take the change of range correction over successive epochs, which can be computed using the following formula:

$$RRC = (PRC(i) - PRC(i-1)) / (t_i - t_{i-1}) \tag{2.2}$$

where RRC is the range rate correction in metres/second, PRC(i), PRC(i-1) are range corrections over subsequent epochs, and $t_i$, $t_{i-1}$ are the GPS times at the present and previous epochs. The interval between epochs is assumed to be of the order of one second.

Another method of computing range rate correction is to use the observed Doppler scaled to range rate correction using the following formula:

$$\mathrm{RRC} = \dot{\rho}_c - \dot{\rho}_{obs} = \left\| \dot{r}^s - \dot{R}_f \right\| - \dot{\rho}_{obs} \tag{2.3}$$

where $\dot{\rho}_c$ is the computed range rate and $\dot{\rho}_{obs}$ is the observed range rate.

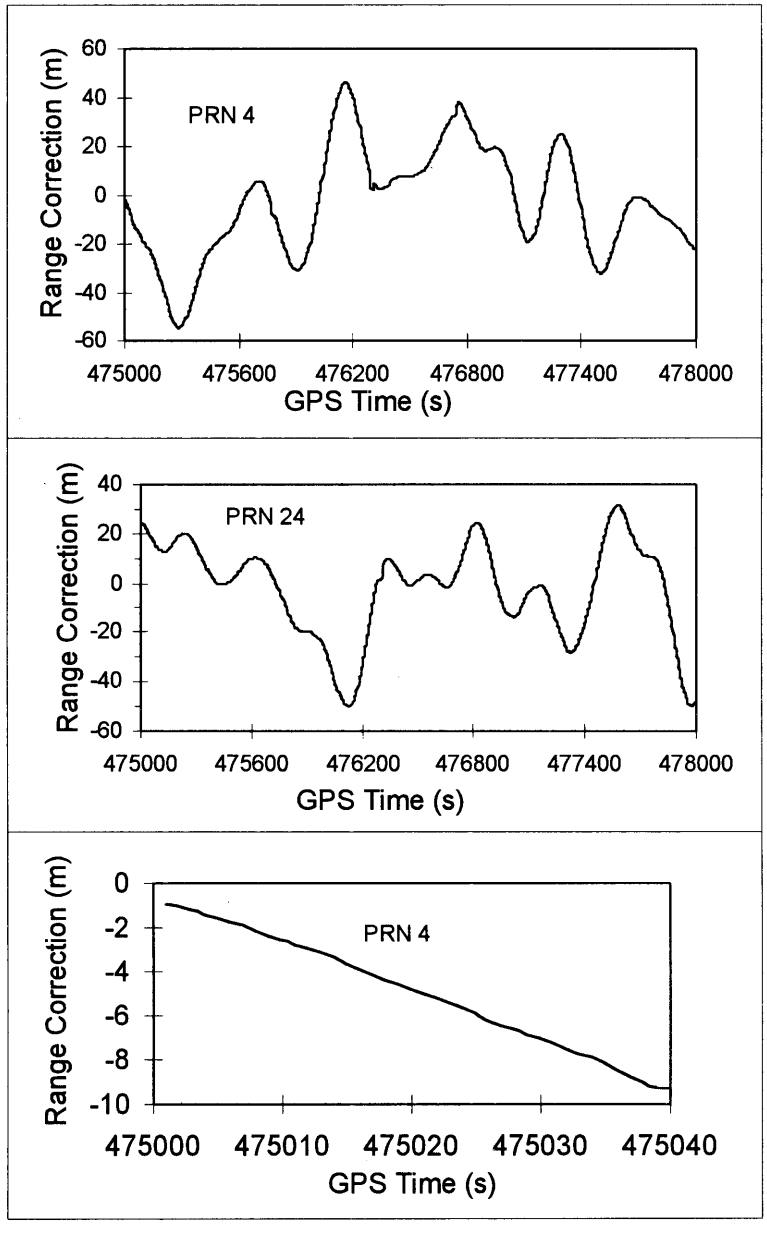


Figure 2.1 Pseudorange Correction Variation over Time

In order to compensate for the time latency, the pseudorange correction must be predicted using the range rate correction. The DGPS correction at the remote receiver can be applied as follows:

$$PR(t) = PRM(t) + PRC(t) \tag{2.4}$$

$$PRC(t) = PRC(t_0) + RRC \bullet (t - t_0) \tag{2.5}$$

where the pseudorange (PR) at time t equals the measured pseudorange (PRM) at time t plus the pseudorange correction (PRC) at time t. The pseudorange correction (PRC) at time t consists of the pseudorange correction (PRC) at the time of applicability $t_0$ plus the range rate correction (RRC) times the difference between time t and $t_0$, i.e., the latency of the correction.

### 2.2.2 Carrier Phase Smoothing of Code

Two basic types of measurements, pseudorange and carrier phase measurements, can be obtained from the GPS satellites. The pseudorange measurement is not ambiguous but noisy, while the carrier phase measurement is accurate but ambiguous because the number of whole cycles (ambiguity) between the satellite and the receiver is unknown. In removing the GPS errors by differential GPS, the pseudorange noise is one of most important error sources which need special attention if metre level accuracy is to be obtained. It has been shown that smoothing pseudorange measurements with carrier phase measurements is an efficient way to reduce pseudorange noises. Different techniques for reducing the pseudorange noise with carrier phase have been proposed [Hatch 1982; Lachapelle et al., 1987; Ashjaee, 1990; Goad, 1990; Euler and Goad, 1991].

The accuracy of the carrier phase derived range difference between two successive epochs is generally better than 1 cm. Since the accuracy of the ambiguity free pseudorange difference is lower, a recursive filter which progressively increases the weight on carrier phase $\Phi$, is used. The carrier phase smoothed pseudorange $\hat{P}_k$ at time k is [Lachapelle, 1995c]

$$\hat{P}_k = W_{p_k} P_k + W_{\Phi_k} \{\hat{P}_{k-1} + (\Phi_k - \Phi_{k-1})\} \tag{2.6}$$

where $P_k$ is the measured pseudorange at epoch k, $W_{p_k}$ and $W_{\Phi_k}$ are the sliding weights assigned to pseudorange and carrier phase measurements. $\Phi_k$ and $\Phi_{k-1}$ are the measured carrier phases at the current and previous epochs. The sliding weights start with a value of 1.0 for the pseudorange and 0.0 for the carrier phase. As the epoch counter increases, the weights slide so that the emphasis is placed on the more accurate phase measurement. To counteract the effect of code and carrier divergence due to the ionosphere, dual ramps operating in parallel are used [Cannon and Lachapelle, 1992]. The concept of the dual ramp carrier phase smoothing of pseudorange is illustrated in Figure 2.2. The ramps are offset by half the selected ramp reset interval. Typically, this moving window technique reduces the time span that either ramp can be used and assumes a negligible divergence between code and carrier phase during the number of epochs between resets. At initialization and after cycle slips, the two ramps are started at the same time. After (reset interval interval/2) epochs, the first filter is reset and the second filter is used for (reset interval/2) more epochs. By this time, the second filter is reset and the first ramp is used again.

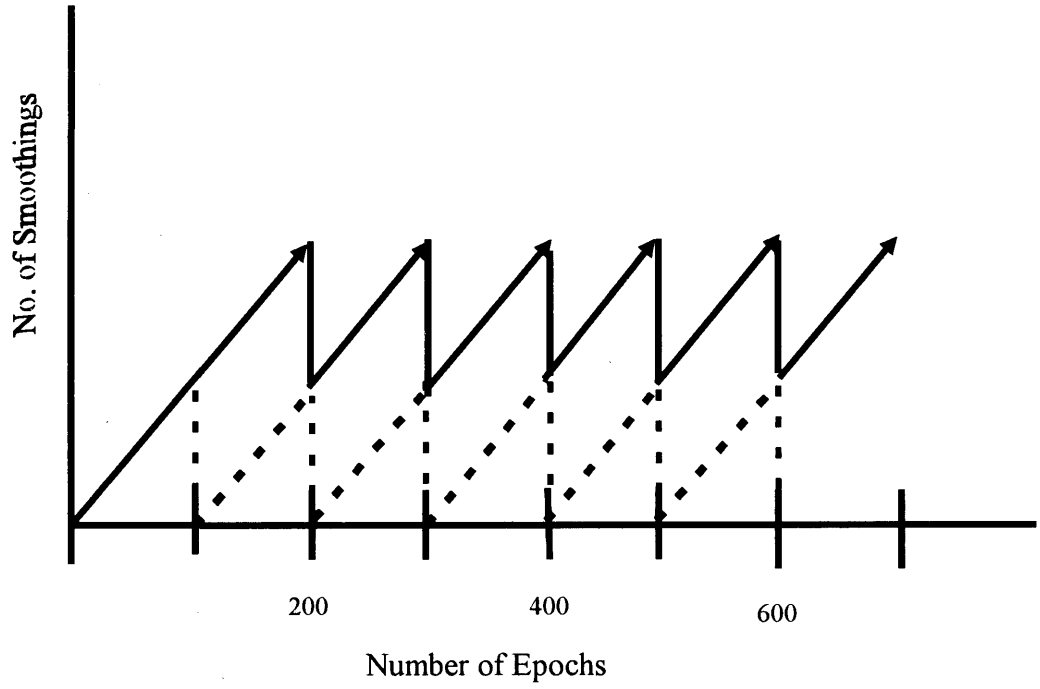


Figure 2.2 Dual Ramp Carrier Phase Smoothing of Pseudorange

Experience has shown that a reasonable value for the reset interval is typically serveral hundred to a few thousand, regardless of the receiver type used. A decision was made to use the C $^3$ NAV™ default value of 400. In order to show that the accuracy is insensitive to the selected reset interval, one day of observations with the GPSCard™ 951 receivers was processed using successively three values for reset interval, namely 400, 1000 and 2000. The results are summarized in Table 2.1. The three sets of RMS results are practically identical in this case. In extreme cases of multipath and undetected cycle slips, the use of a lower value for reset interval would enhance the robustness of the filter at the expense of reducing the accuracy.

Table 2.1 Effect of Reset Interval on the DGPS Positioning Accuracy Using GPSCard™ 951 Receivers, Carrier Phase Smoothing of Pseudorange Measurements

| Reset Interval | Coordinates | Mean (m) | RMS (m) | Min (m) | Max (m) |
|---|---|---|---|---|---|
| 400 | $\phi$ | -0.18 | 0.37 | -1.80 | 1.64 |
| | $\lambda$ | 0.24 | 0.34 | -1.15 | 1.47 |
| | h | -0.06 | 0.55 | -3.01 | 2.27 |
| 1000 | $\phi$ | -0.18 | 0.36 | -1.78 | 1.69 |
| | $\lambda$ | 0.24 | 0.34 | -0.80 | 1.60 |
| | h | -0.05 | 0.53 | -2.88 | 2.19 |
| 2000 | $\phi$ | -0.18 | 0.36 | -1.78 | 1.69 |
| | $\lambda$ | 0.24 | 0.34 | -0.80 | 1.60 |
| | h | -0.05 | 0.53 | -2.88 | 2.19 |

## 2.3 Receiver Selection

The three receiver types selected for the analysis are

(i) C/A code wide correlator spacing : 12-channel Magnavox 9212

This unit is the successor of the 6-channel MX 4200 which has been used successfully in a variety of marine and other applications. Testing of the MX 9212 under foliage has showed a relatively high level of carrier phase tracking loop stability and a relatively good

positioning accuracy [Lachapelle et al., 1995d]; it outperformed two other receiver types in its class, namely the Navstar XR5 M12 and the Motorola PVT-6.

(ii) C/A code Narrow Correlator™ spacing: NovAtel GPSCard™ 951

Since its introduction in 1991, this receiver has consistently delivered a high level of performance under a variety of dynamics. Its narrow correlator spacing technology results in a low C/A code noise and in RMS accuracies at the sub-metre level in each coordinate component when carrier phase smoothing of the code is used [Van Dierendonck et al., 1992; Cannon & Lachapelle, 1992]. See [Lachapelle et al., 1993, 1994] for marine and other applications.

(iii) Semicodeless technology: Ashtech Z-12

This receiver outputs C/A code and associated L1 carrier phase measurements. The Y1 and Y2 code (Y implies that AS is on) and carrier phase measurements are also measured using a semicodeless P-W technology which results in a 14 dB loss compared to much higher losses for other codeless technologies [Ashjaee & Lorenz 1992; Van Dierendonck 1994]. In this study, the emphasis will be on C/A code and carrier phase measurements because these stronger signals would be used to generate Type 9 messages.

## 2.4 Description of Field Measurements

A 424-km baseline was observed during October 13-15, 1994, between Calgary and Havre, Montana using 3 pairs of receivers. Tests with all three receiver classes were conducted simultaneously to avoid performance differences caused by differences in the level of Selective Availability and atmospheric effects. The points occupied in Calgary were located on the Roof of the F-Block of the Engineering Building of The University of

Calgary. Pillars N1, N2 and N3 were occupied with NovAtel, Magnavox and Ashtech antennas (Figure 2.3), respectively. The NovAtel antenna was equipped with an external chokering groundplane. The approximate distance between consecutive pillars is 3 m. The horizon is clear down to an elevation of 0° except in the east direction where the mask angle is approximately 5°. The points occupied in Havre were located in a field of the Northern Agricultural Research Center of Montana State University. Three points, namely N'1, N'2 and N'3, were marked with steel rods in the ground and occupied simultaneously (Figure 2.3). The receivers were housed in a nearby vehicle and were powered by batteries. No external groundplanes were used with any antenna.

The observations with the three receiver types were conducted during the period October 13 (20:00, local time) to October 16 (03:00, local time), 1994. The weather conditions were poor at both ends, due to snow and sleet.

Over 50 hours of data was collected at 1 Hz with the three receiver types selected, except with the Ashtech Z-12 receiver pair. For Ashtech Z-12 pair, the number of hours is down to around 35 due to malfunctioning of the unit in Montana.

For the purpose of the reduction and analysis, the above measurements were divided into two periods of 24 hours, referred to as Day 1 and Day 2 [Lachapelle et al., 1995b]:

Day 1: 20:00, 13 October until 20:00, 14 October 1994,
Calgary local time
Day 2: 20:00, 14 October until 20:00, 15 October 1994,
Calgary local time

This division allowed us to analyze the day to day repeatability of the result.

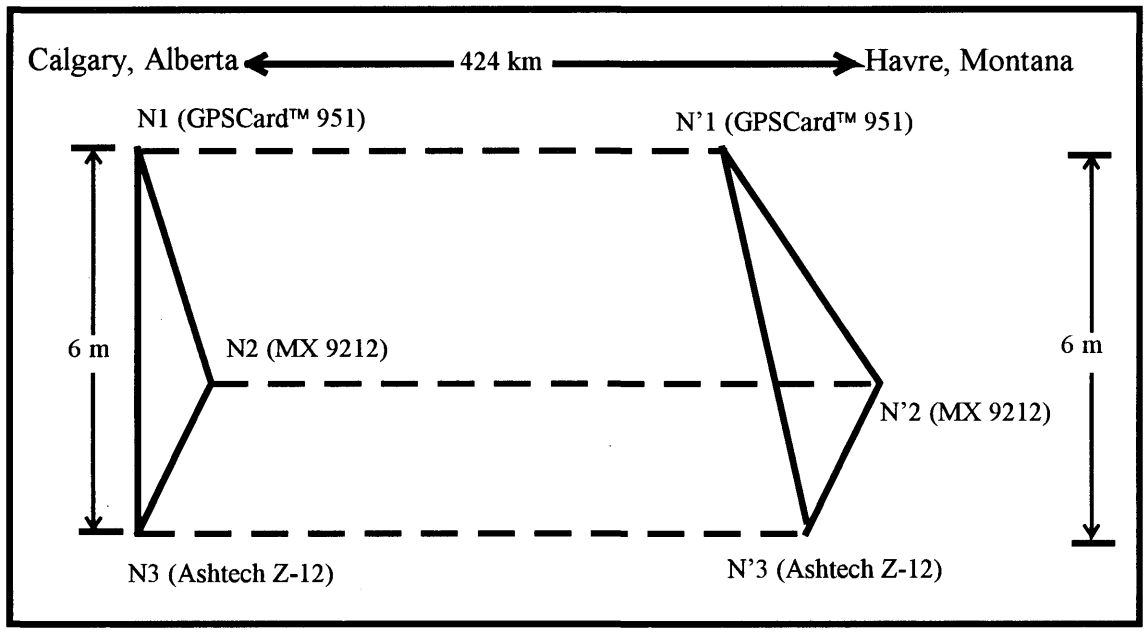


Figure 2.3 Receiver Configuration, Land Test, Calgary - Havre, October 1994

## 2.5 Determination of Reference Coordinates for Calgary and Montana Stations

A DGPS survey was conducted using two Ashtech Z-12 receivers between Priddis and The University of Calgary on December 22, 1994, to transfer the ITRF 1992 - EPOCH 1988.0 coordinates of PRDS to Point N1, shown in Figure 2.3. WGS 84 and ITRF are now compatible within 10 cm [Kouba and Popelar, 1994]. The distance between PRDS and N1 is 25.8 km and the double difference carrier phase integer ambiguities could be resolved using the widelane method. Two widelane solutions for the vector PRDS - N1 were derived, namely one with SEMIKIN™, a software package developed by The University of Calgary [Cannon, 1993], and one with Ashtech software PNAV. Since the difference between these two solutions is at centimetre level, the average of these two solutions was used as the final solution for the ITRF 92 (epoch 1988.0) coordinates of N1. The ITRF coordinates of N2 and N3 were obtained by differentially processing short data

segments between the various receivers used during the measurement campaign of October 13-15, 1994. The fixed integer ambiguity solutions obtained with SEMIKIN™ resulted in the ITRF 92 (epoch 1988.0) coordinates for N2 and N3. These differential solutions are accurate to the millimetre level. The coordinates of the Calgary stations are expected to be better than 10 cm.

In order to determine the WGS-84 coordinates of the Montana Ashtech station (N'3 in Figure 2.3) with respect to N3 in Calgary, two DGPS carrier phase segments of 200 minutes each observed with the Ashtech Z-12 receivers during the period October 13-15 were used. The Ashtech Z-12 units were selected because they provide dual-frequency (L1/L2) measurements which can be used to account for the effect of the ionosphere. This effect is in principle significant over such a long baseline, i.e., 1-3 ppm or 40 to 120 cm. A comparison of L1 and L1/L2 solutions shown in Figure 2.4, however, revealed that the effect of the ionosphere was less than 10 cm in each of the coordinate components. This is due to a relatively quiet ionosphere during the observation period. The two data sets were processed with SEMIKIN™ and Ashtech software GPPS. The solutions are in agreement within 20 cm which is satisfactory for the present purpose. The final coordinates adopted for N'3 are the average of the four solutions. The coordinates of N'1 and N'2 were obtained by differentially processing short data segments between the various receivers. The fixed integer ambiguity solutions were obtained by SEMIKIN™. These differential solutions are accurate to the millimetre level. The coordinates of the Montana stations are expected to be accurate to be better than 1 ppm with respect to those of the Calgary stations.

Table 2.2 Difference between L1/L2 and L1 Solutions

| Software Used | | Cutoff Angle | ΔX (cm) | ΔY (cm) | ΔZ (cm) |
|---|---|---|---|---|---|
| SEMIKIN™ | L1/L2 - L1 | 10° | 7.0 | 2.0 | -2.0 |
| | | 15° | -2.0 | -4.0 | 1.0 |
| | | 20° | 1.0 | -3.0 | 0.0 |
| PNAV | L1/L2 - L1 | 10° | 9.0 | 3.0 | -3.0 |
| | | 15° | 10.0 | 3.0 | -0.1 |
| | | 20° | 4.0 | 0.0 | -1.0 |
| SEMIKIN - PNAV L1 | | 15° | -20.0 | -14.0 | 15.0 |
| | | 20° | -16.0 | -11.0 | 10.0 |

## 2.6 Results and Analysis

### 2.6.1 Latency Effect on Pseudorange Corrections

In order to illustrate the effect of latency on Type 1/9 pseudorange corrections, mean and RMS differences between pseudorange corrections calculated for the 0 second latency case and for latencies of 5, 10, 15 and 25 seconds are shown in Figure 2.4 for a 50-minute data segment observed in Calgary with the GPSCard™ 951 receiver. For all satellites, the RMS difference is below 1 m except for a latency of 25 seconds. This is within anticipated limits with Selective Availability on. PRN 12 is a Block I satellite which is not affected by Selective Availability; this is why the mean and RMS differences are smaller than the other satellites, especially for a latency of 25 seconds.

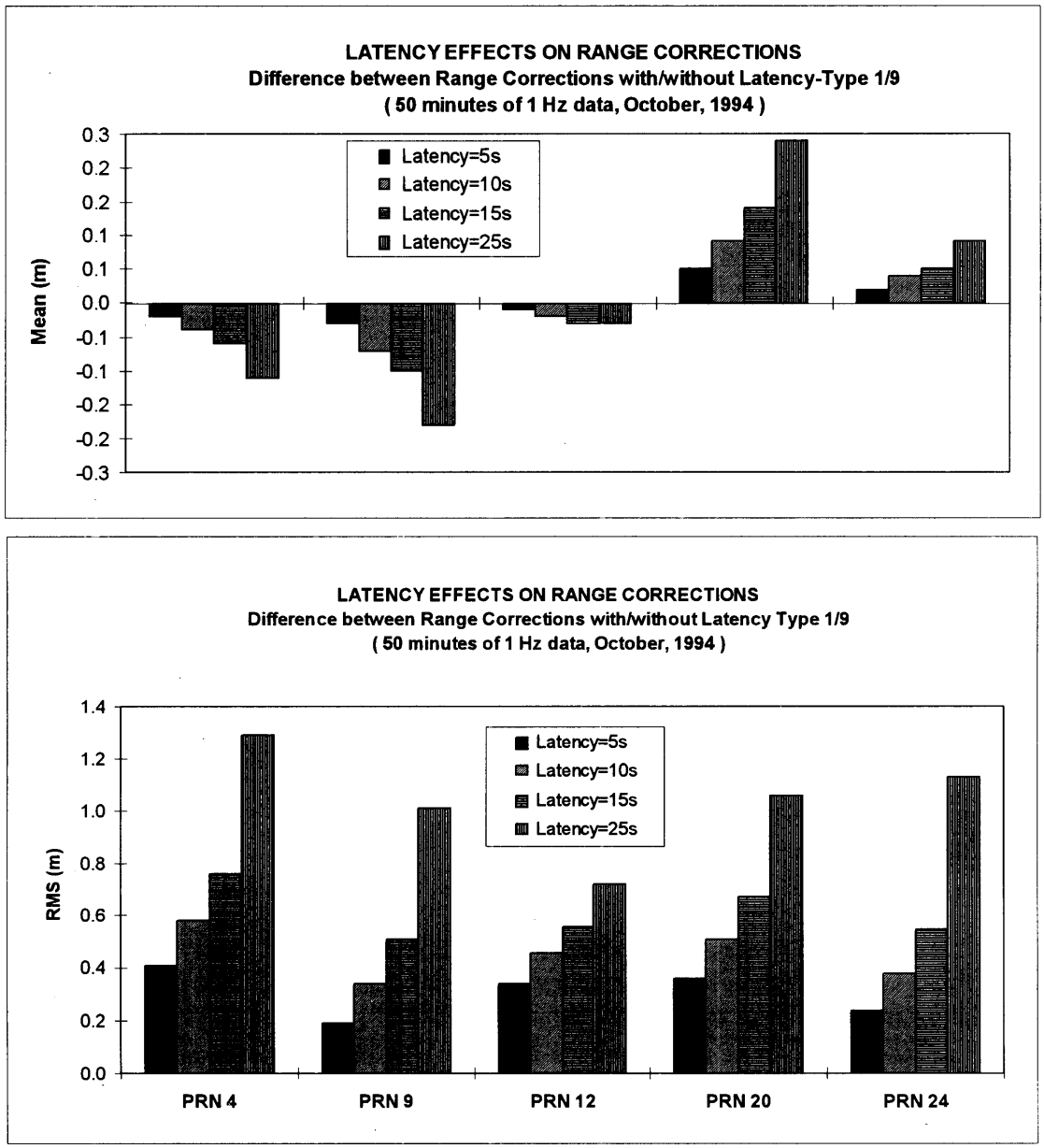


Figure 2.4 Mean and RMS Effect of Latency on Type 1/9 Pseudorange Corrections

### 2.6.2 Results without Latency

The data sets observed during Day1 and Day 2 were first processed using C $^3$ NAV™ with no time latency introduced. The positions obtained at each epoch were compared to the known coordinates of the station selected as the remote. Type 1/9 code versus carrier phase smoothed code solutions are shown in Figure 2.5 for the 0 second latency case, which is equivalent to a post-mission case or an ideal real-time case. The statistics for each of the two days are shown separately to illustrate the high level of repeatability between the two days. The Type 1/9 Ashtech Z-12 Y1 code and carrier phase smoothed code solutions are similar to the Ashtech Z-12 C/A code solution, which indicates that the use of a semicodeless technology to obtain Y1 does not substantially change accuracy in this case. The desired accuracy of 5 m 95th percentile in horizontal position is easily met by the GPSCard™ 951 and Ashtech Z-12 receiver pairs using either code or carrier phase smoothed code. In fact, the 95th percentile horizontal accuracy is $\leq$ 2 m in this case. The best results, namely 1 m accuracy, are obtained using the GPSCard™ 951 receiver pair with carrier phase smoothed code observations. In the case of the MX 9212 receiver pair, the 5 m accuracy is met using carrier phase smoothed code. The height standard deviation ($\approx$ 68th percentile) is less than 2 m for all receiver pairs with code and carrier phase smoothed code solutions except for the MX 9212 pair with code solutions. However, the accuracies obtained herein could be degraded by a few ppm, typically 2 ppm, during periods of high ionospheric activities.

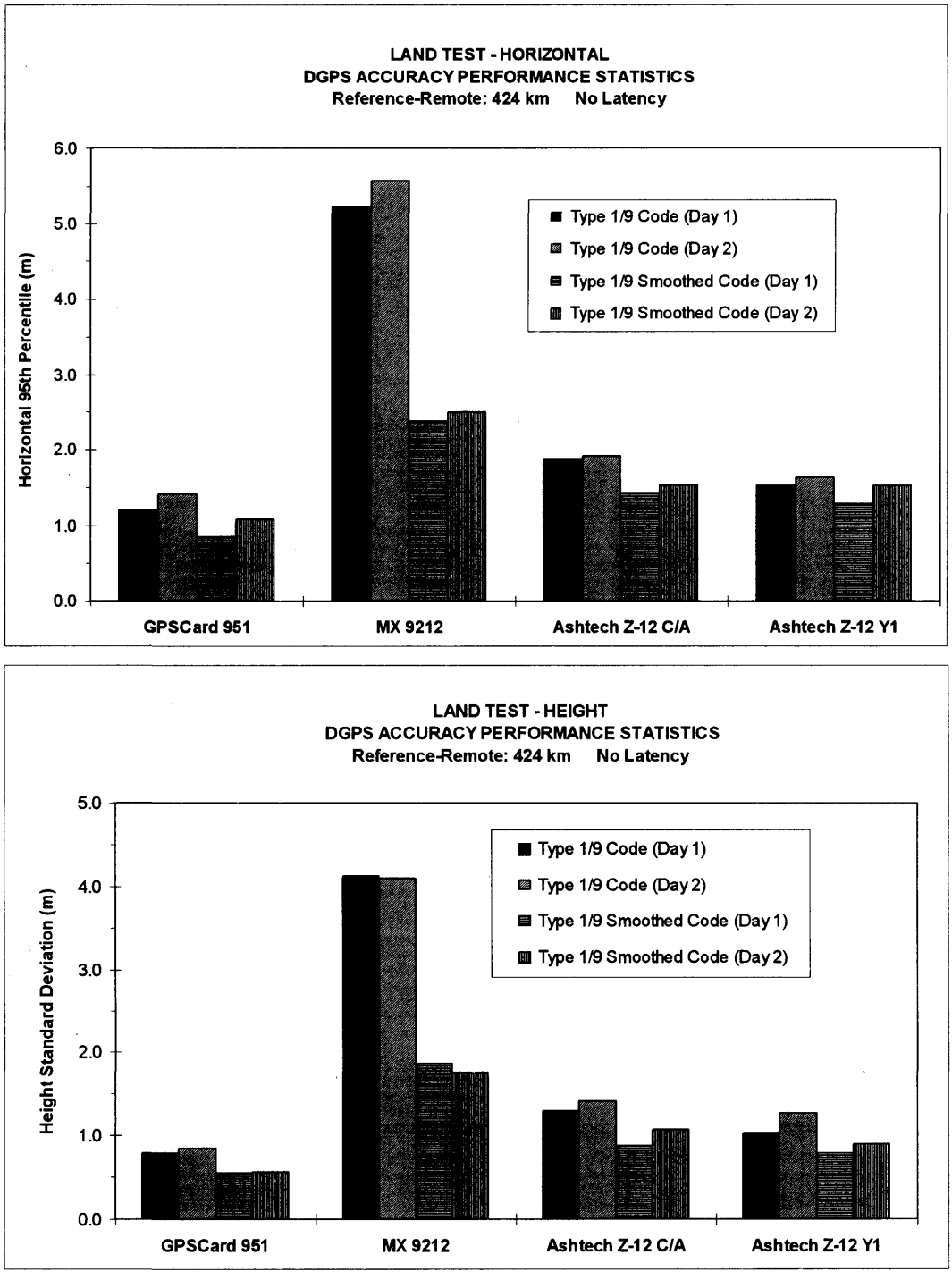


Figure 2.5 Accuracy Performance without Latency

### 2.6.3 Results with Latencies of 5-25 Seconds

In order to simulate latency effects using a conservative scenario, selected latencies were applied to all satellites equally. The worst case is therefore obtained by simulating a latency corresponding to the longest delay which may occur using Type 9 message. The observations made on Day1 were used for these simulations. Calgary was used as the reference station and, Montana as the remote. The accuracies of the Type 1/9 carrier phase smoothed code solutions obtained with all three receiver pairs for latencies of 0, 5, 10, 15 and 25 seconds are shown in Figure 2.6. In this case, the Ashtech Z-12 data used is the C/A code L1 data. The horizontal 95th percentile accuracy is better than 4 m in all cases. This is well within the 5-m threshold anticipated by the Canadian Coast Guard. The height standard deviation ($\approx$ 68th percentile) is lower than 3 m. The best accuracy performance is achieved by the GPSCard™ 951 receiver pair, followed closely by the Ashtech Z-12 C/A code receiver pair. The accuracy performance of the MX 9212 receiver pair is slightly lower due to the use of a wide correlator technology, as anticipated. Again, this is for the case where the effect of the ionosphere is minimal. If one were to assume a 2 ppm effect of the ionosphere, the accuracy obtained with the pair of wide correlator spacing C/A code receivers would deteriorate to slightly below the 5 m level. The effect of a latency of up to 10 seconds on the horizontal 95th percentile and height standard deviation is less than 0.5 m. For a latency of 25 seconds, the effect reaches about 2 m.

### 2.6.4 Accuracy Performance of Mixed Receiver Pairs

The accuracy performance achieved using different receivers at the reference station and the remote using Type 1/9 solutions was analyzed for selected combinations. The results are summarized in Figure 2.7. The accuracies shown for each mixed receiver pair are

approximately half way between the accuracies reported earlier with each identical receiver pair, as anticipated.

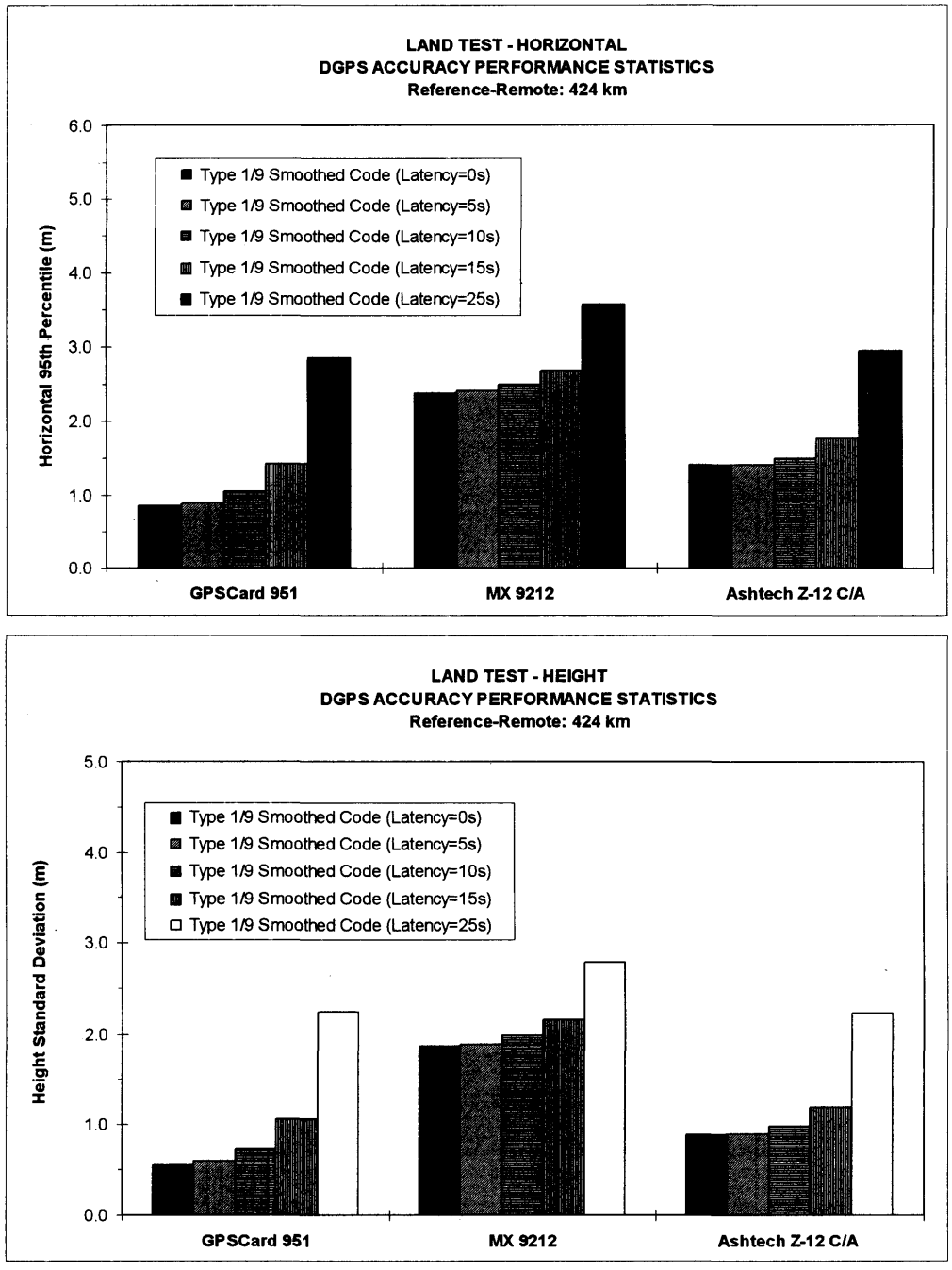


Figure 2.6 Effect of Latency on Type 1/9 Solutions

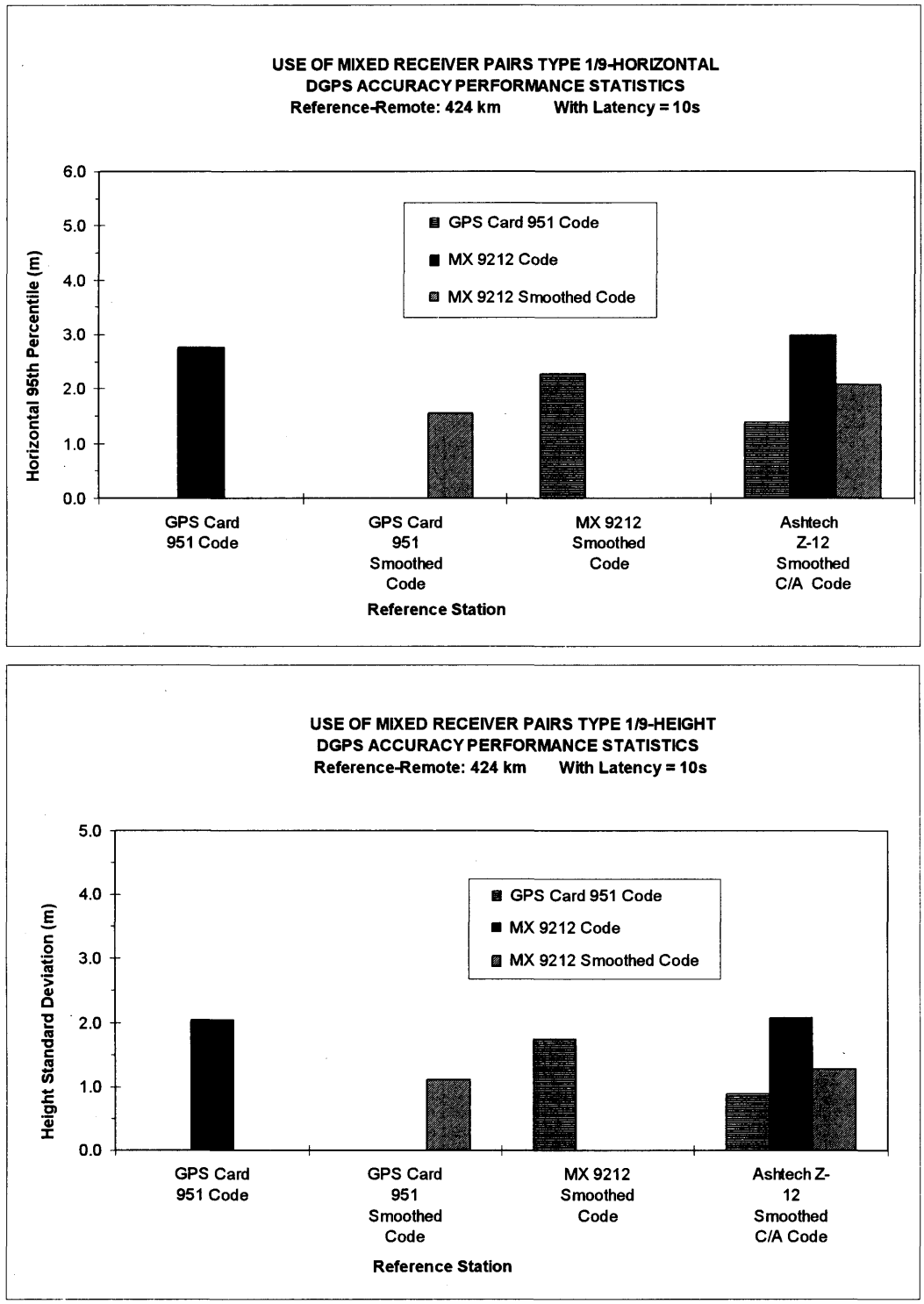


Figure 2.7 Accuracy of Mixed Receiver Pairs for a Latency of 10 Seconds

# CHAPTER 3

## EFFECTS OF WGS 84 REFERENCE STATION POSITION ERRORS ON DGPS REMOTE STATION POSITIONS

Differential operation of GPS is achieved by placing a reference station with a GPS receiver at a known location, determining corrections to the satellite ranging signals, and broadcasting these corrections to users of the service. The coordinates of the reference station should be in WGS 84, which we usually assume is exactly known. In practice, however, the position of the reference station in WGS 84 may not be exactly known due to some practical difficulties. One situation is that there are no known points available in the positioning area and we have to use a single point positioning method to determine the position of the reference station. Another case is that although we have known points available in the working area, the coordinates are not in WGS 84 [Gryglaszewski, 1995]. Therefore, it is of significance to investigate the effect of the reference station position errors on the remote station position.

In this chapter, the effects of WGS 84 reference station position errors on long and short range DGPS static and kinematic remote station positions are investigated. The approach for DGPS static positioning analyzed herein is the double difference carrier phase approach. The approach for DGPS kinematic positioning is the single difference pseudorange approach.

## 3.1 Theoretical Analysis

### 3.1.1 Double Difference Static Positioning

The carrier phase measurement equation can be written as [Wells et al., 1986]:

$$\Phi = \rho + d\rho + c(dt - dT) + \lambda N - d_{ion} + d_{trop} + \varepsilon_{\Phi} \tag{3.1}$$

where $\Phi$ is the carrier phase observation (m)

$\rho$ is the receiver-satellite geometric range (m)

$d\rho$ is the satellite orbit error (m)

c is the speed of light in vacuum (m/s)

dt is the satellite clock offset (s)

dT is the receiver clock offset (s)

$\lambda$ is the carrier phase wavelength (m/cycle)

N is the carrier phase integer ambiguity (cycles)

$d_{ion}$ is the ionospheric delay correction (m)

$d_{trop}$ is the tropospheric delay correction (m)

$\varepsilon_{\Phi}$ is the carrier phase observation noise and multipath (m)

In the following equations, the superscript denotes a satellite and the subscript denotes a receiver. The linearized form of Equation (3.1) at a known reference station m can be expressed as follows when coordinate errors are present:

$$\Phi_m^i = \rho_m^i + d\rho^i + c(dt^i - dT_m) + \lambda N_m^i - d_{ion} + d_{trop} + \mathbf{a}_m^i \delta\mathbf{x}_m + \varepsilon_{\Phi} \tag{3.2}$$

where $\delta\mathbf{x}_m$ is the position error vector of the known reference station

$$\delta\mathbf{x}_m = \left[\delta X_m,\ \delta Y_m,\ \delta Z_m\right]^T,$$

$\mathbf{a}_m^i$ is the coefficient vector, and

$$\mathbf{a}_m^i = \left[\frac{X_m - X^i}{\rho_m^i},\ \frac{Y_m - Y^i}{\rho_m^i},\ \frac{Z_m - Z^i}{\rho_m^i}\right].$$

The corresponding linearized form of Equation (3.1) at an unknown remote station can be expressed as:

$$\Phi_r^i = \rho_r^i + d\rho^i + c(dt^i - dT_r) + \lambda N_r^i - d_{ion} + d_{trop} + \mathbf{a}_r^i \mathbf{x}_r + \varepsilon_\Phi \qquad (3.3)$$

where $\mathbf{x}_r$ is the position correction vector of the unknown remote station

$$\mathbf{x}_r = \left[X_r,\ Y_r,\ Z_r\right]^T,$$

and $\mathbf{a}_r^i$ is the coefficient vector

$$\mathbf{a}_r^i = \left[\frac{X_r - X^i}{\rho_r^i},\ \frac{Y_r - Y^i}{\rho_r^i},\ \frac{Z_r - Z^i}{\rho_r^i}\right],$$

Disregarding error terms which can be canceled or greatly reduced in double differencing, as well as the noise term, the double difference carrier phase equation can be written as:

$$\nabla\Delta\Phi_{rm}^{ik} = \nabla\Delta\rho_{rm}^{ik} + \lambda\nabla\Delta N_{rm}^{ik} + (\mathbf{a}_r^i - \mathbf{a}_r^k)\mathbf{x}_r - (\mathbf{a}_m^i - \mathbf{a}_m^k)\delta\mathbf{x}_m \tag{3.4}$$

$$i = 1, 2, ..., k-1, k+1, ..., n$$

where k and n are the base satellite and number of the satellites used, respectively, and

$$\nabla\Delta\Phi_{rm}^{ik} = \Phi_r^i - \Phi_r^k - (\Phi_m^i - \Phi_m^k) \tag{3.5}$$

$$\nabla\Delta N_{rm}^{ik} = N_r^i - N_r^k - (N_m^i - N_m^k) \tag{3.6}$$

$$\nabla\Delta\rho_{rm}^{ik} = \rho_r^i - \rho_r^k - (\rho_m^i - \rho_m^k) \tag{3.7}$$

Equation (3.4) can be rewritten as

$$l_{rm}^{ik} + (\mathbf{a}_m^i - \mathbf{a}_m^k)\delta\mathbf{x}_m = (\mathbf{a}_r^i - \mathbf{a}_r^k)\mathbf{x}_r \tag{3.8}$$

where $l_{rm}^{ik} = \nabla\Delta\Phi_{rm}^{ik} - \nabla\Delta\rho_{rm}^{ik} - \lambda\nabla\Delta N_{rm}^{ik}$.

If the correct ambiguities are resolved and fixed to integers, the least-squares solution of the estimated position of the unknown remote station can be written as

$$\begin{aligned}\hat{\mathbf{x}}_r &= \{\mathbf{A}_r^T\mathbf{C}_l^{-1}\mathbf{A}_r\}^{-1}\mathbf{A}_r^T\mathbf{C}_l^{-1}(l_{rm} + \mathbf{A}_m\delta\mathbf{x}_m) \\ &= \{\mathbf{A}_r^T\mathbf{C}_l^{-1}\mathbf{A}_r\}^{-1}\mathbf{A}_r^T\mathbf{C}_l^{-1}l_{rm} + \{\mathbf{A}_r^T\mathbf{C}_l^{-1}\mathbf{A}_r\}^{-1}\mathbf{A}_r^T\mathbf{C}_l^{-1}\mathbf{A}_m\delta\mathbf{x}_m\end{aligned}$$

$$= \mathbf{A}_r^T \mathbf{C}_l^{-1} \mathbf{A}_r \}^{-1} \mathbf{A}_r^T \mathbf{C}_l^{-1} l_{rm} + \{\mathbf{A}_r^T \mathbf{C}_l^{-1} \mathbf{A}_r \}^{-1} \mathbf{A}_r^T \mathbf{C}_l^{-1} \{\mathbf{A}_r + \mathbf{A}_m - \mathbf{A}_r \} \delta \mathbf{x}_m$$

$$= \hat{x}^0 + \delta \mathbf{x}_m + \{\mathbf{A}_r^T \mathbf{C}_l^{-1} \mathbf{A}_r \}^{-1} \mathbf{A}_r^T \mathbf{C}_l^{-1} \{\mathbf{A}_m - \mathbf{A}_r \} \delta \mathbf{x}_m \qquad (3.9)$$

where $\hat{\mathbf{x}}_r$ is the estimated position of the unknown remote station, $\mathbf{C}_l$ is the measurement covariance matrix, and $\mathbf{A}_r$ and $\mathbf{A}_m$ are design matrices of the remote and the reference stations, respectively.

The first term of the right side of Equation (3.9) is the estimated position of the remote when there are no errors for reference station coordinates. The second term is position shift which is equal to the shift of reference station coordinates. The third term is the distortion due to errors of reference station coordinates.

Assuming we have N epochs of double difference measurements, then

$$l_{rm} = [l_{rm}^{1k}, l_{rm}^{2k}, \ldots, l_{rm}^{k-1k}, l_{rm}^{k+1k}, \ldots, l_{rm}^{nk}]^T$$

$$\mathbf{A}_r = \begin{bmatrix} \mathbf{A}_{rt_0} \\ \mathbf{A}_{rt_1} \\ \vdots \\ \mathbf{A}_{rt_N} \end{bmatrix}, \qquad \mathbf{A}_m = \begin{bmatrix} \mathbf{A}_{mt_0} \\ \mathbf{A}_{mt_1} \\ \vdots \\ \mathbf{A}_{mt_N} \end{bmatrix},$$

$$\mathbf{A}_{rt_i} = \begin{bmatrix} \mathbf{a}_r^1 - \mathbf{a}_r^k \\ \mathbf{a}_r^2 - \mathbf{a}_r^k \\ \vdots \\ \mathbf{a}_r^n - \mathbf{a}_r^k \end{bmatrix}_{t_i}, \qquad \mathbf{A}_{mt_i} = \begin{bmatrix} \mathbf{a}_m^1 - \mathbf{a}_m^k \\ \mathbf{a}_m^2 - \mathbf{a}_m^k \\ \vdots \\ \mathbf{a}_m^n - \mathbf{a}_m^k \end{bmatrix}_{t_i}$$

Assuming $\rho^i = \rho_r^i = \rho_m^i$, i = 1, 2, ..., n, we have

$$(\mathbf{A}_m - \mathbf{A}_r)_{t_i} = \begin{bmatrix} \mathbf{a}_m^1 - \mathbf{a}_r^1 + \mathbf{a}_r^k - \mathbf{a}_m^k \\ \mathbf{a}_m^2 - \mathbf{a}_r^2 + \mathbf{a}_r^k - \mathbf{a}_m^k \\ \vdots \\ \mathbf{a}_m^n - \mathbf{a}_r^n + \mathbf{a}_r^k - \mathbf{a}_m^k \end{bmatrix}_{t_i} = \begin{bmatrix} \mathbf{d}_{mr}\left(\frac{1}{\rho^1} - \frac{1}{\rho^k}\right) \\ \mathbf{d}_{mr}\left(\frac{1}{\rho^2} - \frac{1}{\rho^k}\right) \\ \vdots \\ \mathbf{d}_{mr}\left(\frac{1}{\rho^n} - \frac{1}{\rho^k}\right) \end{bmatrix}_{t_i} \tag{3.10}$$

where $\mathbf{d}_{mr} = \left[X_m - X_r,\ Y_m - Y_r,\ Z_m - Z_r\right]$.

Equations (3.9) and (3.10) give the analytical relationship between the reference station position errors and their effects on the remote station position.

From the Equations (3.9) and (3.10), it was found that:

a) With other conditions being equal, the distortions of the remote station coordinates are directly proportional to the errors of the reference station position.

b) The difference of satellite geometry between the reference and the remote stations plays an important role in the distortions of remote station coordinates caused by the reference station coordinate errors.

c) The distortions of the remote station coordinates also depend on the direction of reference station error vector, and the length and the direction of the vector formed by

the reference and remote receivers because the third term of the right side of the Equation (3.9) is the inner product of the reference error vector and the reference-remote vector.

### 3.1.2 Single Difference Kinematic Positioning

The pseudorange measurement equation can be written as [Wells et al., 1986]:

$$p = \rho + d\rho + c(dt - dT) + d_{ion} + d_{trop} + \varepsilon_p \tag{3.11}$$

where $p$ is the pseudorange observation (m)

and $\varepsilon_p$ is the pseudorange observation noise and multipath (m)

The linearized form of Equation (3.11) at a reference station can be expressed as:

$$p^i_m = \rho^i_m + d\rho^i + c(dt^i - dT_m) + d_{ion} + d_{trop} + \mathbf{a}^i_m \delta\mathbf{x}_m + \varepsilon_p \tag{3.12}$$

where $\delta\mathbf{x}_m$ is the position error vector of the reference station

$$\delta\mathbf{x}_m = \left[\delta X_m, \quad \delta Y_m, \quad \delta Z_m\right]^T,$$

$\mathbf{a}^i_m$ is the coefficient vector, and

$$\mathbf{a}^i_m = \left[\frac{X_m - X^i}{\rho^i_m}, \quad \frac{Y_m - Y^i}{\rho^i_m}, \quad \frac{Z_m - Z^i}{\rho^i_m}\right],$$

The linearized form of Equation (3.11) at a remote station can be expressed as:

$$p_r^i = \rho_r^i + d\rho^i + c(dt^i - dT_r) + d_{ion} + d_{trop} + \mathbf{a}_r^i \mathbf{x}_r + \varepsilon_p \qquad (3.13)$$

where $\mathbf{x}_r$ is the position correction vector of the remote station

$$\mathbf{x}_r = \left[X_r,\ Y_r,\ Z_r\right]^T,$$

$\mathbf{a}_r^i$ is the coefficient vector, and

$$\mathbf{a}_r^i = \left[\frac{X_r - X^i}{\rho_r^i},\ \frac{Y_r - Y^i}{\rho_r^i},\ \frac{Z_r - Z^i}{\rho_r^i}\right],$$

Disregarding error terms which can be canceled or greatly reduced in between-receivers single differencing , as well as the noise term, the single difference pseudorange equation can thus be written as:

$$\Delta p_{rm}^i = \Delta\rho_{rm}^i - c\Delta dT_{rm} + \mathbf{a}_r^i \mathbf{x}_r - \mathbf{a}_m^i \delta\mathbf{x}_m \qquad (3.14)$$

$$i = 1, 2, \ldots, n$$

where n is the number of the satellites used, and

$$\Delta p_{rm}^i = p_r^i - p_m^i \qquad (3.15)$$

$$\Delta\rho^{i}_{rm} = \rho^{i}_{r} - \rho^{i}_{m} \tag{3.16}$$

$$\Delta dT_{rm} = dT_{r} - dT_{m} \tag{3.17}$$

Equation (3.14) can be further written as

$$l^{i}_{rm} + \mathbf{a}^{i}_{m}\delta\mathbf{x}_{m} = -c\Delta dT_{rm} + \mathbf{a}^{i}_{r}\mathbf{x}_{r} \tag{3.18}$$

where $l^{i}_{rm} = \Delta p^{i}_{rm} - \Delta\rho^{i}_{rm}$.

The least-squares solution of the estimated parameters can be expressed as

$$\begin{aligned}
\begin{bmatrix} \hat{x}_r \\ c\hat{dT}_{rm} \end{bmatrix} &= \{\mathbf{A}_r^T\mathbf{C}_l^{-1}\mathbf{A}_r\}^{-1}\mathbf{A}_r^T\mathbf{C}_l^{-1}\{l_{rm} + \mathbf{A}_m\begin{bmatrix} \delta\mathbf{x}_m \\ 0 \end{bmatrix}\} \\
&= \{\mathbf{A}_r^T\mathbf{C}_l^{-1}\mathbf{A}_r\}^{-1}\mathbf{A}_r^T\mathbf{C}_l^{-1}l_{rm} + \{\mathbf{A}_r^T\mathbf{C}_l^{-1}\mathbf{A}_r\}^{-1}\mathbf{A}_r^T\mathbf{C}_l^{-1}\mathbf{A}_m\begin{bmatrix} \delta\mathbf{x}_m \\ 0 \end{bmatrix} \\
&= \begin{bmatrix} \hat{x}_r^{\,0} \\ c\hat{dT}^{0}_{rm} \end{bmatrix} + \{\mathbf{A}_r^T\mathbf{C}_l^{-1}\mathbf{A}_r\}^{-1}\mathbf{A}_r^T\mathbf{C}_l^{-1}\{\mathbf{A}_r + \mathbf{A}_m - \mathbf{A}_r\}\begin{bmatrix} \delta\mathbf{x}_m \\ 0 \end{bmatrix} \\
&= \begin{bmatrix} \hat{x}_r^{\,0} \\ c\hat{dT}^{0}_{rm} \end{bmatrix} + \begin{bmatrix} \delta\mathbf{x}_m \\ 0 \end{bmatrix} + \{\mathbf{A}_r^T\mathbf{C}_l^{-1}\mathbf{A}_r\}^{-1}\mathbf{A}_r^T\mathbf{C}_l^{-1}\{\mathbf{A}_m - \mathbf{A}_r\}\begin{bmatrix} \delta\mathbf{x}_m \\ 0 \end{bmatrix}
\end{aligned} \tag{3.19}$$

where $\begin{bmatrix} \hat{x}_r \\ c\hat{dT}_{rm} \end{bmatrix}$ is the estimated parameter vector of the unknown remote station., $\mathbf{C}_l$ is the measurement covariance matrix, and $\mathbf{A}_r$ and $\mathbf{A}_m$ are design matrices of the remote and the reference stations, respectively.

The first term of the right side of Equation (3.19) is the estimated parameter vector of the remote when there are no errors in the reference station coordinates. The second term is the position shift which is equal to the shift of reference station coordinates. The third term is the distortions of parameters due to errors of reference station coordinates.

If there are n satellites available,

$$l_{rm} = [l^1_{rm}, l^2_{rm}, \ldots, l^n_{rm}]^T$$

$$\mathbf{A}_r = \begin{bmatrix} \mathbf{a}^1_r & -1 \\ \mathbf{a}^2_r & -1 \\ \vdots & \vdots \\ \mathbf{a}^n_r & -1 \end{bmatrix}, \qquad \mathbf{A}_m = \begin{bmatrix} \mathbf{a}^1_m & -1 \\ \mathbf{a}^2_m & -1 \\ \vdots & \vdots \\ \mathbf{a}^n_m & -1 \end{bmatrix}.$$

Assuming $\rho = \rho^i_r = \rho^i_m$, i = 1, 2, ..., n, we have

$$\mathbf{A}_m - \mathbf{A}_r = \begin{bmatrix} \mathbf{a}^1_m - \mathbf{a}^1_r & 0 \\ \mathbf{a}^2_m - \mathbf{a}^2_r & 0 \\ \vdots & \\ \mathbf{a}^n_m - \mathbf{a}^n_r & 0 \end{bmatrix} = \begin{bmatrix} \dfrac{\mathbf{d}_{mr}}{\rho} & 0 \\ \dfrac{\mathbf{d}_{mr}}{\rho} & 0 \\ \vdots & \\ \dfrac{\mathbf{d}_{mr}}{\rho} & 0 \end{bmatrix} \tag{3.20}$$

where $\mathbf{d}_{mr} = \left[ X_m - X_r, \; Y_m - Y_r, \; Z_m - Z_r \right]$.

Substituting Equation (3.20) into Equation (3.19), we obtain the distortions of the coordinates of the remote station due to the errors of the reference station coordinates are

$$\hat{x}_r - \hat{x}_r^{\,0} - \delta x_m = \{A_r^T C_l^{-1} A_r\}^{-1} A_r^T C_l^{-1} \begin{bmatrix} \frac{d_{mr}}{\rho} \\ \frac{d_{mr}}{\rho} \\ \vdots \\ \frac{d_{mr}}{\rho} \end{bmatrix} \delta x_m \qquad (3.21)$$

Equation (3.21) is the complete formula which gives the analytical relationship between the reference station position errors and the effects on the remote station position.

From the Equation (21), it can also be seen that:

a) With other conditions being equal, the distortions of the remote station coordinates are directly proportional to the errors of the monitor station positions.

b) The difference of satellite geometry between the reference and the remote stations plays an important role in the distortions of the remote station coordinates caused by the reference station coordinate errors.

c) The distortions of the remote station coordinates also depend on the direction of reference station error vector, and the length and the direction of the vector formed by the reference and remote receivers because the right of the Equation (3.21) is the inner product of the reference error vector and the reference-remote vector.

### 3.2 Static Positioning Results and Analysis

The effects of reference position errors on the remote station position can be computed for specified cases by inserting errors in the reference station coordinates and calculating

the resulting distortions on the coordinates of the remote station. In order to illustrate the relationship between the distortions of the remote station coordinates and the errors of the reference station coordinates, different errors can be introduced at the reference station coordinates, while keeping the other conditions the same. In order to demonstrate the relationship between the distortions of the remote station coordinates and the reference-remote separation, the data of different reference-remote separation can be analyzed. The results from the tests with the same and different satellite geometry can be compared to reveal the role of satellite geometry in the distortions of the remote station coordinates.

Different data sets collected on the 424 km baseline used in Chapter 2 and a 16 km baseline were processed and analyzed by inserting different errors in the reference station coordinates and using different data segments. Figures 3.1 and 3.2 show the distortions for 424 km baseline when different errors of the reference coordinates were inserted and different data segments were employed. It is easily found that the distortions are directly proportional to the errors of the reference coordinates and the satellite geometry plays an important role in these distortions because the distortions are different using different data segments. The magnitude of the distortions can reach about 40 centimetres for the 424 km baseline when a 10 m error is inserted into the latitude, longitude and height components of the coordinates of the reference station, which is about $10^{-9}$ of the errors of the reference station coordinates multiplied by the reference-remote separation. Figure 3.3 gives the result of the data segment observed during the same sidereal time period as that of Figure 3.1. By inspecting Figures 3.1 and 3.3, it is found that the distortions are the same because of the same satellite geometry for these two data sets. Figure 3.4 shows the results for the 16 km baseline. The magnitude of the distortions is about 1.6 cm when a 10 m error is inserted into the latitude, longitude and height components of the coordinates of the reference station, which is also about $10^{-9}$ of the errors of the reference station coordinates multiplied by the reference-remote separation.

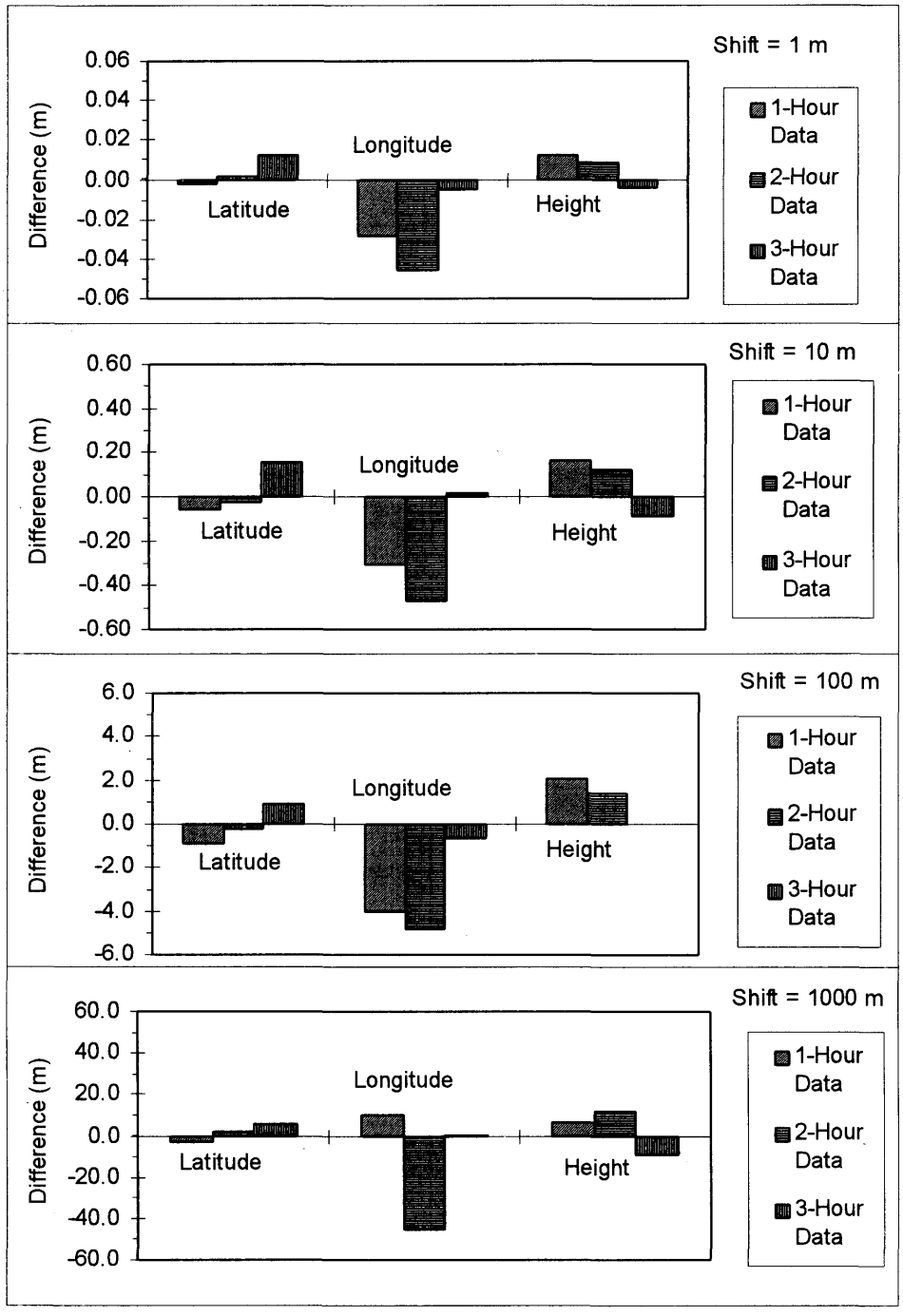


Figure 3.1 Effect of Monitor Station Coordinate Errors on DGPS Position Distortions of Remote Station - Static

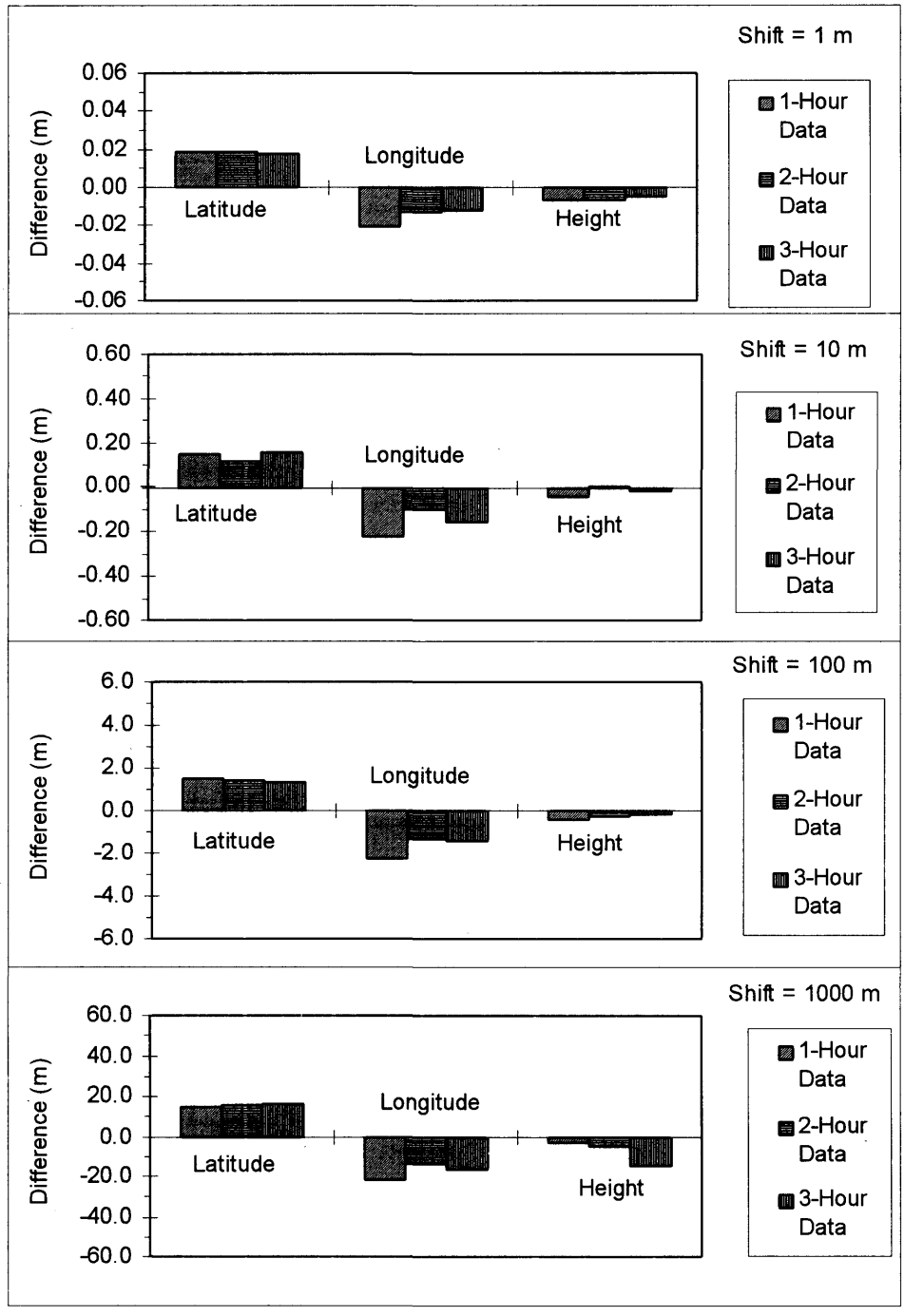


Figure 3.2 Effect of Monitor Station Coordinate Errors on DGPS Position Distortions of Remote Station - Static

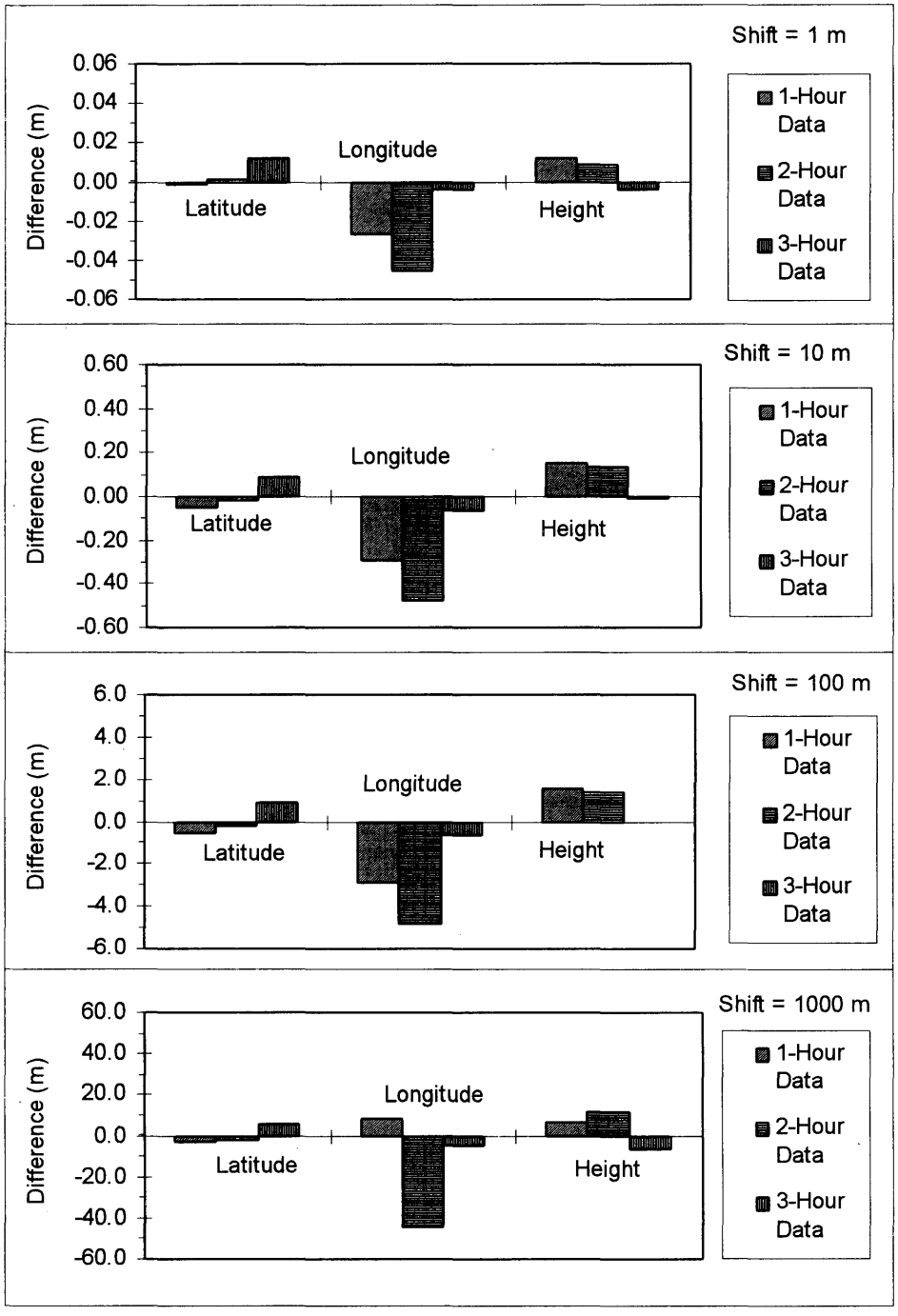


Figure 3.3 Effect of Monitor Station Coordinate Errors on DGPS Position Distortions of Remote Station - Static

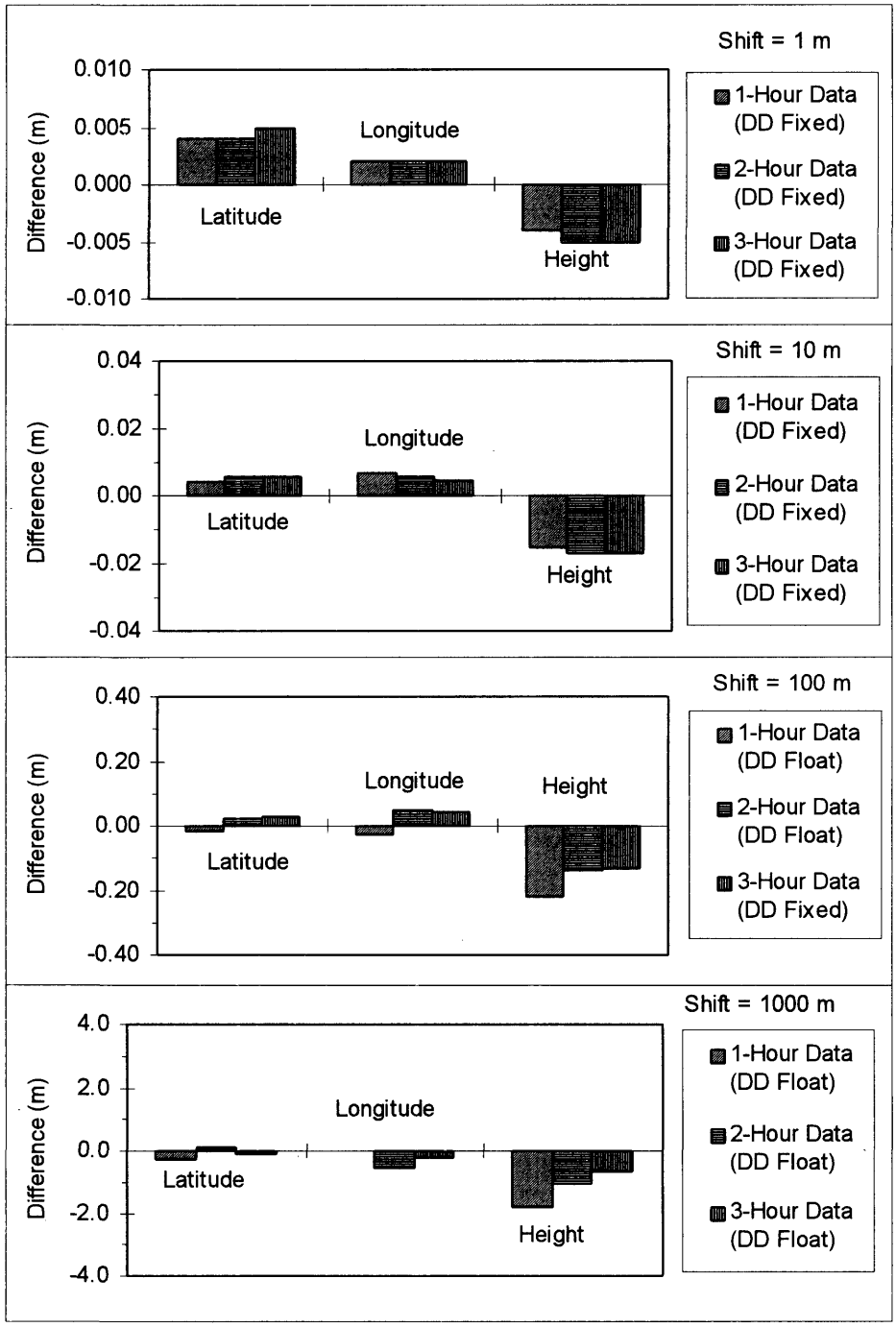


Figure 3.4 Effect of Monitor Station Coordinate Errors on DGPS Position Distortions of Remote Station - Static

### 3.3 Kinematic Positioning Results and Analysis

Figures 3.5, 3.6 and 3.7 show the results of coordinate shifts of 1, 10 and 100 m in latitude, longitude and height components for the data segment observed on the same baseline as that of Figure 3.1 and processed in kinematic mode. It is also shown that the distortions are directly proportional to the errors of the reference station coordinates. Figure 3.8 gives the results for another data segment observed on the same baseline. By comparing Figure 3.7 and Figure 3.8, we can see that the distortions of the remote station coordinates are different, which shows that the satellite geometry plays an important role. But the magnitude of the distortions is about the same. The distortions of the remote station coordinates can reach 20~40 centimetres i.e., $0.5\sim1.0\times10^{-9}$ of the errors of the reference station coordinates multiplied by the reference-remote separation, when an error of 10 m is input in each coordinate component of the reference station. Figure 3.9 shows the results for the 16 km short baseline. The magnitude of the distortions occasionally reachs about 1.6 cm when a 10 m error is inserted into the latitude, longitude and height components of the coordinates of the reference station, which is about $10^{-9}$ of the errors of the reference station coordinates multiplied by the reference-remote separation.

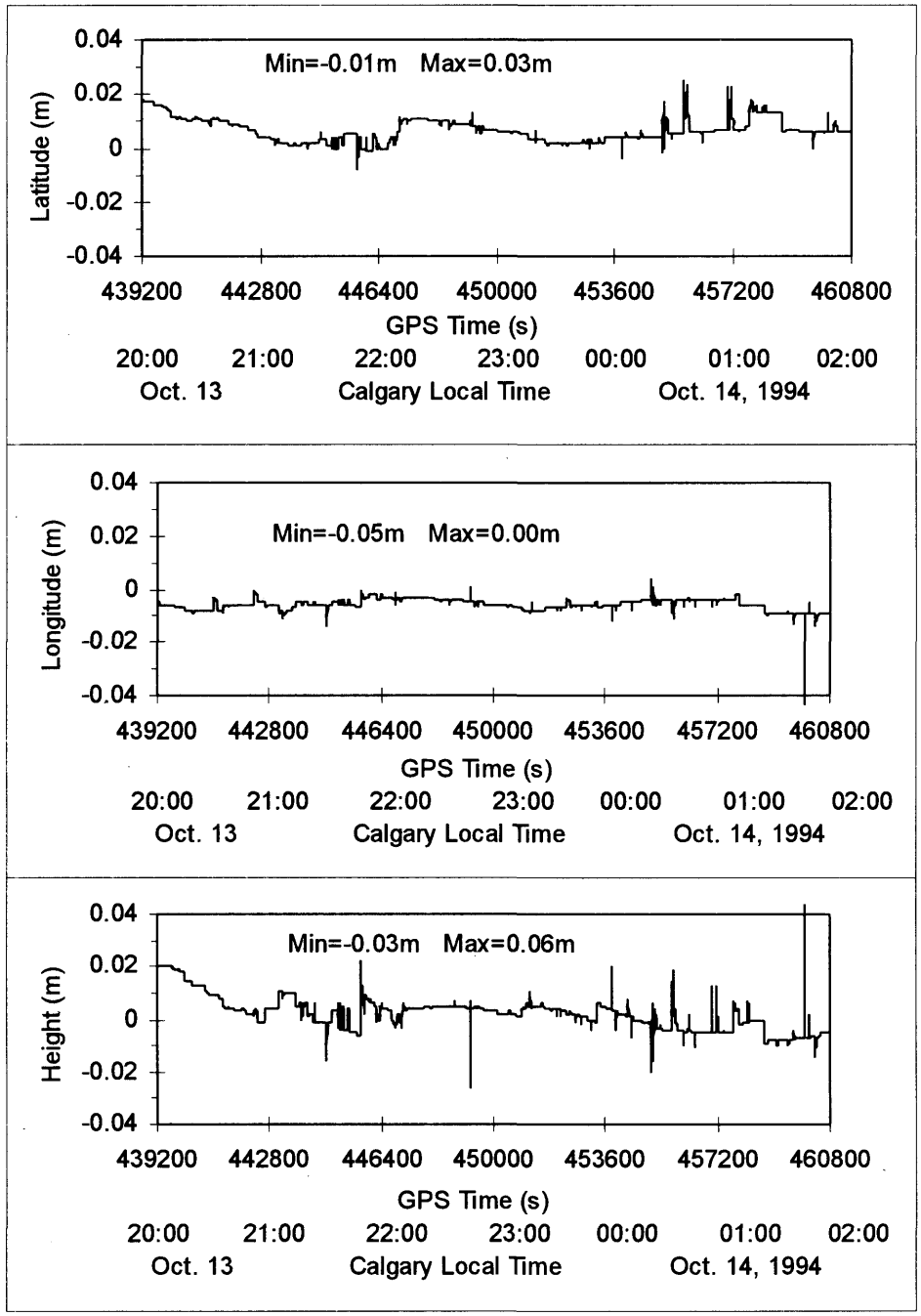


Figure 3.5 Effect of Monitor Station Coordinate Errors on DGPS Position Distortions of Remote Station - Kinematic **1 m shift** in Latitude, Longitude and Height, respectively

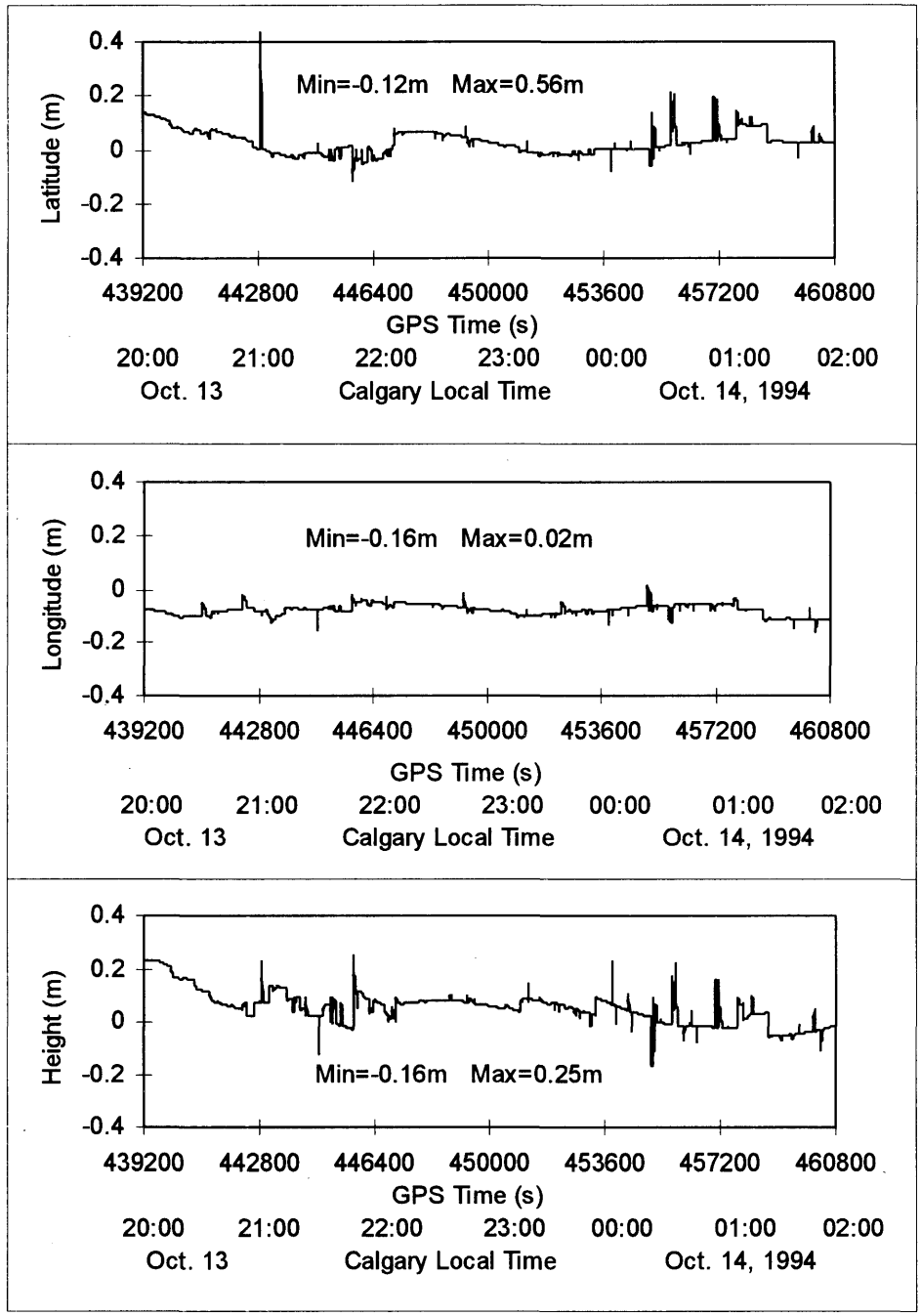


Figure 3.6 Effect of Monitor Station Coordinate Errors on DGPS Position Distortions of Remote Station - Kinematic **10 m shift** in Latitude, Longitude and Height,respectively

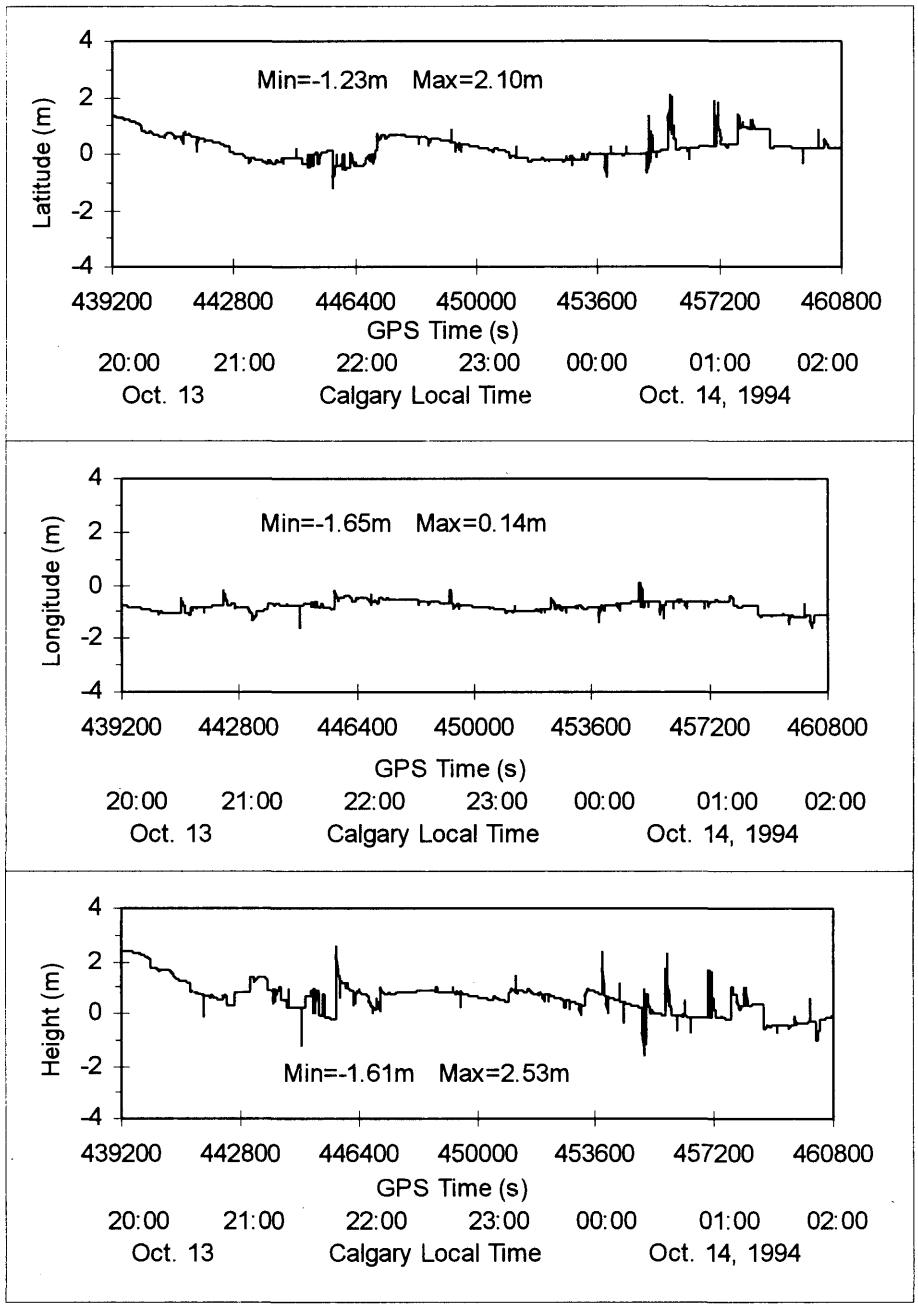


Figure 3.7 Effect of Monitor Station Coordinate Errors on DGPS Position Distortions of Remote Station - Kinematic **100 m shift** in Latitude, Longitude and Height, respectively

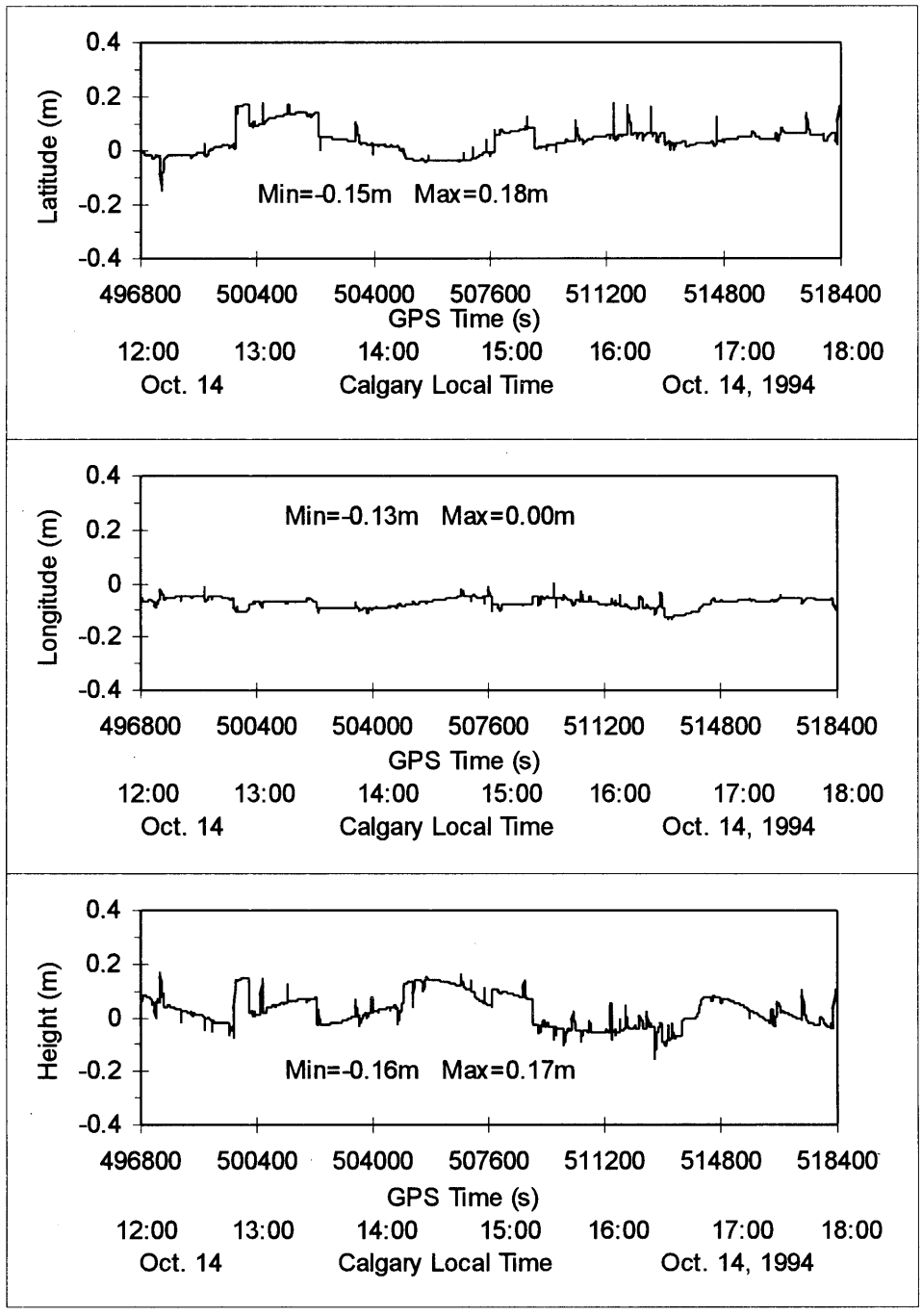


Figure 3.8 Effect of Monitor Station Coordinate Errors on DGPS Position Distortions of Remote Station - Kinematic **10 m shift** in Latitude, Longitude and Height,respectively

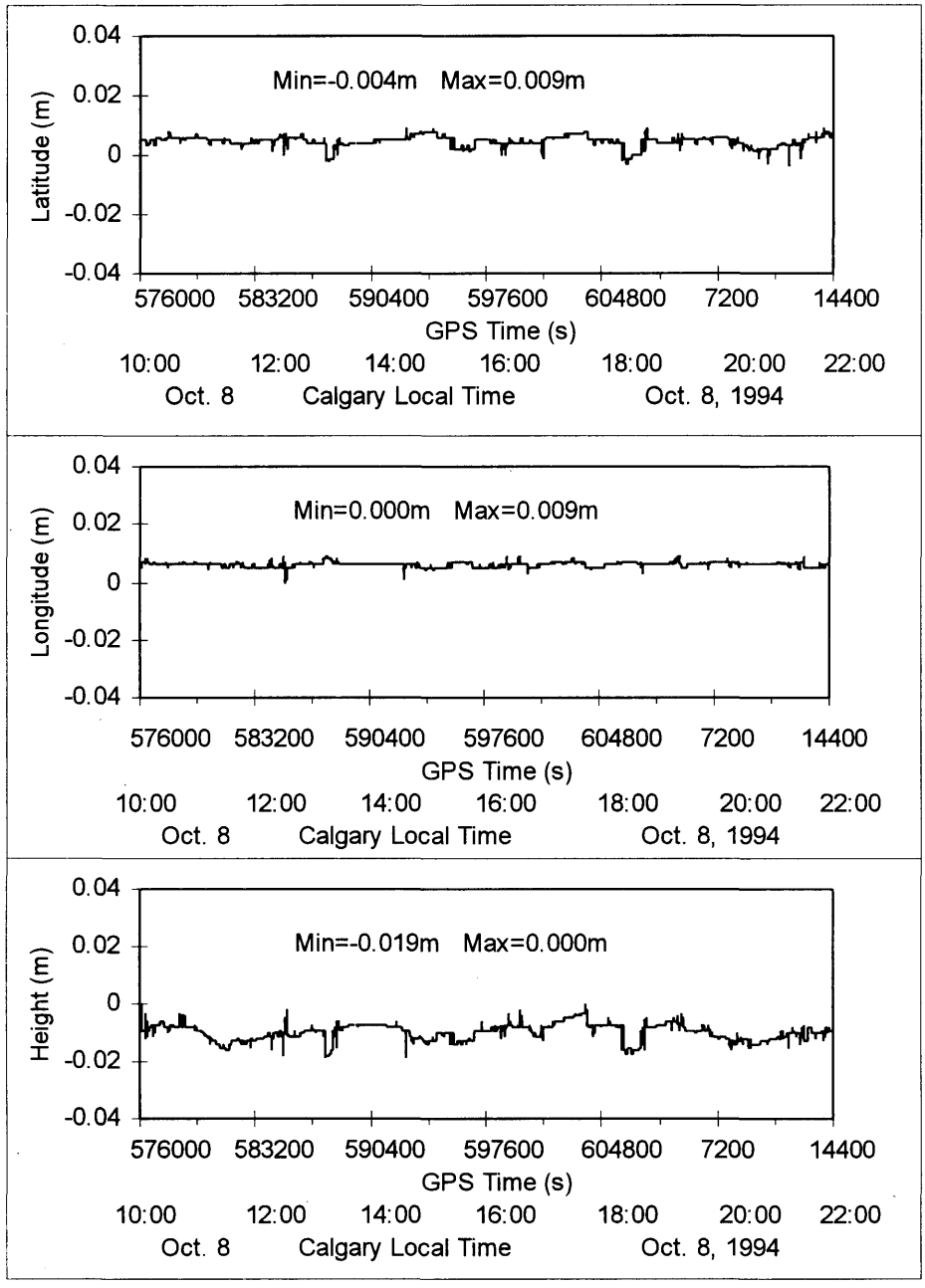


Figure 3.9 Effect of Monitor Station Coordinate Errors on DGPS Position Distortions of Remote Station - Kinematic **10 m shift** in Latitude, Longitude and Height, respectively

# CHAPTER 4

# DGPS PERFORMANCE WITH HEIGHT CONSTRAINTS

The geometry for four-dimensional positioning (latitude, longitude, height and time) will be worse than that for positioning where we reliably know one or more of the solution parameters in advance. In the marine environment, the ship height is normally known to 2~5 m. Let us assume that we have a reasonably good idea of our ship height, for example, and that our primary interest is in horizontal positioning. Then we could hold the 'known' height fixed and solve only for latitude, longitude, and the time offset. However, a better approach is not to hold the height fixed absolutely, but to constrain it within specific bounds (equal to the uncertainty in our knowledge of the height) from the 'known' value. The magnitude of these bounds will be a function of our knowledge of the geoid undulations, the local tide and ship effects such as heave, draft, etc..

Two methods can be used to constrain height. One is weighted constraints, in which the 'known' height information is treated as a quasi-observation and goes into the standard Least-Squares (LS) solution [Krakiwsky, 1992; Leick, 1995]. Another method is the Least-Squares with Inequality constraints (LSI), in which the *a priori* height information is considered by adding inequality constraints [Lawson and Hanson, 1974].

The height constraint method is a useful approach for marine and vehicular navigation, because the height component is normally known to within a few metres. Therefore, investigating the effect of height constraints on final horizontal positioning results is an important aspect of GPS positioning design. The application of height constraint techniques to GPS single point positioning has been studied by [Lu et al., 1993].

In this chapter, DGPS performance with height constraints is investigated. Height constraint approaches and the theory of reliability are first introduced. Different data sets are processed and analyzed to show the effectiveness of DGPS with height constraints. Accuracy performance is analyzed and intercompared using the LSI and the weighted constraint LS for height constraints. Reliability performance results and analysis are presented. The DGPS approach used here is the single difference pseudorange approach and software used for data processing is a modified version of $C^3$ NAV™ [Cannon and Lachapelle, 1992].

## 4.1 Constraint Approaches

### 4.1.1 Least-Squares with Inequality Constraints

There are many applications in applied mathematics, physics, statistics, mathematical programming, economics, control theory, social science, and other fields where the usual least-squares problem must be reformulated by the introduction of certain inequality constraints. These constraints constitute additional information about a problem. The ability to consider least-squares problems with inequality constraints allows us, in particular, to have such constraints on the solution as nonnegativity, or that each variable is to have independent upper and lower bounds, or that the sum of all the variables cannot exceed a specified value.

In mathematical terminology, the least-squares problem with inequality constraints (LSI) can be written as:

LSI

Minimize $\|Ex - f\|$ (4.1)

Subject to $Gx \geq h$, (4.2)

where E is the design matrix, f is the misclosure vector, x is the parameter vector, G is the constraint matrix, and h is the constant vector of the inequality constraints.

There are no algorithms that directly solve the LSI problem. What we do is convert the LSI problem into a least distance programming (LDP) problem [Lu et al., 1993], since the algorithm for solving the LDP problem is well documented [Lawson and Hanson, 1974]. The LDP problem is defined by

LDP

Minimize $\|Z\|$ (4.3)

Subject to $G'z \geq h'$ (4.4)

Once the solution for the LDP problem is determined, the original LSI solution is obtained by the corresponding back transformation from LDP to LSI.

Let the design matrix E in the LSI problem be a m x n matrix with rank equal to n (i.e., full column rank). An orthogonal decomposition of the matrix E can be obtained by the singular value decomposition (SVD) method. That is, E can be expressed as

$$E = USV^T = \begin{pmatrix} U_1 & U_2 \end{pmatrix} \begin{pmatrix} S_1 \\ 0 \end{pmatrix} V^T \tag{4.5}$$

where U, V are m x m and n x n orthogonal matrices, respectively, $S_1$ is the n x n diagonal matrix containing the non-zero singular values.

Since the transformation of an orthogonal matrix does not change the quadratic norm of a vector, the objective function to be minimized in LSI can be written as

$$\begin{aligned}\|Ex - f\| &= \left\|U^T(Ex - f)\right\| \\ &= \left\|U^T(USV^Tx - f)\right\| \\ &= \left\|\begin{pmatrix} S_1 \\ 0 \end{pmatrix} V^Tx - \begin{pmatrix} U_1^T \\ U_2^T \end{pmatrix} f\right\| \\ &= \left\|S_1y - \tilde{f}_1\right\| + \left\|\tilde{f}_2\right\|, \end{aligned} \tag{4.6}$$

where

$$\tilde{f}_1 = U_1^T f, \ \tilde{f}_2 = U_2^T f \text{ and } y = V^Tx$$

with a further substitution of

$$z = S_1y - \tilde{f}_1, \tag{4.7}$$

we may write

$$\|Ex - f\| = \|z\| + \left\|\tilde{f}_2\right\|. \tag{4.8}$$

$\tilde{f}_2$ is a constant term. The only term to be minimized is $\|z\|$. Therefore, the original LSI problem is converted to the following LDP problem:

$$\text{Minimize} \quad \|z\| \tag{4.9}$$

$$\text{Subject to} \quad GVS_1^{-1}z \geq h - GVS_1^{-1}\tilde{f}_1. \tag{4.10}$$

Once the solution $\hat{z}$ for the LDP problem is obtained, the original LSI solution $\hat{x}$ can be determined by

$$\hat{x} = VS_1^{-1}(\hat{z} + \tilde{f}_1). \tag{4.11}$$

In GPS positioning, we not only need to solve for the solution parameters, but also want to determine the covariance matrix of the estimated parameters. For the LSI problem, this is not an easy task since the solution of LDP is an iterative searching process. The error propagation properties through this algorithm are not clear and have not been discussed in the current literature.

In DGPS kinematic positioning using single difference pseudorange approach, the linearized observation equation for the pseudorange at the remote station can be written as

$$\upsilon = A\delta x - l \tag{4.12}$$

where $\upsilon$ is the residual vector, A is the design matrix, $\delta x = \begin{pmatrix} \delta\varphi \\ \delta\lambda \\ \delta h \\ \delta t \end{pmatrix}$ is the correction vector to the approximate unknown parameters, and $l$ is the misclosure vector.

The inequality constraint of **c** metre on the height component can be written as

$$\begin{pmatrix} 0 & 0 & 1 & 0 \\ 0 & 0 & -1 & 0 \end{pmatrix} \begin{pmatrix} \delta\varphi \\ \delta\lambda \\ \delta h \\ \delta t \end{pmatrix} \geq \begin{pmatrix} -\mathbf{c} \\ -\mathbf{c} \end{pmatrix} \tag{4.13}$$

The LSI problem in DGPS kinematic positioning is to minimize $\|A\delta x - l\|$ subject to the above constraints.

### 4.1.2 Weighted Least-Squares Constraints

The *a priori* information of parameters is treated as quasi-observation and goes into the standard least-squares solution in weighted LS constraint approach. The solution can be written as [Leick, 1995]

$$\delta x = \{A^T P_{ll} A + C^0{}_{xx}{}^{-1}\}^{-1}\{A^T P_{ll} l - C^0{}_{xx}{}^{-1} l_{xx}\} \qquad (4.14)$$

where $P_{ll}$ is the weight matrix of the observations, $C^0{}_{xx}$ is the *a priori* covariance matrix of the parameters, and $l_{xx}$ is the difference vector between estimated and *a priori* values of parameters for the current iteration.

## 4.2 Theory of Reliability

Accuracy and reliability are two essential components for the quality control of a GPS positioning system. Accuracy is the measure of the degree of closeness of an estimate to its true, but unknown, value. The accuracy computed using the available data set and configuration can measure the precision of the estimated parameter if and only if the errors included in measurements are random errors. If systematic errors or blunders occur, the accuracy measures will no longer be valid. Reliability is the measure of the capability of a system for detecting blunders in the observations and controlling the effects of the undetectable blunders on the estimated parameters. Therefore, reliability measures have to be combined with accuracy measures to guarantee the robustness of the system output.

Following the suggestion of Baarda, the criteria of the reliability can be classified as Internal Reliability (IR) and External Reliability (ER). The internal reliability refers to the capability of the system of facilitating the detection and localization of blunders in observations without additional information. The external reliability measures the response of the system to undetected blunders in the observations. In other words, it measures the effect of the undetected blunders on the estimated parameters.

### 4.2.1 Internal Reliability Measure

Usually, the internal reliability measure can be represented by the minimum detectable blunders (MDBs) in the observations. For the case with only one blunder and uncorrelated observations, the MDB of the $i^{th}$ observation in the system can be computed as [Li, 1988]

$$\nabla l_i^0 = \sigma_{li} \frac{\delta}{\sqrt{r_i}} \tag{4.15}$$

$$r_i = (Q_{vv} P_{ll})_{ii} \tag{4.16}$$

$$r = \sum_1^n r_i \tag{4.17}$$

$$Q_{vv} = Q_{ll} - AN^{-1}A^T = Q_{ll} - A\{A^T P_{ll} A + C_{xx}^{-1}\}A^T \tag{4.18}$$

where $\nabla l_i^0$ is the minimal detectable blunder associated the ith observation with risk levels $\alpha$ and $\beta$

$\sigma_{li}$ is the standard deviation of the ith observation

$\delta$ is the non-centrality parameter, which depends on $\alpha$ and $\beta$

r is the total redundancy number

$r_i$ is the redundancy contribution of the ith observation to r

$Q_{vv}$ is cofactor matrix of residuals

$P_{ll}$ is the weight matrix of the observations

$Q_{ll}$ is the cofactor matrix of the observations, $P_{ll} = Q_{ll}^{-1}$

A is the design matrix

$C_{xx}$ is the a priori covariance matrix of the parameters

If a blunder in the observation is larger than its respective MDB, this blunder will be able to be detected by the statistical testing on the residuals. However, if a blunder exists in the observation with a value less than the respective MDB, it will not be able to be detected and will corrupt the estimated parameters. Therefore, one objective of the system design is to minimize the MDBs of the observations. This can be accomplished by increasing the accuracy of the measurements or improving the overall design of the system. In GPS positioning, the former approach is impractical, whereas the latter is normally feasible.

### 4.2.2 External Reliability Measure

The parameter estimates from a least-squares adjustment is

$$\hat{X} = N^{-1}A^{T}P_{ll}l \tag{4.19}$$

If there is a blunder $\nabla l$ in the observation, the parameter estimates become

$$\hat{X}' = N^{-1}A^{T}P_{ll}(l + \nabla l) \tag{4.20}$$

Then the effect of blunder $\Delta l$ on the estimated parameters can be written as

$$\nabla\hat{X} = N^{-1}A^{T}P_{ll}\nabla l \tag{4.21}$$

External reliability measure can be quantified by the maximum effect of an undetectable blunder in the observation on the estimated parameters. If we substitute the minimum detectable blunder (MDB) $\nabla l^{0}$ in Equation (4.15) into Equation (4.21), the external reliability measure can be computed as

$$\nabla\hat{X}^{0} = N^{-1}A^{T}P_{ll}\nabla l^{0} \tag{4.22}$$

One aim of the system design is to have acceptable values of external reliability measures in order to minimize the effects of the undetectable blunders on the estimated parameters. The magnitude of the external reliability measures is determined by the system design.

### 4.3 Description of Test Data Sets

To test the performance of height constraints using the LSI and the weighted constraint LS method in comparison with the standard unconstrained LS method, static and shipborne kinematic data sets were analyzed using these two constraint methods.

#### 4.3.1 Static Data Sets

Four static data sets were analyzed using these two constraint methods, respectively. The selected data sets were collected at a data rate of one Hertz in Calgary, Alberta, and also in Havre, Montana, on October 13, 1994. The Calgary station was used as the reference station and the Havre Station as the remote station. The coordinates of both stations are

known as discussed in Section 2.5. The distance between Calgary and Havre is about 424 km. Two types of receivers, the standard wide correlator C/A code receiver MX 9212 and the narrow correlator C/A code receiver GPSCard™ 951 were used in the analysis. Test #1 and Test #2 are MX 9212 data, and Test #3 and Test #4 GPSCard™ 951 data. The satellites observed in Test #1 and Test #3, together with their elevations and azimuths during the selected 40 minute period are listed in Table 4.1. The Test #2 and Test #4 data were obtained by rejecting satellites PRN 19, 24 and 29. Figure 4.1 shows the DOPs and number of satellites observed in Test #1 and Test #2.

Table 4.1

Satellite Elevations and Azimuths - Static Data for Height Constraint Test

| PRN | Elevation (°) | Azimuth (°) | GPS Time (s) |
|---|---|---|---|
| 4 | 16 - 14 | 312 - 295 | 439000 - 441400 |
| 6 | 5 - 7 | 46 - 31 | 439167 - 441400 |
| 14 | 66 - 50 | 223 - 199 | 439000 - 441400 |
| 18 | 21 - 37 | 289 - 296 | 439000 - 441400 |
| 19 | 5 - 14 | 242 - 247 | 440013 - 441400 |
| 22 | 47 - 55 | 127 - 98 | 439000 - 441400 |
| 24 | 5 - 6 | 339 - 335 | 440746 - 441400 |
| 25 | 33 - 17 | 60 - 65 | 439000 - 441400 |
| 29 | 60 - 78 | 296 - 307 | 439000 - 441400 |

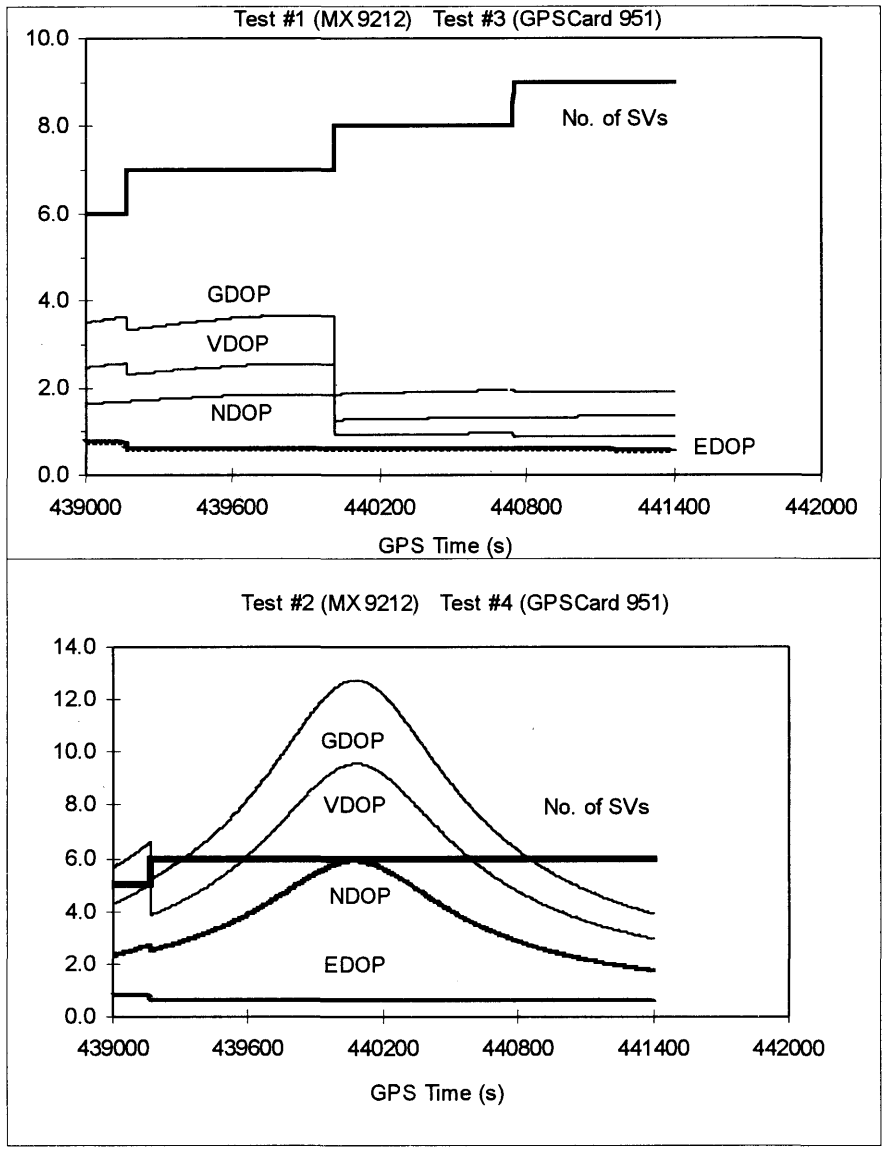


Figure 4.1 DOPs and Number of Satellites Used - Static Test

### 4.3.2 Shipborne Kinematic Data Set

The selected kinematic measurements were made using two NovAtel GPSCard™ 3951 receivers on May 13, 1995 on a Canadian Department of National Defence (DND) ship

off the coast of Vancouver Island [Lachapelle et al., 1996b]. The reference station was located near Victoria, B.C., and the reference antenna was mounted on the top of a 30-ft tower located on the roof of a building at Canadian Forces Base Esquimault. The measurements were made over a period of four hours and the corresponding distance did not exceed 50 km. The reference trajectory of the ship antenna was obtained using carrier phase integer ambiguity solutions derived from The University of Calgary software, FLYKIN™. The satellites observed, together with their elevations and azimuths are listed in Table 4.2. The data used was obtained by rejecting satellites PRN 7 and 15. Figure 4.2 gives number of satellites used and DOPs.

Table 4.2

Satellite Elevations and Azimuths - Shipborne Kinematic Test

| PRN | Elevation (°) | Azimuth (°) | GPS Time (s) |
|---|---|---|---|
| 1 | 9 - 10 | 321 - 321 | 593986 - 593999 |
| 2 | 72 - 14 | 253 - 109 | 579600 - 593071 |
| 4 | 7 - 54 | 161 - 126 | 586948 - 593999 |
| 5 | 16 - 46 | 281 - 296 | 589469 - 593999 |
| 7 | 22 - 37 | 184 - 62 | 579600 - 593999 |
| 9 | 5 - 59 | 303 - 245 | 583227 - 593999 |
| 12 | 11 - 61 | 281 - 157 | 579600 - 593999 |
| 15 | 7 - 6 | 93 - 28 | 579873 - 590002 |
| 16 | 11 - 10 | 251 - 250 | 579600 - 579753 |
| 19 | 37 - 8 | 112 - 129 | 579600 - 584088 |
| 24 | 36 - 8 | 170 - 176 | 590330 - 593999 |
| 26 | 27 - 10 | 312 - 226 | 579600 - 591512 |
| 27 | 73 - 13 | 104 - 142 | 579600 - 587395 |
| 31 | 27 - 5 | 48 - 39 | 579600 - 583286 |

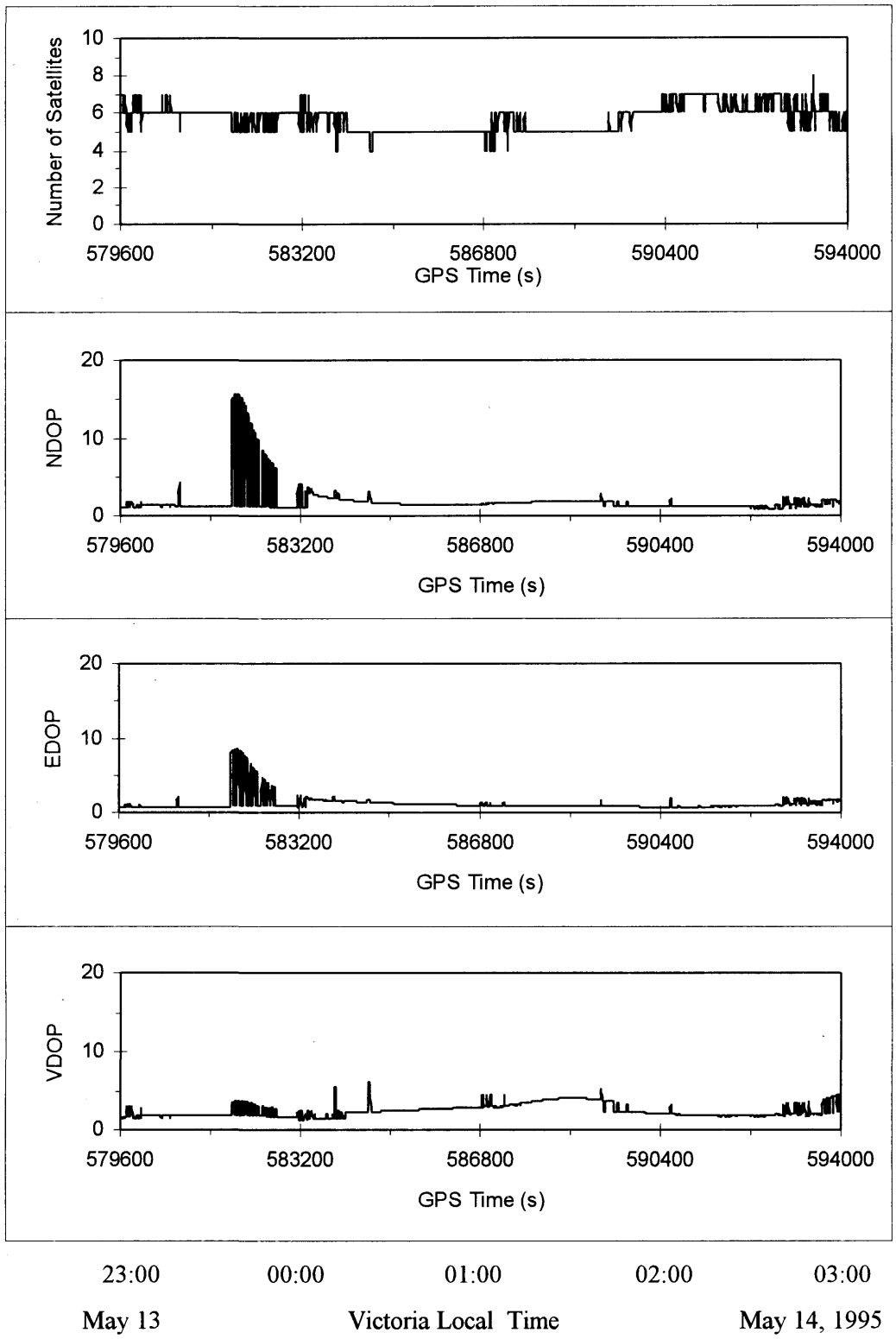


Figure 4.2 DOPs and Number of Satellites Used - Shipborne Kinematic Test

## 4.4 Accuracy Performance Results and Analysis

### 4.4.1 Static Data Sets

In order to investigate the performance of the LSI and the weighted constraint LS methods in height constraints for DGPS positioning, Test #1 and Test #2 data sets were analyzed using these two approaches, and Test #3 and Test #4 data sets processed using the LSI method.

Table 4.3 lists mean and RMS differences of LSI results from the known values with different height constraints using MX 9212 receivers for Test #1 and Test #2. Table 4.4 gives the corresponding mean and RMS differences using the weighted constraint LS approach. From the comparison in Table 4.3 and 4.4, it can be seen that the accuracy of horizontal position is improved significantly, as well as the height component for the wide correlator receivers when the LSI or the weighted constraint LS method is used in DGPS positioning in comparison with the standard LS approach as the mean and RMS differences of LSI results are smaller than the corresponding mean and RMS differences of the unconstrained LS results. It is also shown that a better knowledge of the height is needed for these two methods to improve the position accuracy significantly as the mean and RMS differences of LSI results become smaller when the *a priori* height information is more accurate. It is also found that the weighted constraint LS method seems to be more effective than the LSI method in height constraints for DGPS positioning in this case because mean and RMS differences of the weighted constraint LS approach are smaller than the corresponding mean and RMS differences of the LSI approach.

Table 4.3

Comparison of LSI Results with Different Height Constraints for DGPS (MX 9212)

| Inequality Constraint $\lvert\delta h\rvert \leq$ | Test #1 | | | Test #2 | | |
|---|---|---|---|---|---|---|
| | φ | λ | h | φ | λ | h |
| | Mean/RMS (m) | | | Mean/RMS (m) | | |
| 2.0 | -0.14/2.58 | 0.41/1.58 | -0.65/1.80 | 0.14/2.57 | 0.61/1.69 | -0.15/1.91 |
| 3.0 | -0.23/2.64 | 0.44/1.59 | -0.90/2.55 | 0.10/2.74 | 0.61/1.69 | -0.22/2.78 |
| 4.0 | -0.30/2.73 | 0.46/1.60 | -1.09/3.20 | 0.06/2.96 | 0.61/1.69 | -0.29/3.60 |
| 5.0 | -0.34/2.82 | 0.48/1.60 | -1.22/3.73 | 0.02/3.22 | 0.61/1.69 | -0.36/4.36 |
| 6.0 | -0.36/2.92 | 0.49/1.60 | -1.30/4.15 | -0.02/3.49 | 0.61/1.69 | -0.43/5.06 |
| 7.0 | -0.37/3.01 | 0.50/1.61 | -1.34/4.49 | -0.06/3.76 | 0.61/1.69 | -0.49/5.72 |
| 8.0 | -0.37/3.09 | 0.50/1.61 | -1.35/4.76 | -0.09/4.03 | 0.61/1.69 | -0.55/6.32 |
| 9.0 | -0.37/3.16 | 0.50/1.61 | -1.35/4.99 | -0.12/4.28 | 0.62/1.70 | -0.61/6.86 |
| 10.0 | -0.36/3.23 | 0.50/1.61 | -1.34/5.17 | -0.14/4.53 | 0.62/1.70 | -0.65/7.38 |
| 15.0 | -0.33/3.47 | 0.51/1.61 | -1.29/5.74 | -0.21/5.58 | 0.62/1.70 | -0.78/9.42 |
| 20.0 | -0.31/3.62 | 0.51/1.61 | -1.27/6.02 | -0.23/6.33 | 0.62/1.70 | -0.82/10.83 |
| 30.0 | -0.30/3.75 | 0.51/1.61 | -1.25/6.24 | -0.19/7.27 | 0.62/1.70 | -0.75/12.48 |
| 40.0 | | | | -0.14/7.67 | 0.62/1.70 | -0.68/13.18 |
| No Constraint(LS) | -0.29/3.71 | 0.52/1.59 | -1.23/6.26 | -0.14/7.79 | 0.62/1.68 | -0.71/13.40 |
| Fixed Height(LS) | 0.10/2.51 | 0.36/1.55 | 0.00/0.00 | 0.23/2.47 | 0.60/1.66 | 0.00/0.00 |

Table 4.4

Comparison of Weighted Constraint LS Results with Different Height Constraints for DGPS (MX 9212)

| $3\sigma_{h0}$ | Test #1 | | | Test #2 | | |
|---|---|---|---|---|---|---|
| | φ | λ | h | φ | λ | h |
| | Mean/RMS (m) | | | Mean/RMS (m) | | |
| 2.0 | -0.01/2.50 | 0.37/1.55 | -0.27/0.31 | 0.11/2.45 | 0.60/1.67 | -0.22/0.22 |
| 3.0 | -0.04/2.49 | 0.38/1.55 | -0.34/0.47 | 0.10/2.45 | 0.60/1.67 | -0.22/0.24 |
| 4.0 | -0.06/2.49 | 0.39/1.55 | -0.41/0.70 | 0.10/2.45 | 0.60/1.67 | -0.23/0.27 |
| 5.0 | -0.09/2.49 | 0.40/1.55 | -0.50/0.96 | 0.09/2.44 | 0.60/1.67 | -0.24/0.32 |
| 6.0 | -0.12/2.50 | 0.41/1.56 | -0.58/1.24 | 0.09/2.44 | 0.60/1.67 | -0.25/0.40 |
| 7.0 | -0.15/2.51 | 0.42/1.56 | -0.66/1.52 | 0.08/2.44 | 0.60/1.67 | -0.26/0.49 |
| 8.0 | -0.17/2.53 | 0.43/1.56 | -0.73/1.80 | 0.07/2.43 | 0.60/1.67 | -0.28/0.60 |
| 9.0 | -0.19/2.55 | 0.44/1.56 | -0.80/2.07 | 0.07/2.43 | 0.60/1.67 | -0.29/0.72 |
| 10.0 | -0.21/2.58 | 0.45/1.56 | -0.85/2.33 | 0.06/2.43 | 0.60/1.67 | -0.31/0.86 |
| 15.0 | -0.26/2.76 | 0.47/1.57 | -1.04/3.43 | 0.01/2.48 | 0.60/1.67 | -0.39/1.65 |
| 20.0 | -0.28/2.96 | 0.49/1.58 | -1.12/4.20 | 0.04/2.62 | 0.61/1.67 | -0.48/2.54 |
| 30.0 | -0.29/3.26 | 0.50/1.58 | -1.19/5.10 | 0.11/3.14 | 0.61/1.67 | -0.62/4.31 |
| 40.0 | -0.30/3.42 | 0.51/1.59 | -1.21/5.54 | 0.16/3.78 | 0.61/1.67 | -0.71/5.88 |
| 50.0 | -0.30/3.51 | 0.51/1.59 | -1.22/5.77 | -0.18/4.40 | 0.61/1.67 | -0.75/7.19 |
| 60.0 | -0.29/3.57 | 0.51/1.59 | -1.22/5.91 | -0.19/4.94 | 0.61/1.68 | -0.77/8.26 |
| 80.0 | -0.29/3.62 | 0.51/1.59 | -1.23/6.06 | -0.19/5.76 | 0.62/1.68 | -0.78/9.79 |
| 100.0 | | | | -0.18/6.31 | 0.61/1.68 | -0.77/10.78 |
| 150.0 | | | | -0.16/7.02 | 0.62/1.68 | -0.74/12.05 |
| No Constraint(LS) | -0.29/3.71 | 0.52/1.59 | -1.23/6.26 | -0.14/7.79 | 0.62/1.68 | -0.71/13.40 |
| Fixed Height(LS) | 0.10/2.51 | 0.36/1.55 | 0.00/0.00 | 0.23/2.47 | 0.60/1.66 | 0.00/0.00 |

Table 4.5 lists mean and RMS differences of LSI results from the known values with different height constraints using GPSCard™ 951 receivers for Test #3 and Test #4. From the results for Test #3 listed in Table 4.5, it is found that it does not make much difference using the LSI method in height constraints for the narrow correlator receivers when the

satellite geometry is good. During this test the values of NDOP, EDOP and VDOP are smaller than 4 shown in Figure 4.1. From the results for Test #4 listed in Table 4.5, however, the mean and RMS differences of LSI results are smaller than the corresponding mean and RMS of unconstrained LS results. The mean and RMS differences of LSI results become smaller as the *a priori* height information becomes more accurate. That is because the values of NDOP and VDOP are much larger than the corresponding values in Test #3 as you can see from Figure 4.1. Therefore, when the satellite geometry becomes poorer, the accuracy of position can still be improved significantly using the LSI method in height constraints for narrow correlator receivers.

Table 4.5

Comparison of LSI Results with Different Height Constraints for DGPS

(GPSCard ™ 951)

| Inequality Constraint $\lvert\delta h\rvert \leq$ | Test #3 | | | Test #4 | | |
|---|---|---|---|---|---|---|
| | φ | λ | h | φ | λ | h |
| | Mean/RMS (m) | | | Mean/RMS (m) | | |
| 2.0 | 0.12/0.70 | 0.34/0.45 | -0.03/0.81 | -0.10/0.87 | 0.32/0.47 | 0.02/1.60 |
| 3.0 | | | | -0.08/1.12 | 0.32/0.47 | 0.06/2.12 |
| 4.0 | | | | -0.05/1.32 | 0.32/0.48 | 0.11/2.53 |
| 5.0 | 0.12/0.71 | 0.34/0.45 | -0.04/0.84 | -0.03/1.48 | 0.32/0.48 | 0.15/2.84 |
| 6.0 | | | | -0.01/1.61 | 0.32/0.48 | 0.19/3.10 |
| 7.0 | | | | -0.02/1.73 | 0.32/0.48 | 0.23/3.33 |
| 8.0 | | | | 0.04/1.84 | 0.32/0.48 | 0.27/3.54 |
| 9.0 | | | | 0.06/1.94 | 0.32/0.48 | 0.31/3.73 |
| 10.0 | 0.12/0.71 | 0.34/0.45 | -0.04/0.84 | 0.08/2.03 | 0.32/0.49 | 0.35/3.90 |
| 15.0 | | | | 0.14/2.27 | 0.31/0.49 | 0.45/4.35 |
| 20.0 | | | | 0.15/2.34 | 0.31/0.49 | 0.48/4.47 |
| 30.0 | | | | 0.16/2.40 | 0.31/0.49 | 0.49/4.57 |
| 40.0 | | | | 0.16/2.40 | 0.31/0.49 | 0.49/4.57 |
| No Constraint(LS) | 0.10/0.65 | 0.34/0.45 | -0.05/0.82 | 0.19/2.39 | 0.31/0.49 | 0.53/4.55 |
| Fixed Height(LS) | 0.11/0.59 | 0.34/0.46 | 0.00/0.00 | -0.10/0.43 | 0.32/0.46 | 0.00/0.00 |

Table 4.6 lists minimum and maximum differences of LSI results from the known values with different height constraints using MX 9212 receivers for Test #1 and Test #2. Table 4.7 gives the corresponding minimum and maximum differences using the weighted constraint LS approach. By inspecting Tables 4.6 and 4.7, one can see that the LSI and the weighted constraint LS methods have the advantage of bounding horizontal and height component errors of DGPS when wide correlator MX 9212 receivers are employed.

Table 4.6

Comparison of LSI Results with Different Height Constraints for DGPS (MX 9212)

| Inequality Constraint $\lvert\delta h\rvert \leq$ | Test #1 | | | Test #2 | | |
|---|---|---|---|---|---|---|
| | $\varphi$ | $\lambda$ | h | $\varphi$ | $\lambda$ | h |
| | Min/Max (m) | | | Min/Max (m) | | |
| 2.0 | -11.62/10.84 | -3.88/7.67 | -2.00/2.00 | -11.74/11.30 | -4.71/7.90 | -2.00/2.00 |
| 3.0 | -11.15/10.38 | -3.84/7.67 | -3.00/3.00 | -11.25/11.76 | -4.78/7.89 | -3.00/3.00 |
| 4.0 | -10.67/9.92 | -3.84/7.67 | -4.00/4.00 | -10.86/12.23 | -4.84/7.88 | -4.00/4.00 |
| 5.0 | -10.19/9.46 | -3.89/7.67 | -5.00/5.00 | -10.88/12.25 | -4.91/7.88 | -5.00/5.00 |
| 6.0 | -9.71/9.31 | -3.94/7.67 | -6.00/6.00 | -11.34/12.25 | -4.98/7.87 | -6.00/6.00 |
| 7.0 | -9.68/9.93 | -4.00/7.67 | -7.00/7.00 | -11.49/12.50 | -5.05/7.86 | -7.00/7.00 |
| 8.0 | -9.68/10.53 | -4.05/7.67 | -8.00/8.00 | -11.85/12.98 | -5.12/7.85 | -8.00/8.00 |
| 9.0 | -10.28/10.53 | -4.10/7.67 | -9.00/9.00 | -12.32/13.45 | -5.19/7.84 | -9.00/9.00 |
| 10.0 | -10.90/10.53 | -4.16/7.67 | -10.00/10.00 | -12.78/13.92 | -5.23/7.84 | -10.00/10.00 |
| 15.0 | -13.99/11.14 | -4.17/7.67 | -15.00/15.00 | -13.78/15.10 | -5.23/7.79 | -15.00/15.00 |
| 20.0 | -16.62/13.91 | -4.17/7.67 | -20.00/20.00 | -16.83/16.17 | -5.23/7.75 | -20.00/20.00 |
| 30.0 | -19.07/17.15 | -4.17/7.67 | -29.70/30.00 | -22.92/19.98 | -5.23/7.67 | -30.00/30.00 |
| 40.0 | | | | -27.51/24.91 | -5.23/7.59 | -40.00/40.00 |
| No Constraint(LS) | -19.06/17.27 | -4.18/7.68 | -30.17/31.02 | -30.50/33.39 | -5.22/7.50 | -45.29/56.91 |
| Fixed Height(LS) | -12.18/10.84 | -3.81/7.52 | 0.00/0.00 | -12.47/11.27 | -4.64/7.94 | 0.00/0.000 |

Table 4.7

Comparison of Weighted Constraint LS Results with Different Height Constraints for DGPS (MX 9212)

| $3\sigma_{h0}$ | Test #1 | | | Test #2 | | |
|---|---|---|---|---|---|---|
| | φ | λ | h | φ | λ | h |
| | Min/Max (m) | | | Min/Max (m) | | |
| 2.0 | -12.20/10.63 | -3.82/7.54 | -0.87/0.26 | -12.56/11.16 | -4.63/7.94 | -0.40/-0.08 |
| 3.0 | -12.10/10.49 | -3.81/7.55 | -1.60/0.84 | -12.55/11.15 | -4.64/7.94 | -0.64/-0.09 |
| 4.0 | -11.97/10.31 | -3.80/7.56 | -2.49/1.61 | -12.52/11.14 | -4.64/7.94 | -0.96/0.32 |
| 5.0 | -11.82/10.09 | -3.79/7.57 | -3.45/2.54 | -12.50/11.12 | -4.64/7.94 | -1.35/0.61 |
| 6.0 | -11.63/9.83 | -3.77/7.58 | -4.41/3.60 | -12.46/11.10 | -4.66/7.94 | -1.80/0.93 |
| 7.0 | -11.44/9.56 | -3.76/7.59 | -5.32/4.76 | -12.42/11.08 | -4.66/7.94 | -2.31/1.30 |
| 8.0 | -11.22/9.26 | -3.77/7.60 | -6.18/5.98 | -12.38/11.05 | -4.67/7.94 | -2.86/1.69 |
| 9.0 | -11.01/8.97 | -3.79/7.61 | -7.39/7.23 | -12.33/11.02 | -4.68/7.94 | -3.43/2.12 |
| 10.0 | -10.79/8.67 | -3.81/7.62 | -8.60/8.49 | -12.28/10.99 | -4.69/7.93 | -4.03/2.55 |
| 15.0 | -10.26/8.22 | -3.92/7.64 | -14.19/14.31 | -11.97/10.82 | -4.76/7.92 | -7.01/4.77 |
| 20.0 | -12.08/10.62 | -3.99/7.66 | -18.45/18.75 | -11.62/10.64 | -4.82/7.90 | -9.57/8.00 |
| 30.0 | -15.10/13.49 | -4.08/7.67 | -23.51/24.04 | -11.01/11.73 | -4.94/7.86 | -14.64/15.44 |
| 40.0 | -16.59/14.91 | -4.12/7.68 | -26.02/26.67 | -11.00/12.82 | -5.02/7.82 | -18.29/22.73 |
| 50.0 | -17.40/15.68 | -4.14/7.68 | -27.37/28.09 | -13.60/16.56 | -5.07/7.77 | -22.72/29.03 |
| 60.0 | -17.87/16.13 | -4.15/7.68 | -28.17/28.92 | -15.97/19.66 | -5.11/7.73 | -26.44/34.16 |
| 80.0 | -18.37/16.61 | -4.17/7.68 | -29.01/29.80 | -19.79/24.04 | -5.15/7.67 | -31.60/41.41 |
| 100.0 | | | | -22.50/26.76 | -5.17/7.62 | -34.73/45.92 |
| 150.0 | | | | -26.24/30.09 | -5.20/7.57 | -39.79/51.44 |
| No Constraint(LS) | -19.06/17.27 | -4.18/7.68 | -30.17/31.02 | -30.50/33.39 | -5.22/7.50 | -45.29/56.91 |
| Fixed Height(LS) | -12.18/10.84 | -3.81/7.52 | 0.00/0.00 | -12.47/11.27 | -4.64/7.94 | 0.00/0.000 |

Table 4.8 lists minimum and maximum differences of LSI results from the known values with different height constraints using GPSCard™ receivers for Test #3 and Test #4. It is seen that the height constraint LSI does not have the advantage of bounding position errors if the satellite geometry is good. However, the height constraint LSI can still have the advantage of bounding horizontal and height component errors when the satellite geometry becomes poor.

Table 4.8

Comparison of LSI Results with Different Height Constraints for DGPS

(GPSCard ™ 951)

| Inequality Constraint $\lvert\delta h\rvert \leq$ | Test #3 | | | Test #4 | | |
|---|---|---|---|---|---|---|
| | φ | λ | h | φ | λ | h |
| | Min/Max (m) | | | Min/Max (m) | | |
| 2.0 | -2.62/2.29 | -0.54/1.20 | -2.00/2.00 | -2.92/1.68 | -1.10/1.36 | -2.00/2.00 |
| 3.0 | | | | -3.39/2.16 | -1.10/1.40 | -3.00/3.00 |
| 4.0 | | | | -3.85/2.56 | -1.10/1.44 | -4.00/4.00 |
| 5.0 | -2.62/2.29 | -0.54/1.20 | -3.08/2.38 | -3.91/3.11 | -1.10/1.44 | -5.00/5.00 |
| 6.0 | | | | -4.03/3.10 | -1.10/1.44 | -6.00/6.00 |
| 7.0 | | | | -4.57/4.09 | -1.10/1.44 | -7.00/7.00 |
| 8.0 | | | | -4.92/4.64 | -1.10/1.44 | -8.00/8.00 |
| 9.0 | | | | -5.32/5.15 | -1.10/1.47 | -9.00/9.00 |
| 10.0 | -2.62/2.29 | -0.54/1.20 | -3.08/2.38 | -5.80/5.69 | -1.10/1.50 | -10.00/10.00 |
| 15.0 | | | | -8.52/7.93 | -1.10/1.55 | -15.00/15.00 |
| 20.0 | | | | -9.97/10.77 | -1.10/1.55 | -18.01/20.00 |
| 30.0 | | | | -9.97/15.29 | -1.58/1.55 | -18.01/28.19 |
| 40.0 | | | | -9.97/15.29 | -1.58/1.55 | -18.01/28.19 |
| No Constraint(LS) | -2.51/2.06 | -0.45/1.22 | -3.02/2.39 | -9.98/15.29 | -1.58/1.55 | -18.04/28.19 |
| Fixed Height(LS) | -1.90/2.36 | -0.50/1.22 | 0.00/0.00 | -1.90/1.17 | -1.02/1.30 | 0.00/0.00 |

Figure 4.3 shows position differences from the known values using the LSI with 5 m height constraint and the standard LS methods for Test #1. The corresponding mean and RMS differences can be found in Table 4.3, and minimum and maximum differences in Table 4.7. It is obvious that the differences of the results using the LSI with 5 m height constraint are much smaller than the corresponding differences using the unconstrained LS approach. One can easily notice that there are jumps in height and latitude components using the unconstrained LS method when the values of DOPs change shown in Figure 4.1. However, the jumps disappear when the LSI with 5 m height constraint approach is

employed. The improvement in the latitude component is the one which is significant since errors in excess of 15 m have been reduced to 5 m.

Figure 4.4 gives position differences from the known values using the LSI with 5 m height constraint and the standard LS methods for Test #2. One may notice from Figure 4.1, the values of NDOP and VDOP are much larger than those in Test #1, which means the geometry of Test #2 is much poorer than that of Test #1. By inspecting Figure 4.4, one will find that the accuracy improvement of height and latitude components using the LSI with 5 m height constraint is more significant than in Test #1 while the geometry is much better.

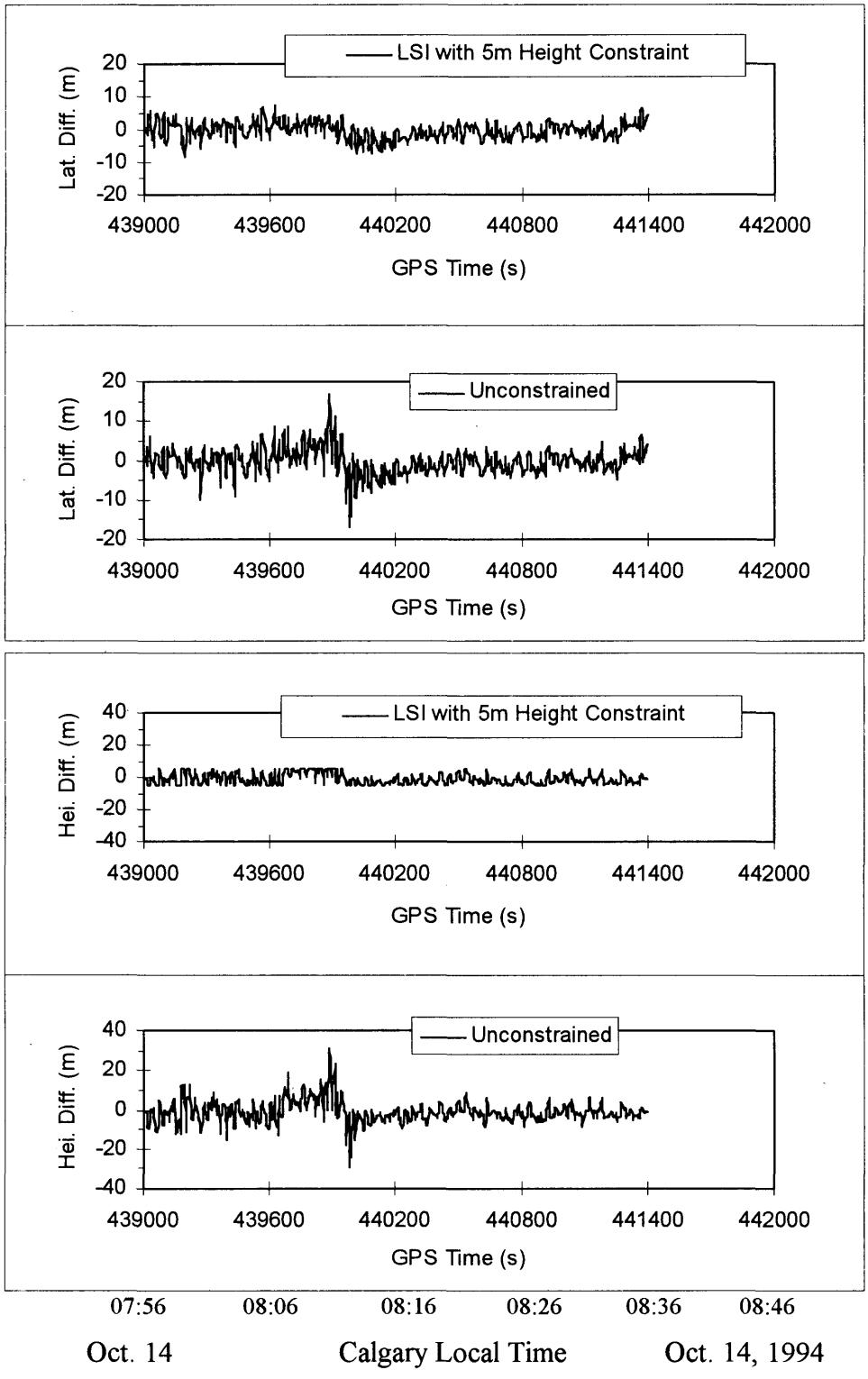


Figure 4.3 Comparison of Position Differences from the Known Position LSI versus LS for DGPS Test #1 (MX 9212)

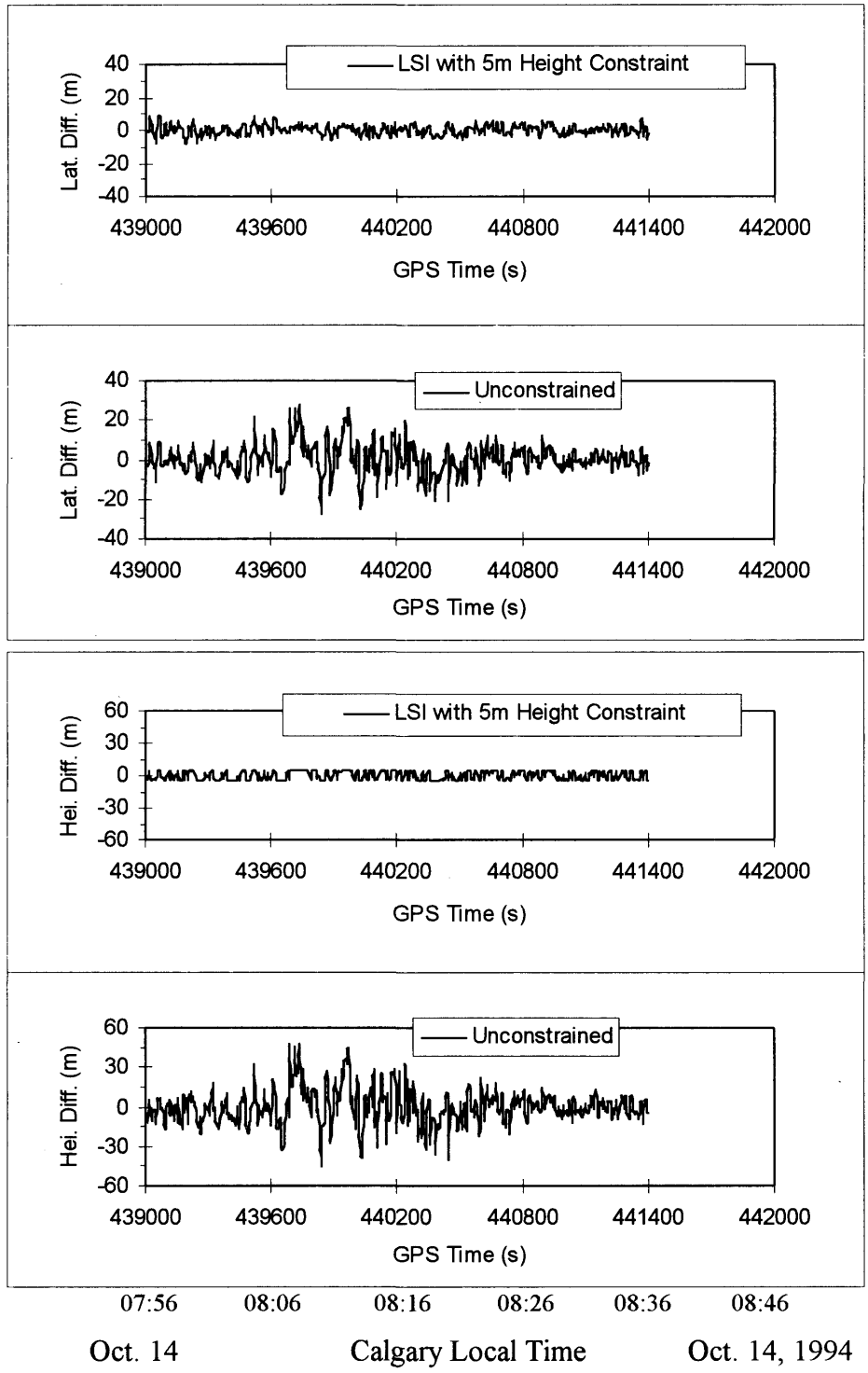


Figure 4.4 Comparison of Position Differences from the Known Position LSI versus LS for DGPS Test #2 (MX 9212)

### 4.4.2 Shipborne Kinematic Data Set

It is shown using static data sets in Section 4.4.1 that the accuracy improvement of horizontal and vertical components can be significant when employing height constraint approaches. The weighted constraint LS method seems to be more effective than the LSI method in height constraints for DGPS positioning.

In order to further investigate the performance of the weighted height constraint LS method for DGPS positioning in kinematic environments, the shipborne kinematic data set described in Section 4.3.2 was processed and analyzed using the weighted height constraint LS and the unconstrained LS. Table 4.9 summarizes the mean, RMS, minimum and maximum differences from the reference coordinates for different height constraints using the weighted height constraint LS and the unconstrained LS. From the comparison in Table 4.9, it can be seen that the accuracy of the horizontal position is improved significantly, as well as the height component when the weighted constraint LS method is used in DGPS positioning in comparison with the standard LS as the mean, RMS, minimum, and maximum differences of the weighted constraint LS results are smaller than the corresponding mean and RMS differences of the unconstrained LS results. It is also shown that a better knowledge of the height is needed for the weighted height constraint approach to improve the position accuracy significantly as the mean, RMS, minimum and maximum differences of the weighted constraint LS results become smaller when the a priori height information is more accurate.

Table 4.9

Comparison of Weighted Constraint LS Results with Different Height Constraints for DGPS (GPSCard ™ 3951) - Shipborne Kinematic Test

| $3\sigma_{h0}$ | Kinematic Test | | | | | |
|---|---|---|---|---|---|---|
| | φ | λ | h | φ | λ | h |
| | Mean/RMS (m) | | | Min/Max (m) | | |
| 2.0 | -0.05/1.52 | -0.15/0.95 | -0.02/0.48 | -19.10/8.57 | -10.07/4.99 | -1.36/1.42 |
| 5.0 | -0.06/1.51 | -0.15/0.94 | -0.01/0.47 | -19.11/8.04 | -10.06/4.89 | -1.50/2.50 |
| 10.0 | -0.08/1.52 | -0.14/0.94 | 0.00/0.71 | -19.13/9.43 | -10.01/5.47 | -3.13/7.38 |
| 20.0 | -0.11/1.68 | -0.14/1.02 | 0.04/1.30 | -19.15/16.49 | -9.89/9.51 | -6.85/15.68 |
| 30.0 | -0.13/1.88 | -0.14/1.12 | 0.08/1.63 | -19.16/23.20 | -10.09/13.20 | -8.57/19.91 |
| 40.0 | -0.14/2.02 | -0.14/1.20 | 0.09/1.82 | -19.16/27.24 | -10.27/15.43 | -9.37/21.99 |
| 50.0 | -0.14/2.11 | -0.14/1.25 | 0.10/1.92 | -20.02/29.68 | -11.21/16.77 | -9.79/23.12 |
| No Constraint(LS) | -0.15/2.34 | -0.14/1.37 | 0.12/2.17 | -24.17/35.37 | -13.52/19.91 | -10.64/25.43 |

Figure 4.5 shows the position differences from the known values using the weighted constraint LS with 5 m height constraint and the standard LS methods. The corresponding mean, RMS, minimum and maximum differences can also be found in Table 4.9. All the data was used for the calculation of statistics, but the sampling interval for Figure 4.5 is five seconds. That is why the maximum difference of the height component using the unconstrained LS approach is 25.43 m, but we cannot see it in Figure 4.5a. It is obvious that the differences of the results using the weighted constraint LS approach are much smaller than the corresponding differences using the unconstrained LS approach. The RMS difference of height component is greatly reduced from 2.17 m to 0.47 m. The RMS difference improvement for horizontal components is also significant. The RMS difference is reduced from 2.34 m to 1.51 m for the latitude component, and from 1.37 m to 0.94 m for the longitude component. One can easily notice that there are large jumps in latitude and longitude components using the unconstrained LS method when the values of DOPs change at

that time as shown in Figure 4.2. However, the values of the jumps are greatly reduced when the weighted height constraint LS approach is employed. It means that the weighted height constraint LS has the advantage of greatly reducing or eliminating horizontal position jumps.

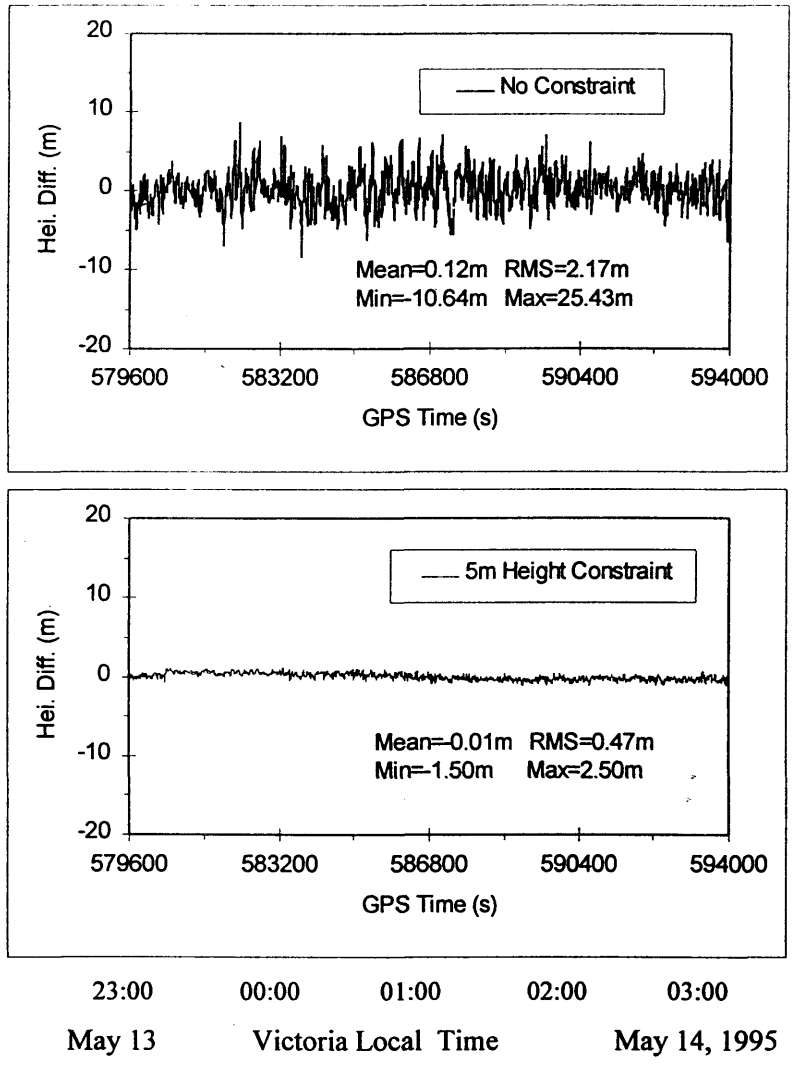


Figure 4.5a Height Result Comparison with/without Height Constraint

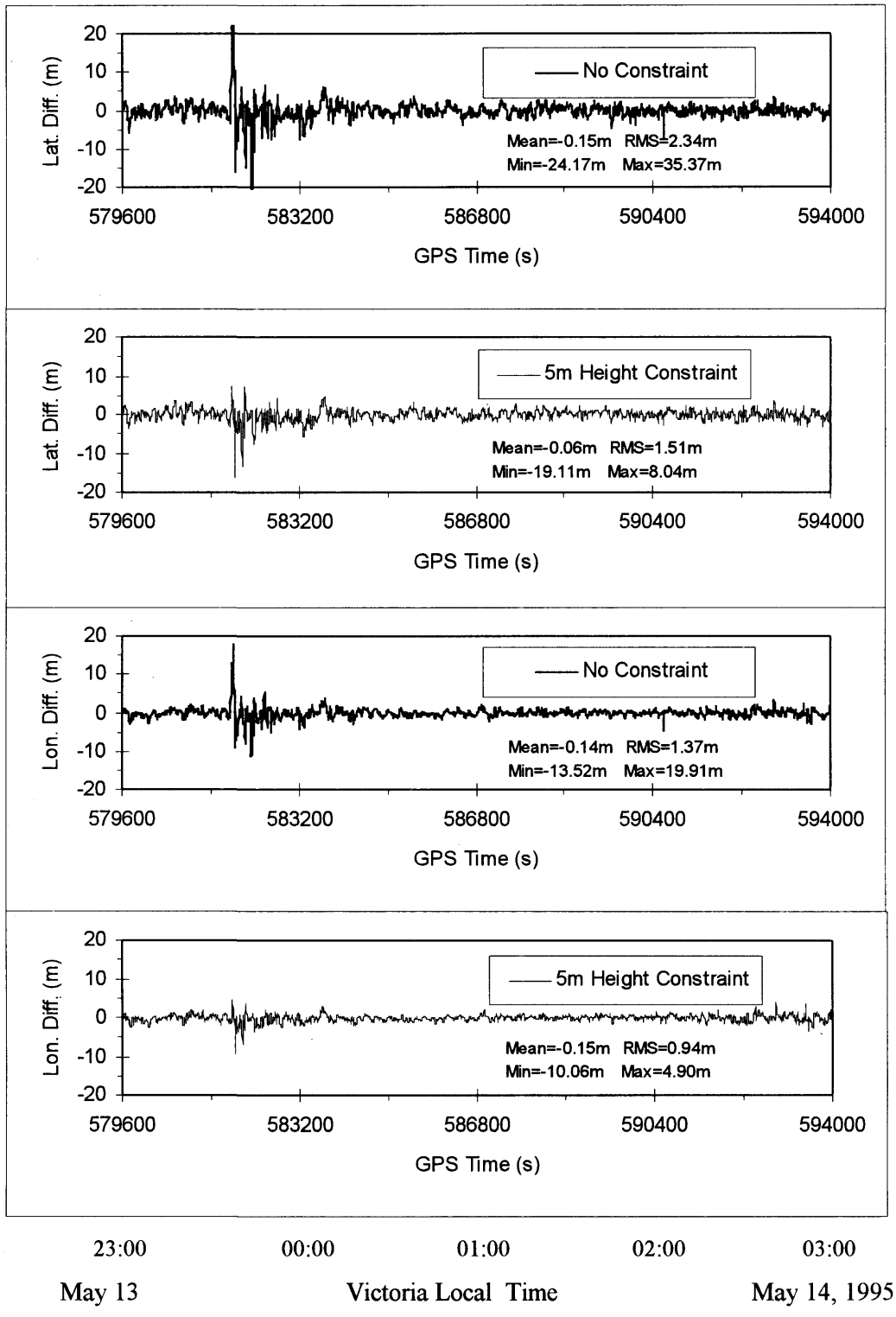


Figure 4.5b Horizontal Position Result Comparison with/without Height Constraint

## 4.5 Reliability Performance Results and Analysis

The accuracy performance using the height constraint approaches instead of the unconstrained LS approach has been studied and analyzed in the previous section. This section is devoted to the reliability of the weighted constraint LS approach in comparison with the unconstrained LS approach. Here, the weighted height constraint approach is chosen over the LSI approach for the reliability performance study and comparison because the accuracy performance of the weighted constraint LS approach is similiar to or better than the LSI height constraint technique, and the error propagation of LSI is more complex.

In order to compare the reliability performance of the weighted constraint LS approach with that of the unconstrained LS technique in DGPS positioning, static data sets of Test #1 and Test #2 were kinematically processed using these two approaches in DGPS mode. Figure 4.6 shows the results of pseudorange MDBs with and without height constraints for Test #1. By inspecting the figures, one can easily notice the reduction of pseudorange MDBs, especially for satellite PRN 29, using the weighted constraint LS approach. By comparing Figure 4.6 with the DOP values of Test #1 in Figure 4.1, one can see that values of MDBs decrease as the values of DOPs drop in this case, and the internal reliability performance improvement is more significant when the satellite geometry becomes poor.

Figure 4.7 gives the results of pseudorange MDBs with and without height constraints for Test #2. One can also find that there is a reduction of pseudorange MDBs, for satellites PRN 14 and PRN 25 when employing the weighted constraint LS technique. By checking the DOP values of Test #2 in Figure 4.1, one will also see that values of MDBs decrease

as the values of DOPs drop. The internal reliability performance improvement is more significant when the satellite geometry becomes poor.

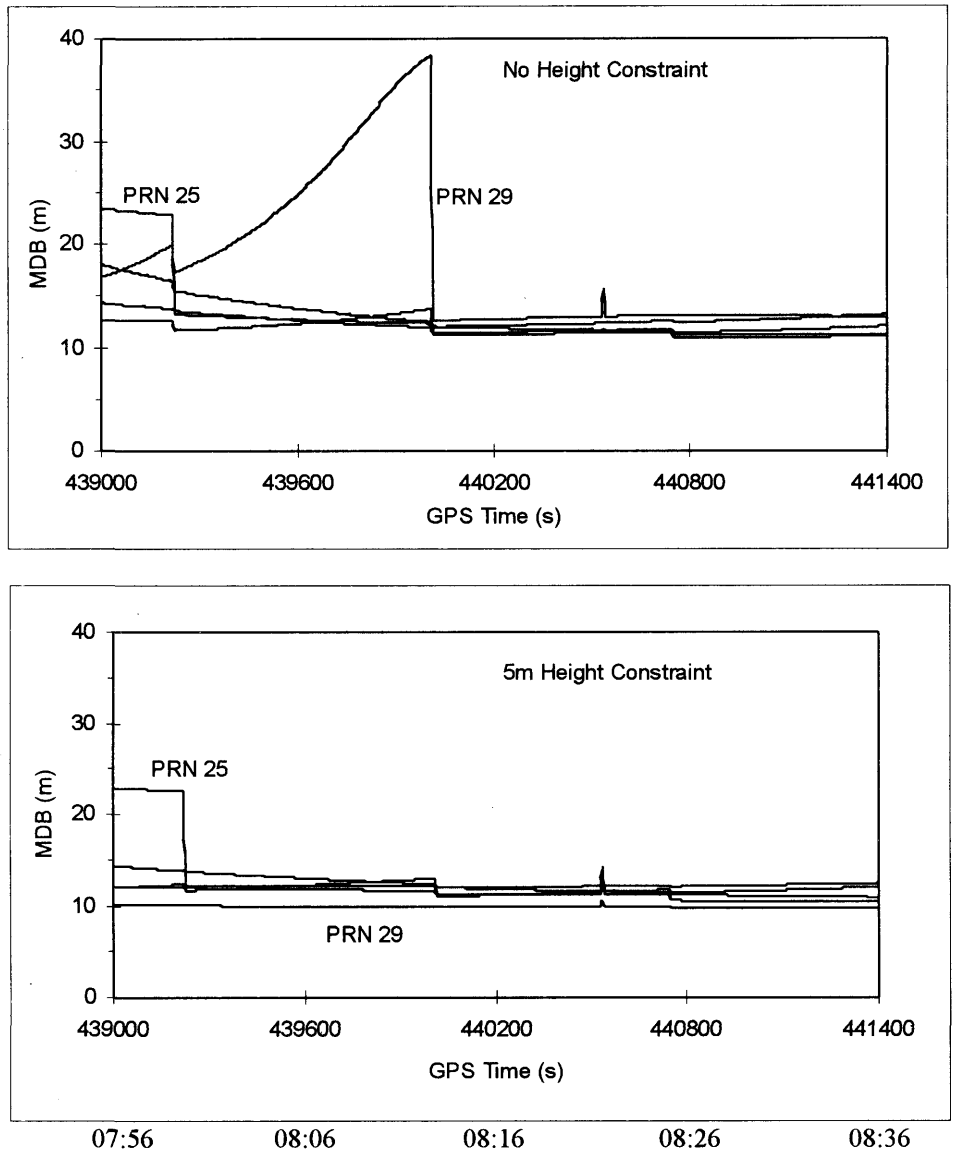


Figure 4.6 Comparison of Pseudorange MDBs with/without Height Constrained for DGPS Test #1

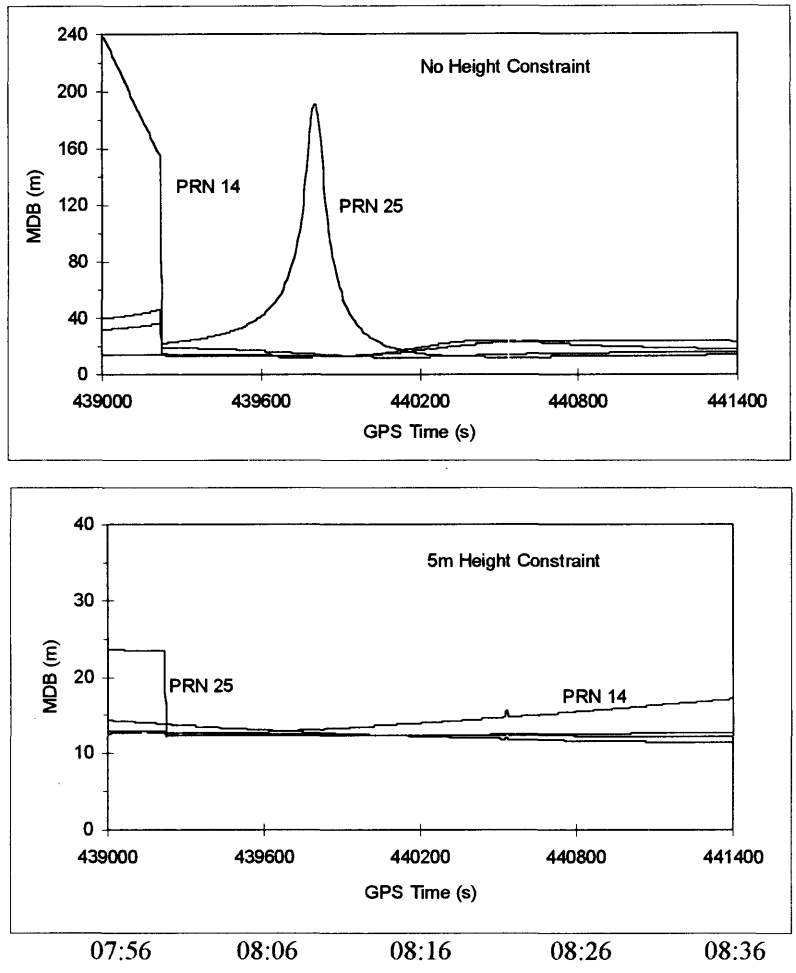


Figure 4.7 Comparison of Pseudorange MDBs with/without height constrained for DGPS Test #2

Comparing Figure 4.7 with Figure 4.6 and checking the corresponding DOP values in Figure 4.1, one can conclude that the reduction of the MDBs of the pseudorange measurements when using a height constraint is more significant as the geometry becomes poorer.

Figure 4.8 gives latitude external reliability measures, i.e. the influences of MDBs on the latitude component, with and without height constraints for Test #1. One can see that the

magnitude of the MDB influences on the latitude component is significantly reduced using the weighted height constraint approach instead of the unconstrained LS technique. Checking the DOP values in Figure 4.1, one will also see that the values of the MDB influence on the latitude component decreases as the values of DOPs drop in this case, and the latitude external reliability performance improvement when using a height constraint becomes more significant as the satellite geometry becomes poorer.

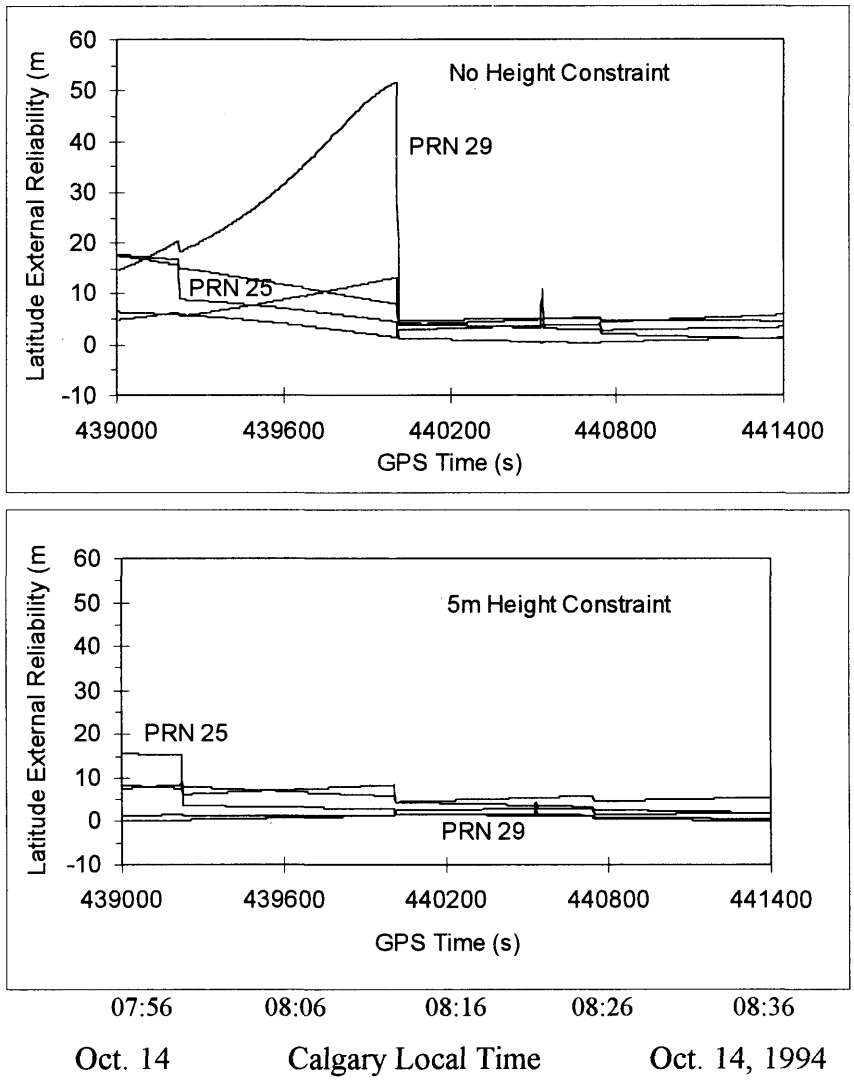


Figure 4.8 Comparison of Pseudorange MDB Influences on Latitude with/without Height Constrained for DGPS Test #1

Figure 4.9 shows corresponding height external reliability measures, i.e. the influences of MDBs on the height component, with and without height constraints for Test #1. One can find that the magnitude of the MDB's influence on the height component is significantly reduced when using the weighted height constraint approach instead of the unconstrained LS technique.

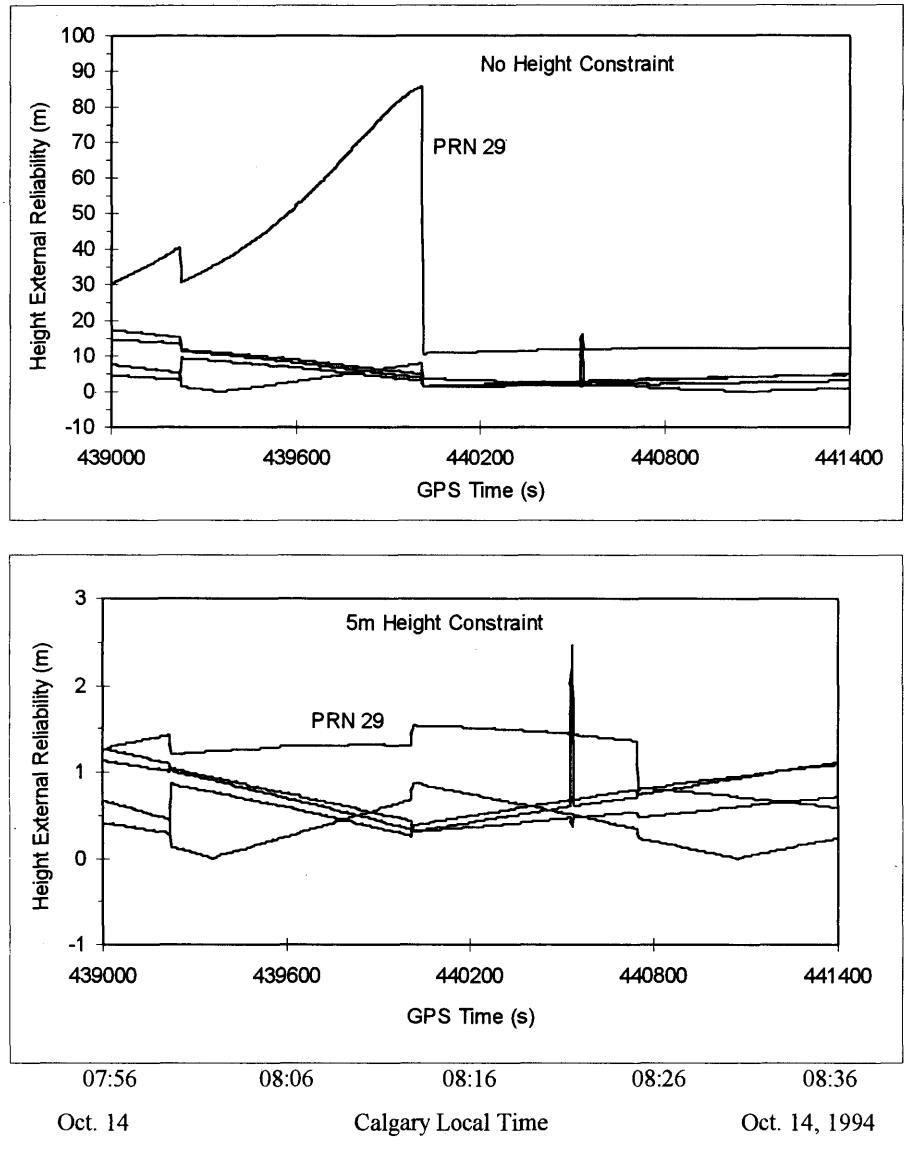


Figure 4.9 Comparison of Pseudorange MDB Influences on Height with/without Height Constrained for DGPS Test #1

By comparing pseudorange MDB influences on the height component in Figure 4.9 with those on the latitude component in Figure 4.8, one will discover that the height external reliability performance improvement is more significant than the corresponding latitude component using the weighted height constraint approach in this case. Checking the DOP values in Figure 4.1, one will also see that values of the MDB influences on the height component decrease as the values of DOPs drop. The height external reliability performance improvement is more significant when the satellite geometry becomes poorer.

Figures 4.10 and 4.11 show the latitude and the height external reliability measures, i.e. the influences of MDBs on the latitude and the height components, with and without height constraints for Test #2. By inspecting Figures 4.10, 4.11 and checking the corresponding DOP values of Test #2 in Figure 4.1, one can derive the similiar conclusions as those for Test #1.

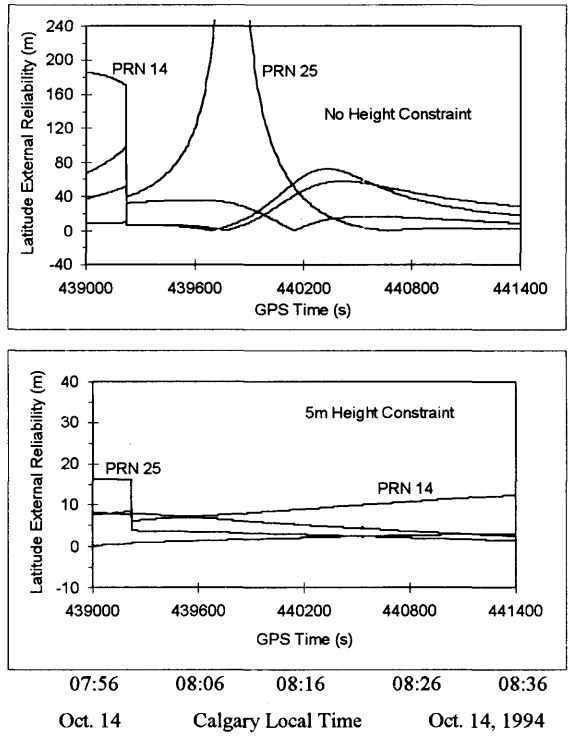


Figure 4.10 Comparison of Pseudorange MDB Influences on Latitude with/without Height Constrained for DGPS Test #2

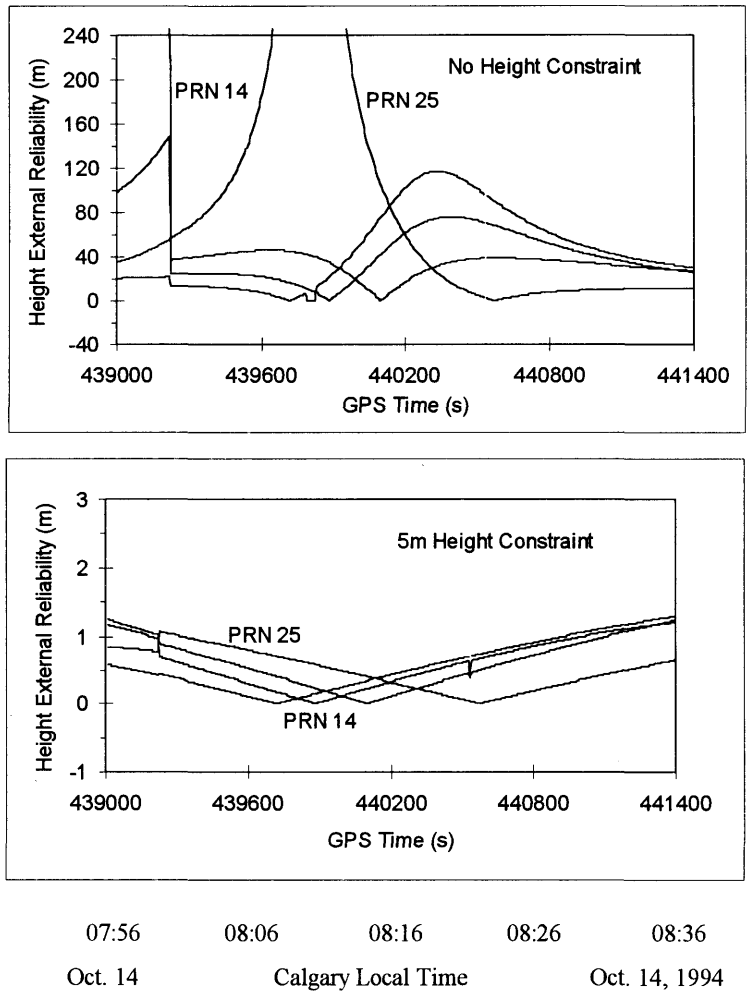


Figure 4.11 Comparison of Pseudorange MDB Influences on Height with/without Height Constrained for DGPS Test #2

Comparing the external reliability measures of Test #2 in Figures 4.10 and 4.11 with those of Test #1 in Figures 4.8 and 4.9 and checking the corresponding DOP values for Test #1 and Test #2 in Figure 4.1, one can conclude that the external reliability performance improvement is more significant using the weighted height constraint approach when the geometry becomes poorer.

It has been shown using static data sets that the reliability performance improvement of horizontal and vertical components can be significant using the weighted height constraint LS approach. In order to further investigate the reliability performance of the weighted

height constraint LS method for DGPS positioning in kinematic environments, the shipborne kinematic data set described in Section 4.3.2 was processed and analyzed using the weighted height constraint LS with 5 m height constraints and the unconstrained LS.

Figure 4.12 shows the results of pseudorange MDBs of satellites PRN 12 and PRN 9 with and without height constraints for the shipborne kinematic test. By inspecting the figures, one can easily notice the reduction of pseudorange MDBs using the weighted constraint LS approach. By comparing Figure 4.12 with the number of satellites used and the DOP values in Figure 4.2, one can also find that the blunders are undetectable using the standard LS when there is no redundancy because the number of satellites drops to 4. However, the blunders can be detected and the effects of the undetectable blunders on positioning results can be avoided if the weighted height constraint LS method is used.

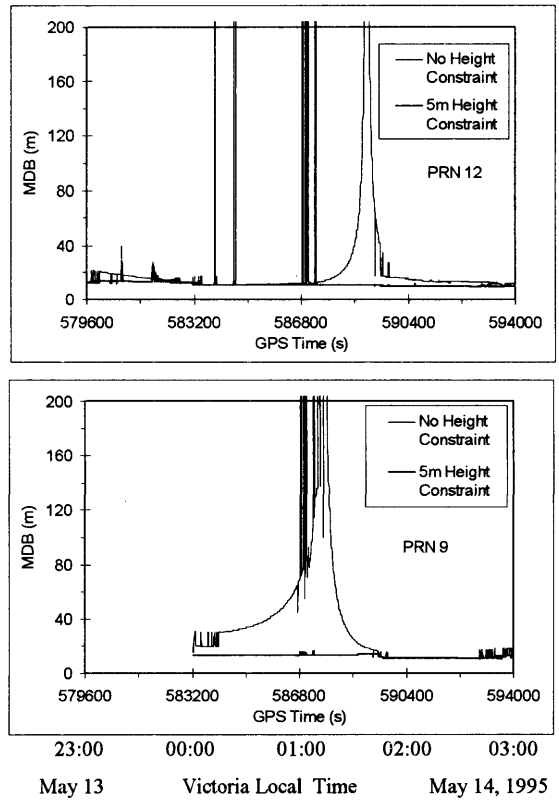


Figure 4.12 Comparison of Pseudorange MDB with/without Height Constrained - Shipborne Kinematic Test

Figure 4.13 gives height, latitude and longitude external reliability measures, i.e. the influences of MDBs of satellites PRN 12 and PRN 9 on height, latitude, and longitude components, with and without height constraints for the shipborne kinematic test. By inspecting Figure 4.13, one can see that the magnitude of the MDB influences on horizontal and vertical component is reduced dramatically using the weighted height constraint approach instead of the unconstrained LS technique, especially when there is no redundant measurements because the number of satellites drops to 4.

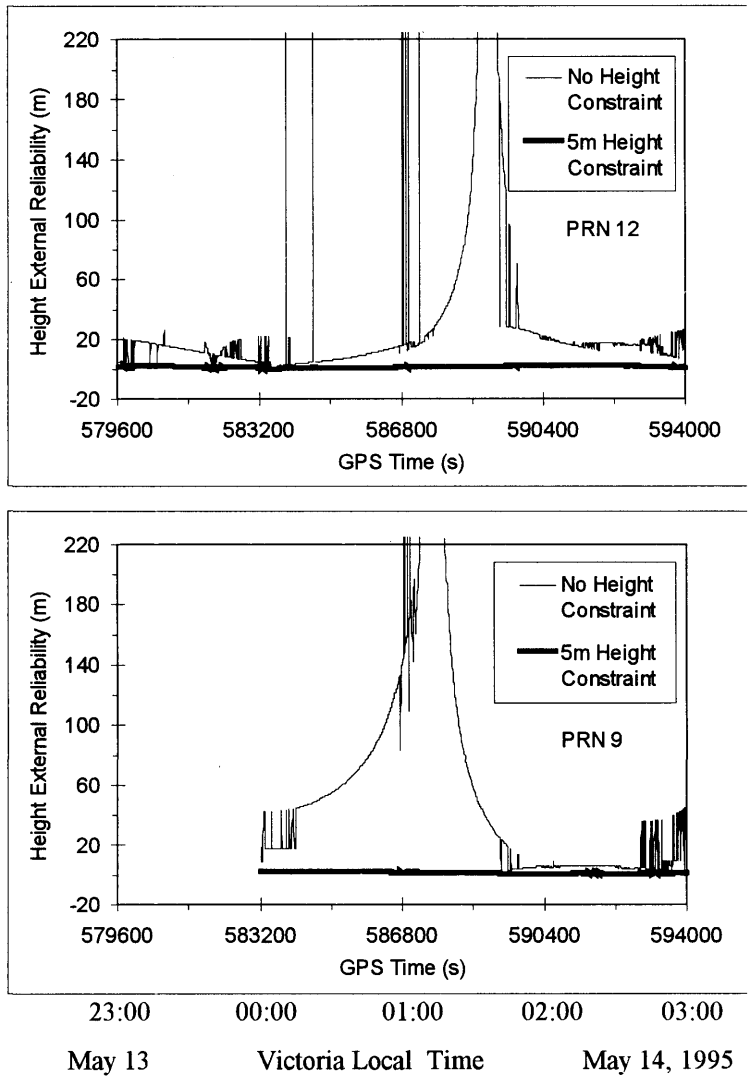


Figure 4.13a Comparison of Pseudorange MDB Influences on Height with/without Height Constrained - Shipborne Kinematic Test

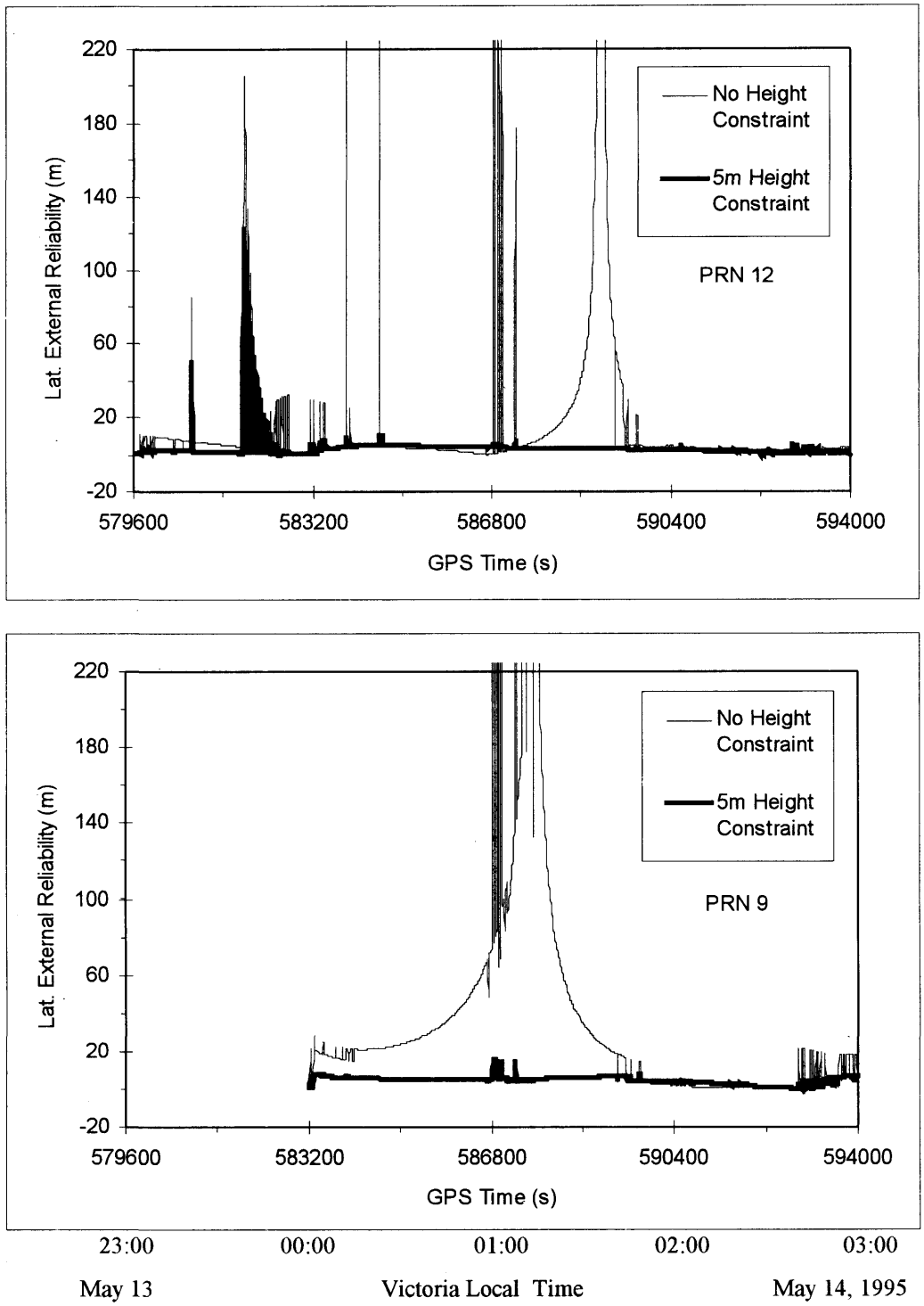


Figure 4.13b Comparison of Pseudorange MDB Influences on Latitude with/without Height Constrained - Shipborne Kinematic Test

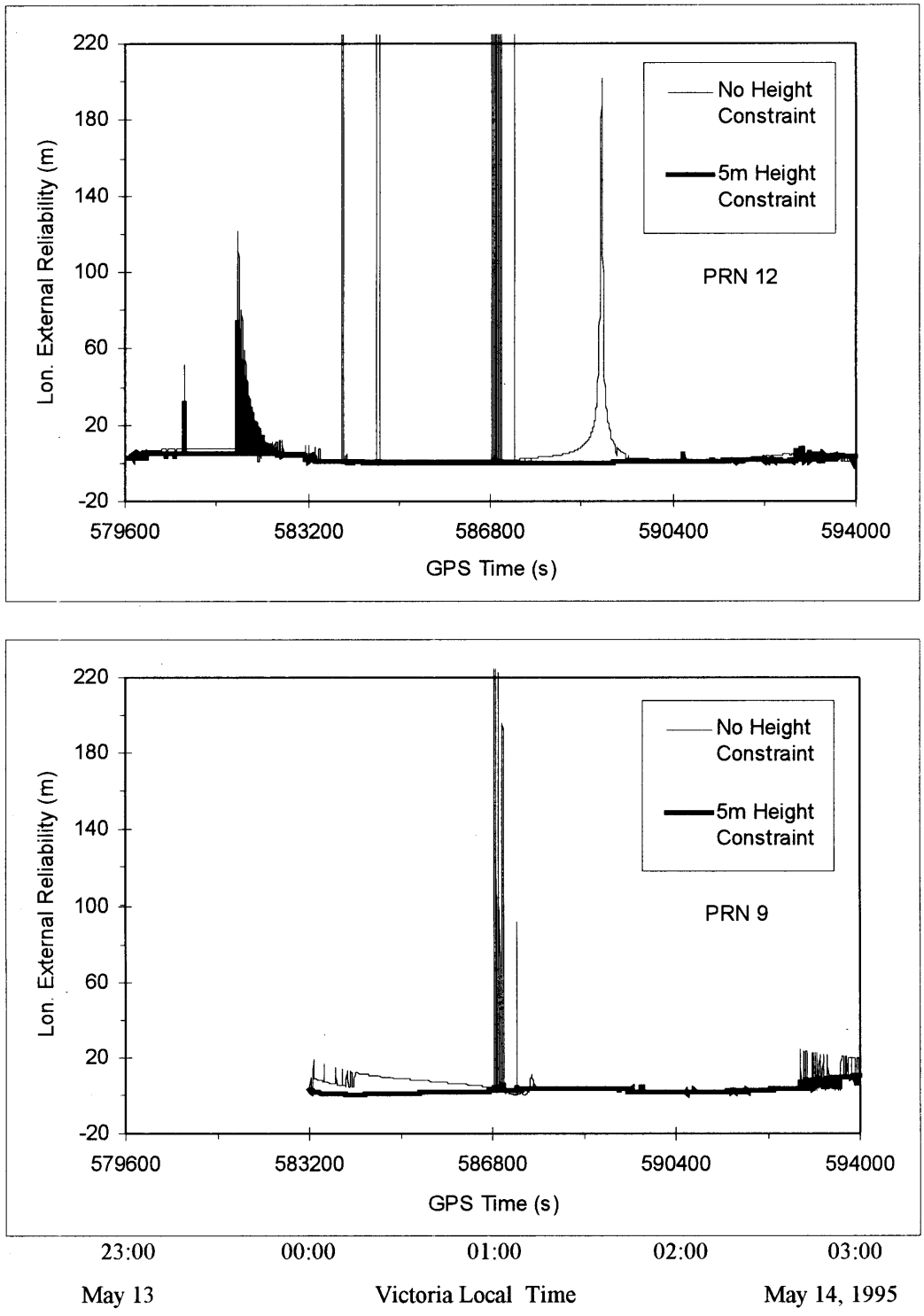


Figure 4.13c Comparison of Pseudorange MDB Influences on Longitude with/without Height Constrained - Shipborne Kinematic Test

# CHAPTER 5

# DGPS PERFORMANCE AIDED WITH EXTERNAL PRECISE CLOCKS

Research has shown that the receiver clock bias can be predictable depending on the stability characteristics of the clock [Misra et al., 1995a]. This characteristic of the receiver clock stability has previously been exploited for navigation and integrity monitoring with 'clock coasting' over a relatively short period when the satellite geometry becomes poor [Sturza, 1983; Lee, 1993]. If the receiver clock bias is relatively stable over a period, we can adaptively model the clock bias from the past measurements and expect to be able to predict the clock bias for the future. Then we can take advantage of the estimated clock stability characteristic regularly and continuously to improve positioning performance by fixing or constraining the receiver clock bias after we have modeled and predicted it.

In this chapter, DGPS performance aided with external precise clocks is investigated. The impact of precise clock augmentation of GPS receivers is described. A DGPS test using two NovAtel GPSCard™ receivers aided with external precise clocks is introduced. Differential reciver clock bias adaptive modeling at the remote station is presented. Finally, the results and analysis are given to demonstrate the performance improvement. The DGPS approach used here is the single difference pseudorange approach.

## 5.1 Impact of Precise Clock Augmentation of GPS Receivers

Current and previous analyses suggest that adding a low-cost atomic clock to a GPS receiver will significantly improve the vertical accuracy and navigation system availability

which in turn promises to lead to a major improvements in safety, integrity, and continuity of service of the GPS satellite-based navigation system [Murphy et al., 1994]. GPS navigation using three satellites and a precise clock is studied and a formula for computing PDOP, HDOP and VDOP as a function of three-satellite geometry and clock stability is presented in [Sturza, 1983]. It is found that clock coasting with a micro-miniature atomic clock would significantly improve Receiver Autonomous Integrity Monitoring (RAIM) availability [Lee, 1993]. It is also discovered that the ability to meet an availability requirement of 99.999% appears to be possible when a low-cost atomic clock is combined with a GPS receiver system [Murphy et al., 1994]. An approach to GPS navigation based on receiver clock modeling to predict its bias is analyzed and a significant improvement in the accuracy of the vertical position estimates is shown in [Misra et al., 1995a]. An approach to RAIM based on receiver clock modeling to predict its bias, referred to as clock-aided RAIM, has been found to offer a significant improvement in availability of fault detection and exclusion functions as shown in [Misra et al., 1995b].

## 5.2 Test Description

To test the performance of DGPS positioning using narrow correlator receivers aided with external precise clocks, two NovAtel GPSCard™ receivers aided with precise external clocks are used. Four hours of data are collected at a rate of one Hz on the roof of Engineering Building at The University of Calgary using a GPSCard™ 951 receiver aided with an external Efratom Model FRK rubidium clock, and on the roof of NovAtel Communications Ltd. using a GPSCard™ 3951 receiver aided with an external FTS 4040A RS cesium clock from Frequiency and Time Systems, Inc. in Beverly, MA, USA. The Allan variance of Efratom Model FRK is $1.0 \times 10^{-11}$ for a 10-second time interval sampling and $3.0 \times 10^{-12}$ for a 100-second time interval sampling. The baseline length between these two stations is about 7 km. In the kinematic processing of the data, the

university station was chosen as the reference station because its coordinates are known. The NovAtel station is the remote station. The reference coordinates of the NovAtel station for the purpose of this comparison are obtained by processing a subset of the collected data using SEMIKIN™.

### 5.3 Differential Receiver Clock Bias Adaptive Modeling at the Remote Station

Assuming we have GPS measurements over a time period ($t_0$, t) at both the reference and the remote stations during which the drift or drift rate of the receiver clocks is stable, we can model the differential receiver clock bias between the reference and the remote stations at time t as a linear or quadratic function, namely

$$b_t = b_0 + b_1(t - t_0), \tag{5.1}$$

or

$$b_t = b_0 + b_1(t - t_0) + b_2(t - t_0)^2, \tag{5.2}$$

and estimate the parameters $b_0$, $b_1$, and $b_2$ using the differential receiver clock biases computed from a single snapshot of the differentially-corrected pseudorange measurements.

After we get the differential clock bias model, we expect to be able to predict the differential clock bias for a certain time $\Delta t$ in the future. After time $\Delta t$, we slide the measurement window for $\Delta t$, estimate the differential clock bias model, and predict the differential clock bias for the next time period of $\Delta t$.

In order to determine whether the differential clock bias at the remote station is modellable, the data described in Section 5.2 was processed using a modified version of C$^3$NAV™. Figure 5.1 gives the snapshot estimated differential clock bias from the 4D approach using the differentially-corrected pseudorange measurements and corresponding predicted differential clock bias using Equation (5.1) at the remote station in DGPS positioning. Fifteen minutes of data is used for the establishment of the differential clock bias model and the measurement window is slided every minute. These figures show that the differential receiver clock bias is modellable and predictable at the remote station in DGPS positioning. In the simulation, Equation (5.2) is also used to model the differential receiver clock bias for the comparison. The results show that Equations (5.1) and (5.2) give similar results for the differential receiver clock bias. The five-minute sliding window is aslo tested to predict the differential receiver clock bias. It gave results that are similar to the one-minute sliding window. The predicted differential clock bias in Figure 5.1 is not smooth because the model is frequently updated.

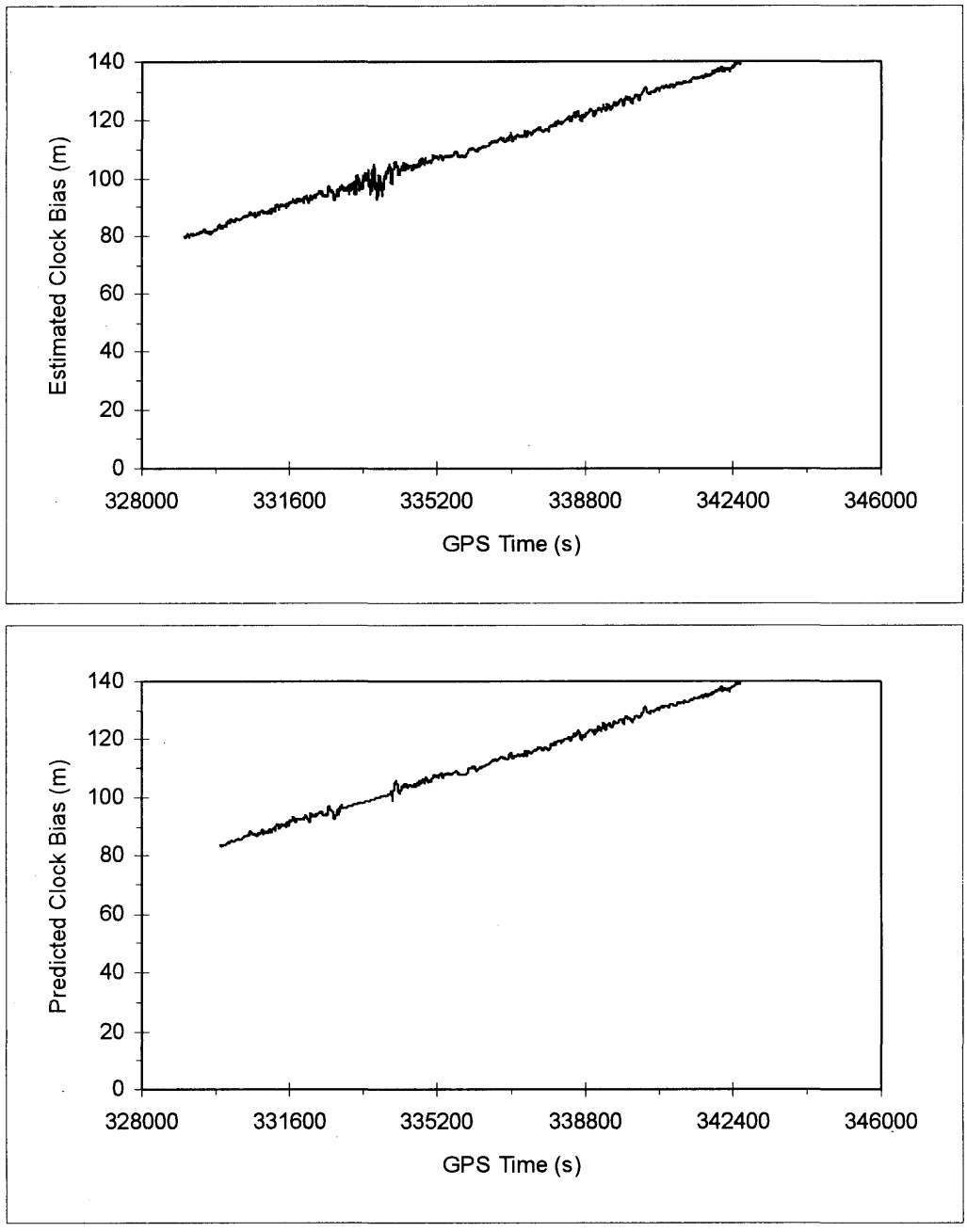


Figure 5.1 Estimated versus Predicted Receiver Clock Bias

## 5.4 Results and Analysis

In order to investigate DGPS performance aided with external precise clocks, the test data described in Section 5.2 was processed using modified C$^3$ NAV™.

After we accurately modelled the differential receiver clock bias using the past available measurements at the remote station, we can predict it for the future and fix it to estimate the 3D user position. In order to demonstrate the impact of GPS receivers aided with external precise clocks on the dilution of precision (DOP), the DOP values are computed for the cases with the differential clock bias fixed or not. Figure 5.2 gives the number of satellites used, NDOP, EDOP and VDOP when the differential clock bias is fixed or not. It is evident that the NDOP and VDOP values are reduced for 3D positioning with the differential clock bias fixed. The results shown in Figure 5.2 also indicate that VDOP can actually be lower than NDOP and EDOP at the remote station for DGPS positioning aided with external precise clocks.

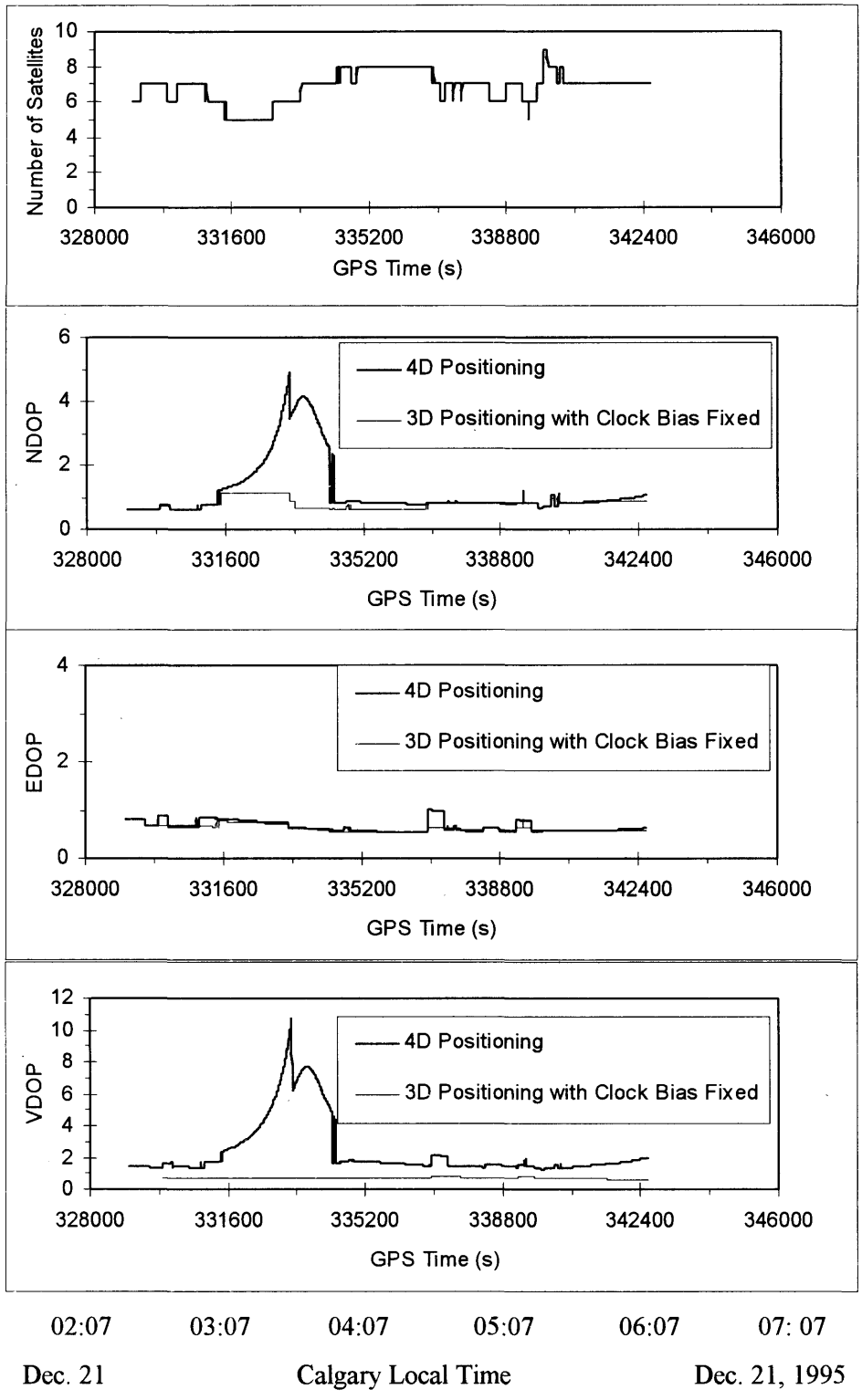


Figure 5.2 Number of Satellites and DOPs with/without Receiver Clock Bias Fixed

Figure 5.3 shows the DGPS positioning results for height and latitude components in different positioning modes; i.e., 4D positioning, 3D positioning with the differential receiver clock bias fixed, and 3D positioning with the differential receiver clock bias fixed and 5 m height constraint. By inspecting Figure 5.3a, we can see that the accuracy of the height component is improved from 1.57 m for the 4D positioning to 1.04 m for this specific data set using the approach of the 3D positioning with the differential receiver clock bias fixed. More importantly, the peak errors of the 4D positioning when the satellite geometry becomes poor as shown in Figure 5.2 is reduced by using the 3D positioning with the clock bias fixed. Comparing the results of the 3D positioning with the differential receiver clock bias fixed and a 5 m height constraint to those of the 3D positioning with the differential receiver clock bias fixed, we can find that the accuracy is improved from 1.04 m to 0.19 m. By checking the latitude component results with and without the differential receiver clock bias fixed in Figure 5.3b, it is seen that the approach of the 3D positioning with the differential receiver clock bias fixed does not improve the accuracy of the latitude component in comparison with the 4D positioning. It does reduce the peak errors when the satellite geometry becomes poor. The results of the latitude component can still be improved by constraining the height.

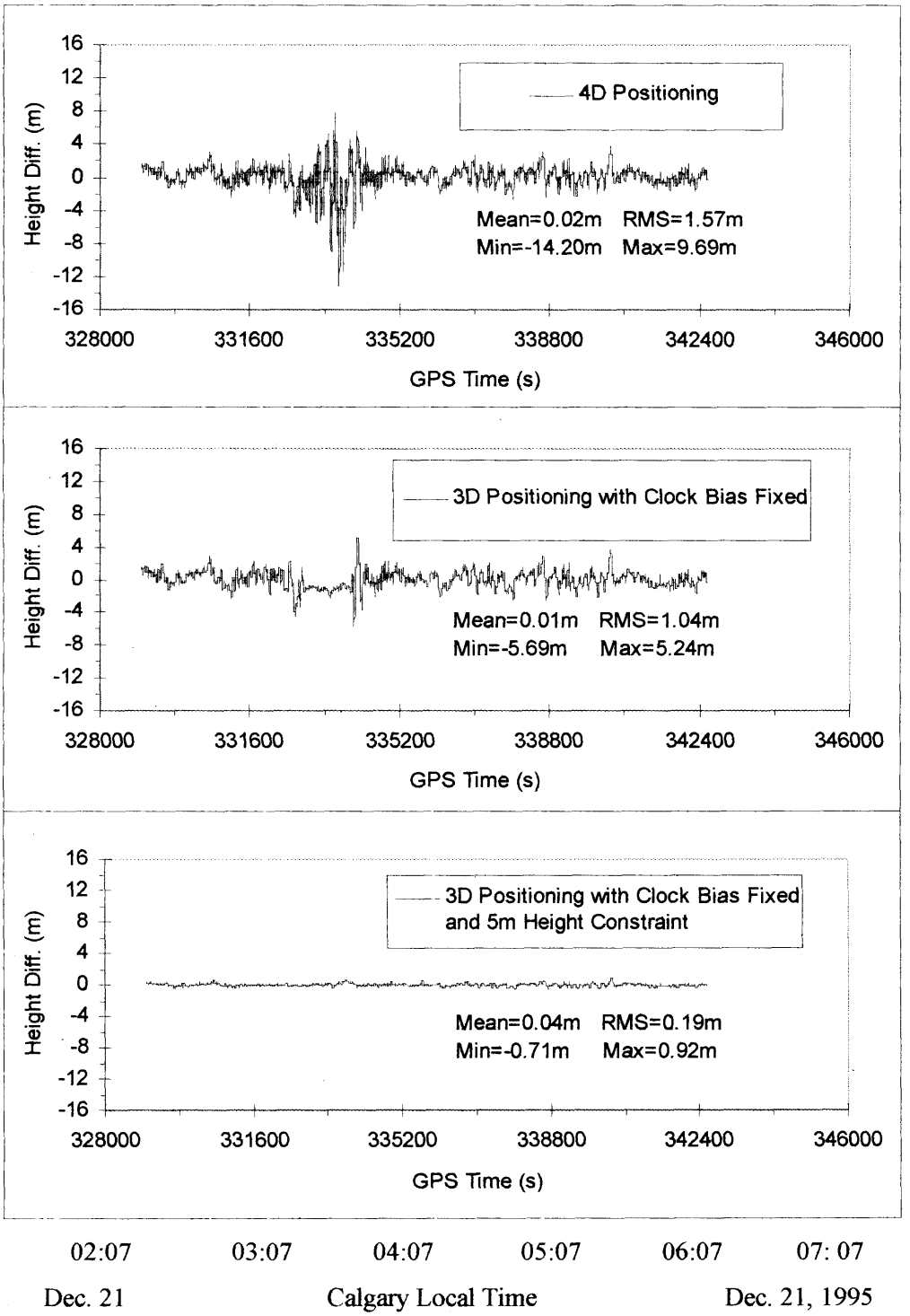


Figure 5.3a Position Result Comparison with/without Receiver Clock Bias Fixed and/or Height Constrained - Height

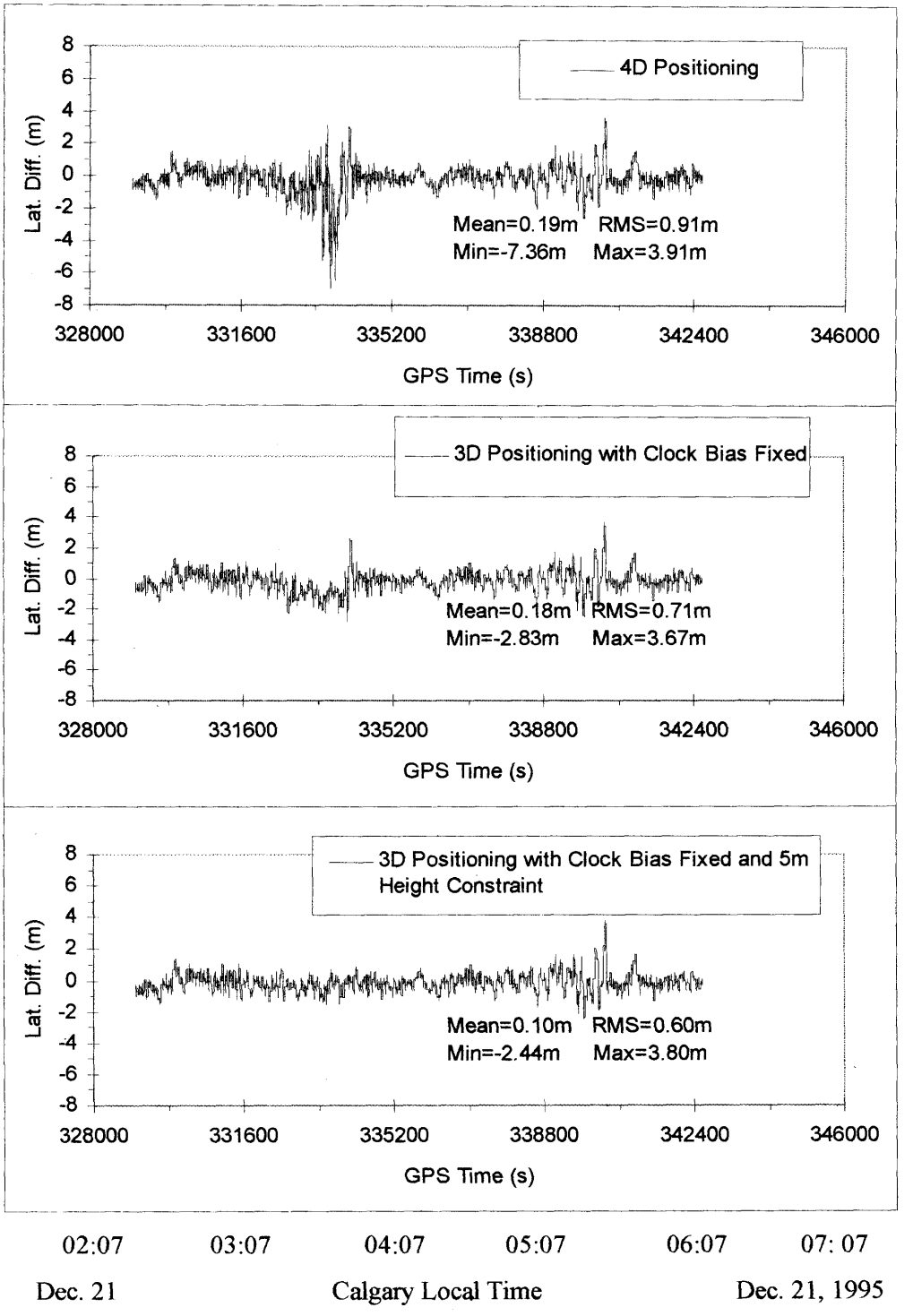


Figure 5.3b Position Result Comparison with/without Receiver Clock Bias Fixed and/or Height Constrained - Latitude

In order to analyze the reliability performance of DGPS positioning aided with external precise clocks, the internal and external reliability measures are computed for different DGPS modes using the test data.

Shown in Figure 5.4 are minimum detectable biases (MDB) for three satellites using different approaches, i.e., 4D positioning, 3D positioning with the differential receiver clock bias fixed, and 3D positioning with the differential receiver clock bias fixed and a 5 m height constraint. One can see that the MDBs of the pseudorange measurements are reduced using the 3D positioning with the differential receiver clock bias fixed, and the 3D positioning with the differential receiver clock bias fixed and 5 m height constraint, for satellites PRN 22 and PRN 14 during the period of poor geometry. The MDB reduction is small when comparing the results of the 3D positioning with the differential receiver clock bias fixed, and the 3D positioning with the differential receiver clock bias fixed and a 5 m height constraint.

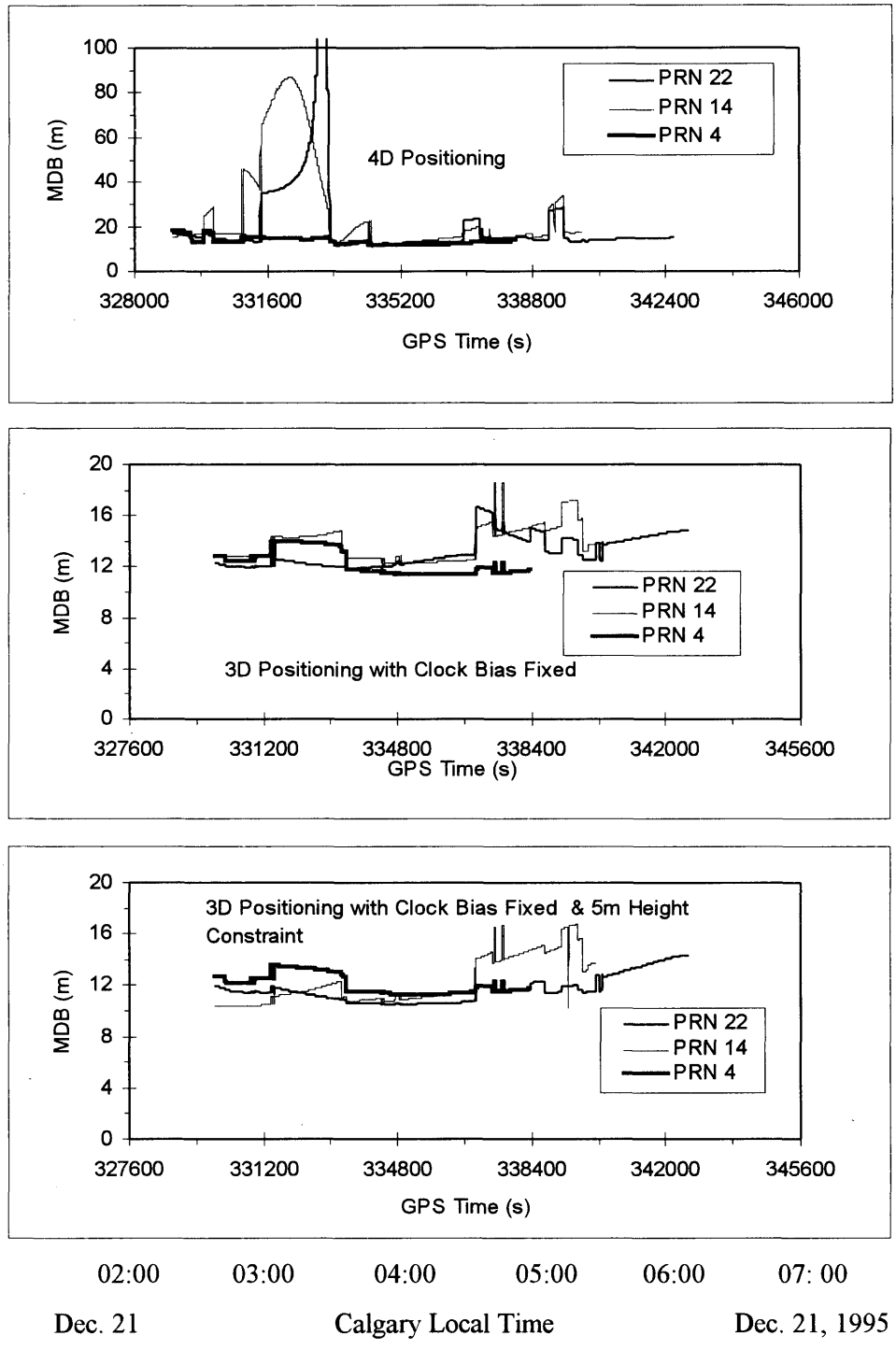


Figure 5.4 Comparison of Pseudorange MDBs with/without Receiver Clock Bias Fixed and/or Height Constrained

Figure 5.5a shows the height external reliability measures, i.e., the influences of pseudorange MDBs on the height component, for the 4D positioning, the 3D positioning with the differential receiver clock bias fixed, and the 3D positioning with the differential receiver clock bias fixed and 5 m height constraint. One can easily notice that the magnitude of the MDB influences on the height component is significantly reduced using the approaches of the 3D positioning with the differential receiver clock bias fixed and the 3D positiong with the differential receiver clock bias fixed and a 5 m height constraint instead of the 4D positioning approach.

Checking the VDOP values in Figure 5.2, the magnitude of the MDB's influence on the height component decreases as the VDOP values drop. The height external reliability performance improvement is more significant as the satellite geometry becomes poor. Comparing height external reliability measures of the 3D positioning with the differential receiver clock bias fixed and a 5 m height constraint to those of the 3D positioning with the differential receiver clock bias fixed, the height external reliability improves.

Figure 5.5b gives the corresponding latitude external reliability measures, i.e., the influences of pseudorange MDBs on the latitude component, using the 3D positioning with the differential clock bias fixed, and the 3D positioning with the differential clock bias fixed and a 5 m height constraint compared with the 4D positioning case. The magnitude of the MDB's influence on the latitude component is significantly reduced using approaches of the 3D positioning with the differential receiver clock bias fixed and the 3D positiong with the differential receiver clock bias fixed and a 5 m height constraint. By checking the NDOP values in Figure 5.2, one will also find that the magnitude of the MDB's influence on the latitude component decreases as the NDOP values drop. The latitude external reliability performance improvement is more significant as the satellite geometry becomes poor. Comparing the latitude external reliability measures of the 3D

positioning with the differential receiver clock bias fixed and a 5 m height constraint to those of the 3D positioning with the differential receiver clock bias fixed, the latitude external reliability improves.

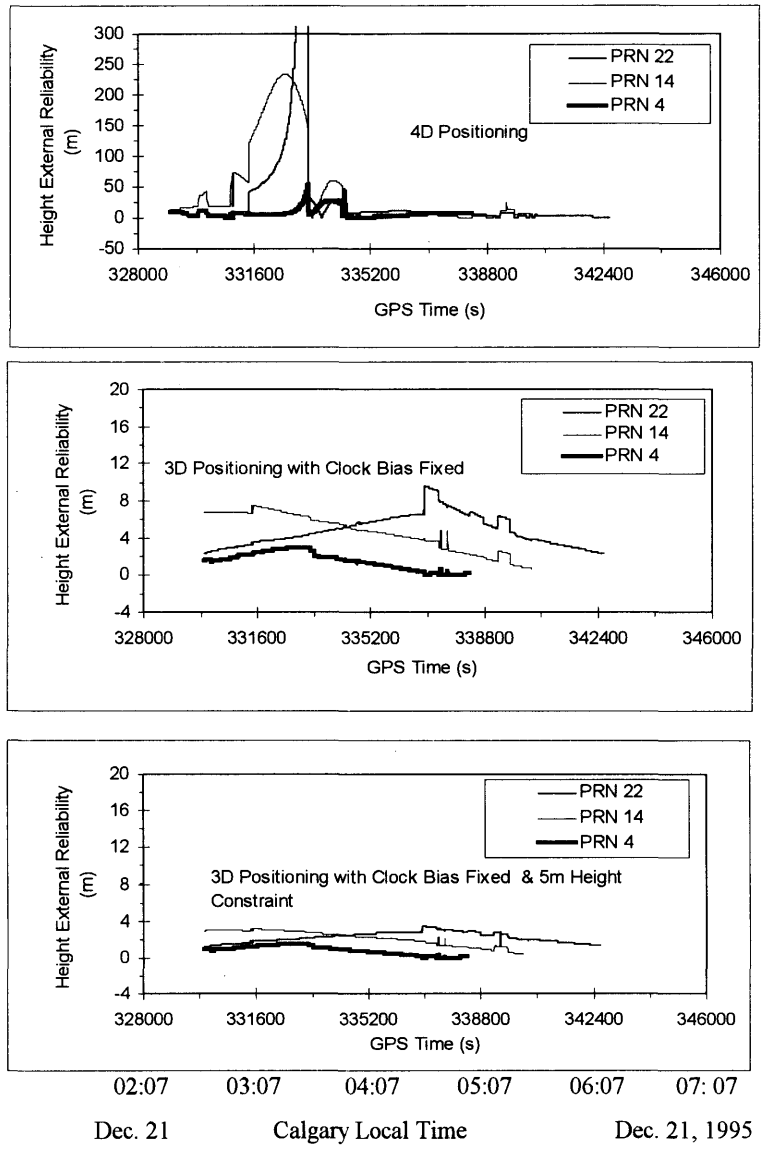


Figure 5.5a Comparison of Pseudorange MDB Influences on Height with/without Receiver Clock Bias Fixed and/or Height Constrained

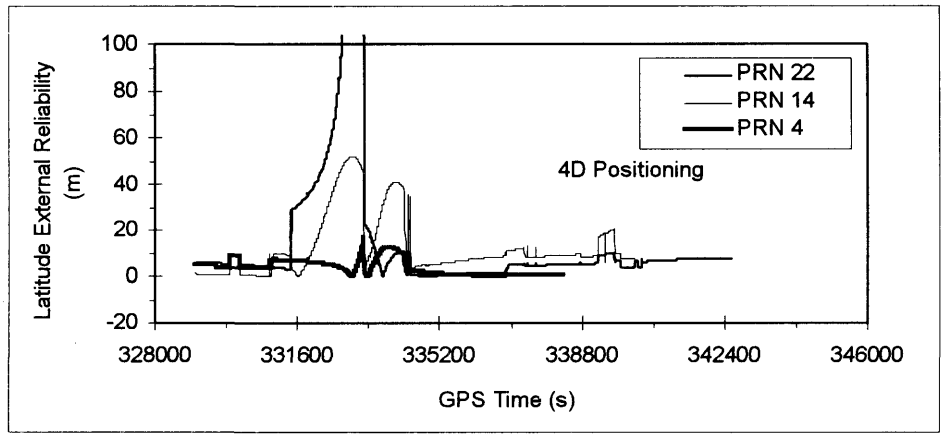


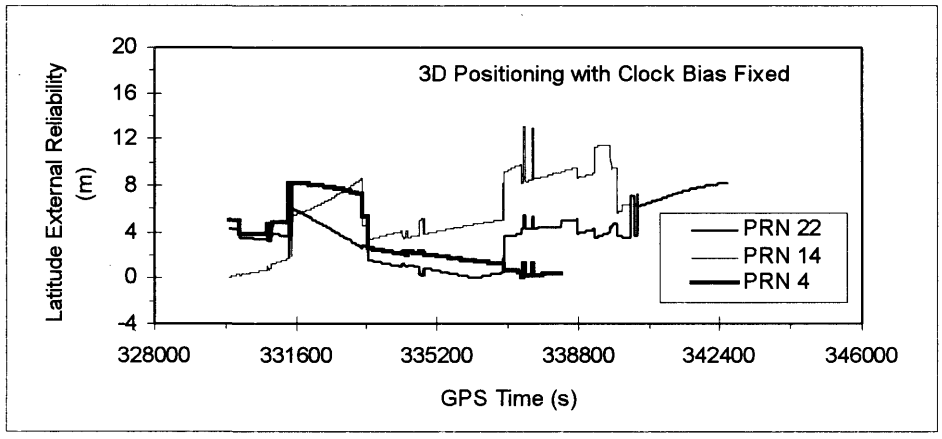


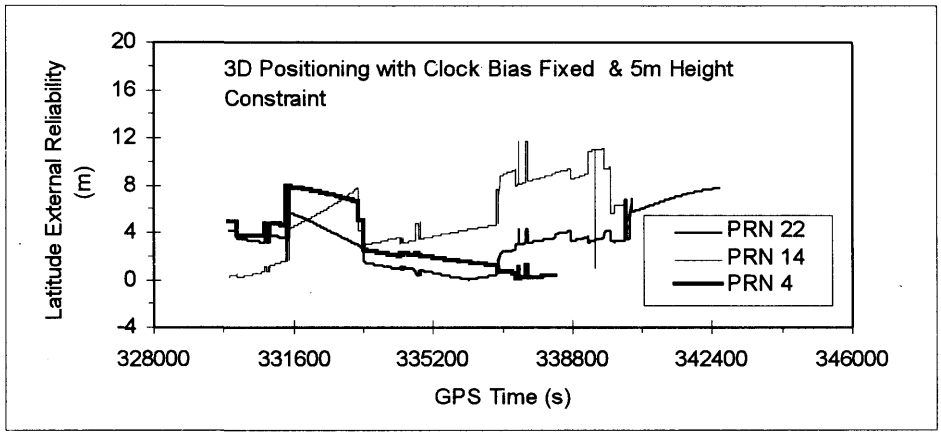




Figure 5.5b Comparison of Pseudorange MDB Influence on Latitude with/without Receiver Clock Bias Fixed and/or Height Constrained

# CHAPTER 6

# CONCLUSIONS AND RECOMMENDATIONS

## 6.1 Conclusions

Based on the investigations reported herein and the results obtained from these tests, the major conclusions are as follows:

1) Real-time DGPS accuracy of all receiver technologies using RTCM message Types 1/9 can easily meet the 95th percentile horizontal accuracy requirement of 5 m set by the Canadian Coast Guard for latencies in excess of 15 seconds, which is well beyond the 5 to 8 seconds latency expected for most firmware systems operating in conjunction with marine radiobeacons. The wide correlator spacing technology is the only technology which must utilize carrier phase smoothed code to attain the accuracy stated. The desired accuracy of 5 m 95th percentile in horizontal position is easily met by the Narrow Correlator™ and the semicodeless P-W technologies using either code or carrier phase smoothed code. Actually, the 95th percentile horizontal accuracy is better than 2 m with latency less than 15 seconds. The 95th percentile horizontal accuracy using different receiver technologies at the reference station and the remote with latency of 10 seconds is better than 3 m, which also meets the stated accuracy requirements. However, the accuracies obtained herein could be degraded by a few ppm, typically 2 ppm, during periods of high ionospheric activities.

2) With other conditions being equal, the distortions of the remote station coordinates are directly proportional to the errors of the monitor station coordinates. The difference of

satellite geometry between the reference and the remote stations, however, plays an important role on the distortions of remote station coordinates caused by the reference station coordinate errors. The distortions of the remote station coordinates also depend on the direction of reference station error vector, and the length and the direction of the inter-station vector formed by the reference and remote stations. The magnitude of the distortions of the DGPS remote coordinates was estimated to be about $10^{-9}$ of the errors of the reference station coordinates multiplied by the reference-remote separation.

3) The accuracy of horizontal position is improved significantly, as well as the height component for the wide correlator receivers when using the LSI or the weighted constraint LS method is used for height constraints in DGPS positioning in comparison with the standard unconstrained LS method. A relatively good knowledge of the height is needed for these two methods to improve the position accuracy significantly. The weighted constraint LS method seems to be more effective than the LSI method in height constraints for DGPS positioning. It does not make much difference using the LSI method in height constraints for the Narrow Correlator™ receivers when the satellite geometry is good. But when the satellite geometry becomes poorer, the accuracy of position can still be improved significantly using the LSI method in height constraints.

4) The LSI and the weighted constraint LS methods have the advantage of bounding the horizontal and height component errors of DGPS positioning when the wide correlator technology is employed. When the Narrow Correlator™ technology is used, the height constraint LSI does not have the advantage of bounding the position errors if the satellite geometry is good because its pseudorange measurement accuracy is very high. However, the height constraint LSI does have the advantage of bounding the horizontal and height component errors when the satellite geometry becomes poor.

5) The reduction of the MDBs of the pseudorange measurements is significant when the weighted height constraint approach is used instead of the standard LS. This effect is more significant when the geometry becomes poor. The performance improvement of the external reliability measure, is significant, especially for the horizontal component, which will be more significant when the satellite geometry becomes poor. A blunder is undetectable using the standard LS when there is no redundancy. A blunder can be detected and the effects of the blunder on horizontal positioning results can be reduced if the height constraint method is used, even when the number of satellites grops to 4.

6) The differential receiver clock bias at the remote station for DGPS positioning is modellable and predictable using external precise clocks. The DOP values at the remote station can be significantly reduced by using external precise clocks. The accuracy and reliability improves for the height component when the approach of the 3D positioning with the differential receiver clock bias fixed, and the approach of the 3D positioning with the differential receiver clock bias fixed and a 5 m height constraint are employed instead of the 4D positioning approach. The peak errors of the 4D positioning when the satellite geometry becomes poor is avoided by using the 3D positioning with the differential receiver clock bias fixed. The peak errors of the 4D positioning when the satellite geometry becomes poor are avoided by using the 3D positioning with clock bias fixed. Internal and external reliability measures are improved by using the approach of the 3D positioning with the differential receiver clock bias fixed and the approach of the 3D positioning with the differential receiver clock bias fixed and a 5 m height constraint instead of the 4D positioning approach.

## 6.2 Recommendations

The research reported in this thesis is a contribution to the investigation of the accuracy and reliability of various DGPS approaches. There are several problems left to be studied further. The following are recommendations for further investigations:

1) The real-time DGPS performance, including accuracy, reliability, coverage and availability using height constraints and RTCM message Type 9 for different receiver technologies need to be investigated and tested based on radiobeacon transceivers in the real marine environment.

2) In land and airborne mode, a barometer is one choice which is inexpensive and convenient to use for height determination. However, the accuracy of pressure heights are affected by many factors such as the vehicle dynamics and temperature changes. Therefore, DGPS performance with height constraints using aided barometers should be investigated and tested.

3) Investigations and tests of DGPS performance using different receiver technologies aided with oven-controlled crystal oscillator (OCXO), which is less stable, but lower cost than cesium and rubidium clocks, are required.

# REFERENCES

Ashjaee, J., R. Lorenz, R. Sutherland, J. Dutilloy, J. Minazio, R. Abtahi, J. Eichner, J. Kosmalska, and R. Helkey (1989): "New GPS Developments and Ashtech M-XII." Proceedings of ION GPS-89, The Institute of Navigation, Washington, D.C., pp. 195-198.

Ashjaee, J. (1990): "Ashtech XII GPS Technology.", IEEE PLANS '90.

Ashjaee, J., R. Lorenz (1992): "Precision GPS Surveying After Y-Code.", Proceedings of GPS-92 (Albuquerque, September 16-18), The Institute of Navigation, Alexandria, VA, pp. 285-299.

Cannon, M.E. (1987): "Kinematic Positioning Using GPS Pseudorange and Carrier Phase Observations." MSc. Thesis, UCSE Report No. 20019, Department of Geomatics Engineering, The University of Calgary.

Cannon, M.E. (1990a): "High-Accuracy GPS Semi-Kinematic Positioning: Modeling and Results.", Navigation, Journal of the U.S. Institute of Navigation, Vol. 37, No.1, pp. 53-64.

Cannon, M.E., G. Lachapelle, H. Ayers, and K.P. Schwarz (1990b): "A Comparison of SEMIKIN and KINSRVY for Kinematic Applications.", Proceedings of ION GPS-90, Colorado Springs.

Cannon, M.E., and G. Lachapelle (1992): "Analysis of a High Performance C/A Code GPS Receiver in Kinematic Mode.", Navigation, Journal of the U.S. Institute of Navigation, Vol. 39, No. 3, pp. 285-299.

Cannon M.E. and Lachapelle G. (1993): "C3NAV™ Operating Manual", Department of Geomatics Engineering, The University of Calgary.

Cannon M.E.(1993): "SEMIKIN™ Operating Manual", Department of Geomatics Engineering, The University of Calgary.

Caspary, W.T. (1987): "Concepts of Network and Deformation Analysis.", Monograph 11, School of Surveying, The University of New South Wales, Australia.

Enge, P.K., P. Levin, A. Hansen, and R. Kalafus (1992): "Coverage of DGPS/Radiobeacons.", Navigation, Journal of the U.S. Institute of Navigation, Vol. 39, No. 4.

Euler, H.J., and C.C. Goad (1991): "On optimal filtering of GPS dual frequency observations without using orbit information.", Bulletin G□od□sique, Springer Verlag, No. 65, pp. 130-143.

Forbes, F., S. Ryan, and S. Wee (1994), The Canadian Coast Guard DGPS Project, Proceedings of ION GPS-94, Salt Lake City, pp. 1451-1460.

Goad, C.C. (1990): "Optimal Filtering of Pseudoranges and Phases from Single-Frequency GPS Receivers.", Navigation, Journal of the U.S. Institute of Navigation, Vol. 37, No. 3, pp. 249-262.

Gryglaszewski, B. (1995): "User Position Errors due to Reference Receiver Translation", Presented at the Special Meeting of RTCM.

Hatch, R. (1982): "The Synergism of GPS Code and Carrier Measurements.", Proceedings of the Third International Geodetic Symposium on Satellite Doppler Positioning, DMA/NGS, Washington, D.C., pp. 1213-1232.

Hwang, P.Y.C. (1990): "GPS Navigation: Combining Pseudorange with Continuous Carrier Phase Using a Kalman Filter.", Navigation, Journal of the U.S. Institute of Navigation, Vol. 37, No. 2.

Kouba, J., and J. Popelar (1994): "Modern Reference Frames in Precise Positioning and Navigation.", Proceedings of International Symposium on Kinematic Systems in Geodesy, Geomatics and Navigation - KIS 94, Department of Geomatics Engineering, The University of Calgary, pp. 79-85.

Krakiwsky, E.J. (1992): "The Method of Least Squares: A Synthesis of Advances.", UCSE Report No. 10003, Department of Geomatics Engineering, The University of Calgary.

Lachapelle, G., W. Falkenberg, and M. Casey (1987): "Use of Phase Data for Accurate GPS Differential GPS Kinematic Positioning.", Bulletin Geodesique, International Association of geodesy, Paris, Vol. 61, No. 4, pp. 367-377.

Lachapelle, G., W. Falkenberg, J. Hagglund, D. Kinlyside, M. Casey, P. Kielland, and H. Boudreau (1988): "Shipborne GPS Kinematic Positioning for Hydrographic Applications.", Navigation, Vol. 35, No. 1, The institute of navigation, Alexanndria, VA, pp. 73-78.

Lachapelle, G., P. Kielland, and M. Casey (1992a): "GPS for Marine Navigation and Hydrography.", International hydrographic review, Monaco, Vol. LXIX, No. 1, pp. 43-69.

Lachapelle, G., M.E. Cannon, and G. Lu (1992b): "High Precision GPS Navigation With Emphasis on Carrier Phase Ambiguity Resolution.", Marine Geodesy, Vol. 15, No. 4, pp. 253-269.

Lachapelle, G., C. Liu, G. Lu, B. Townsend, M.E. Cannon, and R. Hare (1993): "Precise Marine DGPS Positioning Using P Code and High Performance C/A Code Technologies", Geomatica, Canadian Institute of Geomatics, Ottawa, Vol. 47, No. 2, pp. 117-128.

Lachapelle, G., H. Sun, M.E. Cannon, and G. Lu (1994): "Precise Aircraft-to-Aircraft Positioning Using a Multiple Receiver Configuration", Canadian Aeronautics and Space Journal, Ottawa, Vol. 40, No. 2, pp. 74-78.

Lachapelle, G.. R. Klukas, D. Roberts, W. Qiu, and C. McMillan (1995a): "One-Metre Level Kinematic Point Positioning Using Precise Orbit and Timing Information.", Geomatica, Canadian Institute of Geomatics, Ottawa, Vol. 49, No. 2, pp. 193-203.

Lachapelle, G., and C. Tang (1995b): "Analysis of Receiver Technologies to Generate Differential Information at Permanent (Radiobeacon) Sites, Contract Report, Electronic Engineering Directorate - AMTJ, Annadian Coast Guard, Department of Transport, Ottawa.

Lachapelle, G. (1995c): "GPS Theory and Applications", ENGO 625 Lecture Notes, Department of Geomatics Engineering, The University of Calgary.

Lachapelle, G., and J. Henriksen (1995d): "GPS Under Cover: The Effect of Foliage on Vehicular Navigation.", GPS World, Vol. 6, No. 3, pp. 26-35.

Lachapelle, G., M.E. Cannon, C. Tang, H. Lan, S. Wee, S. Ryan, and F. Forbes (1996a): "Shipborne and Airborne DGPS Positioning Accuracies Using Various Receiver Technologies and RTCM Message Types 1/9 and 18-21.", Canadian Aeronautics and Space Journal, Vol. 42, No. 1, pp. 37-44.

Lachapelle, G., A. Bruton, J. Henriksen, and M.E. Cannon (1996b): "Evaluation of High Performance Multipath Reduction Technologies for Precise DGPS Shipborne Positioning.", Proceedings of ION National Technical Meeting, Institute of Navigation, Santa Monica, California, January 22-24.

Lawson C.L., R.J. Hanson (1974): "Solving Least Squares Problems.", Prentice-Hall Inc., Englewood Cliffs, N.J..

Lee, Y.C (1993): "RAIM Availability for GPS Augumented with Barometric Altimeter Aiding and Clock Coasting.", Navigation, Journal of the U.S. Institute of Navigation, Vol. 40, No.2, pp. 179-193.

Li, D. (1988): "Error Processing and Reliability Theory.", Publishing House of Surveying and Mapping of China, Beijing, P.R. China.

Loomis, P., G. Kremer, and J. Reynolds (1989): "Correction Algorithms for Differential GPS Reference Stations.", Navigation, Journal of the U.S. Institute of Navigation, Vol. 36, No.2, pp. 179-197.

Lu, G. (1991): "Quality Control for Differential Kinematic GPS Positioning." MSc. Thesis, UCSE Report No. 20042, Department of Geomatics Engineering, The University of Calgary.

Lu, G., and G. Lachapelle (1991): "Reliability Analysis for Kinematic GPS Position and Velocity Estimation.", Proceedings of IAG International Symposium No. 107 on Kinematic systems in Geodesy, Surveying and Remote Sensing, Springer Verlag, New York, pp. 273-284.

Lu, G., E.J. Krakiwsky, and G. Lachapelle (1993): "Application of inequality constraint least squares to GPS navigation under selective availability.", Manuscripta Geodaetica, Vol. 18, No. 3, Springer Verlag, pp. 124-130.

Mark, Lt., J. Spalding, and M. Dowd (1995): "Verification of USCG DGPS Broadcast Parameters.", Proceedings of ION GPS-95 (Palm Springs, California, September 12-15), The Institute of Navigation, Alexandria, VA, pp. 889-897.

Misra, P., M. Pratt, B. Burke, and R. Ferranti (1995a): "Adaptive Modeling of Receiver Clock for Meter-Level DGPS Vertical Positioning.", Proceedings of ION GPS-95 (Palm Springs, California, September 12-15), The Institute of Navigation, Alexandria, VA, pp. 1127-1135.

Misra, P., M. Pratt, R. Muchnik, and B. Manganis (1995b): "A General RAIM Algorithm Based on Receiver Clock.", Proceedings of ION GPS-95 (Palm Springs,

California, September 12-15), The Institute of Navigation, Alexandria, VA, pp. 1941-1948.

Parkinson, B.W., and P. Axelrad (1988): "Autonomous GPS Integrity Monitoring Using the Pseudorange Residual.", Navigation, Journal of the U.S. Institute of Navigation, Vol. 35, No.2, pp. 255-271.

Poppe, D.. D. Last and M. Searle (1994): "Coverge Prediction of DGPS Radio-Beacon System.", Proceedings of 1994 National Technical Meetings, pp. 843-850.

RTCM (1994): "RTCM Recommended Standards for Differential Navstar GPS Service.", Version 2.1, RTCM SC-104, Washington, D.C..

Sturza, M.A. (1983): "GPS Navigation Using Three Satellites and a Precise Clock.", Navigation, Journal of the U.S. Institute of Navigation, Vol. 30, No.2, pp. 146-156.

Sturza, M.A. (1988): "Navigation System Integrity Monitoring Using Redundant Measurements.", Navigation, Journal of the U.S. Institute of Navigation, Vol. 35, No.4, pp. 483-501.

Teunissen, P.J.G. (1990): "Quality Control in integrated Navigation Systems.", Proceedings of IEEE PLANS'90, Las Vegas, USA.

Van Dierendonck, A.J. (1994): "Understanding GPS Receiver Terminology: A Tutorial on What Those Words Mean.", Proceedings of International Symposium on Kinematic Systems in Geodesy, Geomatics and Navigation-KIS 94.", Department of Geomatics Engineering, The University of Calgary, pp. 15-24.

Van Dierendonck, A.J., P. Penton, and T. Ford (1992): "Theory and Performance of Narrow Correlator Spacing in a GPS Receiver.", Navigation, The U.S. Institute of Navigation, Alexandria, VA, Vol. 39, No. 3, pp. 265-283.

Wells, D.E., N. Beck, D. Delikaraoglou, A. Kleusberg, E.J. Krakiwsky, G. Lachapelle, R.B. Langley, M. Nakiboglu, K.P. Schwarz, J.M. Tranquilla, P. Vanicek (1986): "Guide to GPS Positioning.", Canadian GPS Associates, Fredericton, New Brunswick, Canada.